

Sieve-based deterministic particle displacement for suspension separation J.P. Dijkshoorn

# Sieve-based deterministic particle displacement for suspension separation

Bridging the gap between microfluidics and microfiltration

Jaap Dijkshoorn

## Invitation

It is my pleasure to invite you to the public defence of my PhD thesis entitled:

### Sieve-based deterministic particle displacement for suspension separation

On Friday, the 12th of October at 13:30 in the Aula of Wageningen University, Generaal Foulkesweg 1 in Wageningen

After the defence you are invited to join the reception, dinner and drinks at *Onder de Linden*, Haagsteeg 16 in Wageningen

#### Jaap Dijkshoorn

#### Paranymphs

**Ricardo Cunha**  
JorgeRicardo.Cunha@wetsus.nl

**Rik de Vries**  
R.d.Vries@wln.nl

# Propositions

1. Dispersion separation can be improved by controlling the process on the scale of individual particles.  
(this thesis)
2. Many suspension separation techniques are similar but some are more similar than others.  
(this thesis)
3. Water is also food.
4. For patenting scientific results, you need to know the science of patenting.
5. Writing is like a separation experiment, you need the right flow.
6. The border between news and fake news is gradual.

Propositions belonging to the thesis, entitled

## **Sieve-based deterministic particle displacement for suspension separation**

*Bridging the gap between microfluidics and microfiltration*

Jaap Dijkshoorn

Wageningen, 12 October 2018

# Sieve-based deterministic particle displacement for suspension separation

*Bridging the gap between microfluidics and microfiltration*

Jaap Dijkshoorn

## **Thesis committee**

### **Promotor**

Prof. Dr R.M. Boom  
Professor of Food Process Engineering  
Wageningen University & Research

### **Co-promotors**

Dr M.A.I. Schutyser  
Associate professor, Laboratory of Food Process Engineering  
Wageningen University & Research

Dr R.M. Wagterveld  
Scientific project manager, Wetsus,  
European Centre of Excellence for Sustainable Water Technology  
Leeuwarden

### **Other members**

Prof. Dr A.H. Velders, Wageningen University & Research  
Prof. Dr R.G.H. Lammertink, University of Twente, Enschede  
Prof. Dr D.C. Nijmeijer, Eindhoven University of Technology  
Dr A.D.A. Harbiye, VECO precision metals, Eerbeek

This research was conducted under the auspices of the Graduate School VLAG  
(Advanced Studies in Food Technology, Agrobiotechnology, Nutrition and Health Sciences)

# Sieve-based deterministic particle displacement for suspension separation

*Bridging the gap between microfluidics and microfiltration*

**Jaap Dijkshoorn**

**Thesis**

submitted in fulfilment of the requirements for the degree of doctor

at Wageningen University

by the authority of the Rector Magnificus,

Prof. Dr A.P.J. Mol,

in the presence of the

Thesis Committee appointed by the Academic Board

to be defended in public

on Friday 12 October 2018

at 1:30 p.m. in the Aula.

Jaap Dijkshoorn

Sieve-based deterministic particle displacement for suspension separation

*Bridging the gap between microfluidics and microfiltration,*

158 pages.

PhD thesis Wageningen University, Wageningen, the Netherlands (2018)

With references, with summaries in English and Dutch

ISBN: 978-94-6343-497-3

DOI: <https://doi.org/10.18174/457801>

# Content

Summary	7
Samenvatting	10
<b>Chapter one</b>	15
<i>Introduction and outline</i>	
<b>Chapter two</b>	25
<i>A comparison of microfiltration and inertia-based microfluidics for large scale suspension separation</i>	
<b>Chapter three</b>	43
<i>Sieve-based lateral displacement technology for suspension separation</i>	
<b>Chapter four</b>	63
<i>Reducing the critical particle diameter in (highly) asymmetric sieve-based lateral displacement devices</i>	
<b>Chapter five</b>	85
<i>Visualizing the hydrodynamics in sieve-based lateral displacement systems</i>	
<b>Chapter six</b>	105
<i>Deterministic displacement of particles and oil droplets in a cross-flow microsieve module</i>	
<b>Chapter seven</b>	127
<i>General discussion and outlook</i>	
References	141
Acknowledgements	151
About the author	155
Publications	156
Overview of completed training activities	157





# Summary

Large industries such as for food and chemicals production, and for wastewater treatment always strive to improve their processes. Separation processes are amongst the most common and most energy intensive processes and therefore subjected to continuous improvement efforts. In this thesis, the aim is to improve the industrial scale separation of dispersed particles or droplets in suspension by scaling up a microfluidic separation principle. Microfluidic (micron-sized) separation techniques are extremely effective and precise, but unfortunately, these systems only process very small volumes. To apply these systems on an industrial scale their throughput must be increased by several orders of magnitude. For this reason, we investigated methods to increase the throughput of microfluidic techniques in order to function as alternative to existing separation techniques, such as microfiltration.

In *chapter 2*, several microfluidic techniques were identified, compared to cross-flow microfiltration and evaluated for their potential to process larger volumes. We discussed the current state-of-the-art of microfiltration and of microfluidic techniques, and their advantages and challenges for use on industrial scale. Three promising systems were selected with potential for industrial-scale use: fluid skimming microfiltration, sparse lateral displacement arrays and inertial spiral microchannel. These three systems were evaluated on four important aspects required for industrial use. Conceptual large scale designs were proposed.

The conceptual design of the sparse lateral displacement array was selected and further investigated in *chapter 3*. This system was selected because it separates particles that are smaller than the gaps throughout the system, which lowers the pressure drop and the risk of (irreversible) internal fouling. The throughput was increased by replacing the traditional obstacles by sieves. Initially the introduction of sieves adversely affected the separation because of the inhomogeneous pressure difference across the sieve over its length. This pressure

difference was stabilized by optimizing the outflow conditions of the outlets, which improved the performance of the system. This demonstrated that deterministic displacement of particles is possible in a sieve-based lateral displacement system as long as the flow conditions are adapted to it.

This concept was found to work well for displacing large particles ( $D_p = 785\mu\text{m}$ ) in *chapter 3*. However, decreasing the critical particle size was not straightforward, because traditional deterministic lateral displacement (DLD) scaling guidelines do not apply to the asymmetric sieve-based lateral displacement system. Therefore, in *chapter 4* we present an analysis of the influence of the geometric DLD parameters on the hydrodynamics and particle displacement in sieve-based lateral displacement systems. This analysis led to different guidelines to scale the critical particle diameter than are valid for original DLD systems.

The analysis of the relation between geometric parameters, hydrodynamics and particle displacement showed the large influence of the hydrodynamics on displacement and thus separation. In *chapter 5* we investigated the hydrodynamics in a sieve-based lateral displacement system both experimentally and numerically. This was done by visualizing the flow lanes with high speed imaging and subsequent analysis of the velocity components for different inflow velocities. The experimental observations were confirmed with two dimensional numerical simulations. Thorough analysis of both experimental and numerical results revealed the underlying fundamentals of the flow lanes and the hydrodynamic requirements to change the critical particle diameter. With this understanding on the hydrodynamic requirements, we proposed a simplified design that would allow deterministic displacement of particles at high throughputs.

A cross-flow module with a microsieve was designed and constructed to evaluate the findings in *chapter 5*, which was discussed in *chapter 6*. Computational Fluid Dynamics (CFD) simulations were done to obtain the required hydrodynamic conditions, which were confirmed by experimental visualization of the flow field. Experiments verified that at the right

hydrodynamic conditions, there is significant retention of particles and/or oil droplets that are smaller than the pores in the sieve. These results demonstrated that the microfluidic DLD separation can be applied in a microfiltration-like system to displace particles that are smaller than the pores on a much larger scale, which is not possible with conventional microfiltration. The main findings and conclusions are discussed in *chapter 7*. This discussion is followed by a short evaluation of the feasibility of deterministic displacement on industrial scale compared to microfiltration. The chapter is concluded by an outlook for future research. As stated before, the principle of deterministic displacement of particles on industrial scales can be very interesting because of the lower pressure loss, lower risk of (irreversible) fouling, and the possibility to effectively concentrate deformable particles and droplets. However, to achieve increased throughput, scale-up of the technique is required. In this thesis, a large-scale cross-flow microsieve (CFM) module is proposed. Its relatively simple design makes its manufacturing well feasible. Even though deterministic displacement in a CFM system has benefits compared to microfiltration, the novelty of the technique also brings its questions and risks. In the outlook we discuss several aspects that still need additional research, such as: the optimum industrial scale design, the minimum particle diameter that can be displaced, how the concentration polarisation affects displacement and fouling mechanisms. Concluding, an established, off-the-shelf technology like microfiltration may seem an easy and safe option, but we believe that the benefits of deterministic displacement may outweigh its current, initial risks, leading to a new generation of separation processes.

# Samenvatting

Grote industriële bedrijven zoals bijvoorbeeld in de levensmiddelensector, in de chemie en in de waterzuivering zijn continu bezig om hun processen te verbeteren en hun afvalstromen te verminderen. Omdat scheidingsprocessen tot de meest voorkomende en meest energie intensieve processen behoren, wordt er veel onderzoek gedaan om deze te verbeteren. In dit proefschrift wordt onderzocht hoe industriële scheidingsprocessen, die deeltjes of druppels afscheiden van een vloeistof, kunnen worden verbeterd door het opschalen van een microfluidisch scheidingsprincipe. Microfluidische scheidingsprincipes zijn erg efficiënt en heel precies, maar zoals de naam al doet vermoeden kunnen deze micro-systemen maar hele kleine hoeveelheden behandelen (microvolumes). Om deze systemen toe te passen op industriële schaal moet hun capaciteit sterk worden vergroot. Dit is wat wij hebben onderzocht, door de capaciteit van deze microfluidische systemen te vergroten kunnen ze een alternatief zijn ten opzichte van bestaande technieken zoals bijvoorbeeld microfiltratie.

In *hoofdstuk 2* zijn verschillende microfluidische technieken beschreven, vergeleken met microfiltratie en geëvalueerd of ze geschikt zijn voor hogere doorstroom. De nieuwste microfiltratie- en microfluidische technieken worden beschreven en hun voordelen en nadelen benoemd die betrekking hebben op het toepassen van deze technieken op industriële schaal. Drie veelbelovende systemen met potentie om gebruikt te worden op grote schaal zijn geselecteerd, namelijk: vloeistof-afromende microfiltratie (fluid-skimming microfiltration), een vereenvoudigd systeem dat deeltjes zijwaarts verplaatst (sparse lateral displacement arrays) en een spiraalvormig microkanaal waar gebruik wordt gemaakt van vloeistof inertie (inertial spiral microchannel). Deze drie systemen zijn daarna nogmaals vergeleken op vier punten die belangrijk zijn voor toepassing in de industrie. Van deze drie systemen zijn conceptuele ontwerpen voorgesteld die op grote schaal zouden kunnen worden toegepast.

Van de drie systemen hebben we het sparse lateral displacement systeem geselecteerd om verder te onderzoeken (*hoofdstuk 3*). De naam van dit systeem beschrijft wat het doet, het kan namelijk deeltjes zijwaarts in een vloeistof verplaatsen zodanig dat de deeltjes aan één kant kunnen worden opgevangen. De reden dat we dit systeem hebben geselecteerd is omdat het deeltjes kan tegenhouden die kleiner zijn dan de openingen, daardoor is de drukval en de kans dat de deeltjes deze openingen blokkeren kleiner. Om de doorstroom van dit systeem te verhogen wordt het originele ontwerp aangepast door het te combineren met een speciaal soort zeef. Maar de scheiding verslechterde nadat deze zeven in het systeem geplaatst waren. Dit kwam doordat de zeven de drukverdeling in het systeem veranderden. Door de uitstroom per afvoerkanaal aan te passen kon de drukverdeling worden hersteld en lukte het weer om deeltjes tegen te houden. Deze resultaten lieten zien dat het mogelijk was om met een aangepaste (hybride) systeem deeltjes te scheiden die kleiner waren dan de poriën in de zeef.

Tot zover werkte de scheiding goed voor grote deeltje met een diameter van ongeveer 0.8 mm (beschreven in *hoofdstuk 3*). Deze deeltjes zijn veel groter dan deeltjes die in de praktijk in industriële processen voorkomen en daarom vervolgden we ons onderzoek om ook de kleinere deeltjes te kunnen scheiden. Het scheiden van kleinere deeltjes bleek echter niet eenvoudig, mede omdat de bestaande theorie niet werkte voor het aangepaste systeem met schuine zeven. Dus is er gezocht naar nieuwe richtlijnen om ook de kleinere en industrieel relevante deeltjes te kunnen scheiden. In *hoofdstuk 4* werd de invloed van de geometrie op de vloeistofstroming en op de scheiding van verschillende deeltjesgroottes geanalyseerd. Deze analyse leidde tot nieuwe inzichten en richtlijnen, die het mogelijk maken om ook kleinere deeltjes met dit systeem te kunnen scheiden.

De analyse over de relatie tussen de geometrische parameters, de vloeistofstroming en scheiding gaf een nieuw inzicht in de mate waarop de vloeistofdynamica invloed heeft op de scheiding. In *hoofdstuk 5* onderzochten we de hydrodynamica in het aangepaste hybride zeefstelsel (sieve-based lateral displacement device) zowel experimenteel als modelmatig. Dit

werd gedaan door de vloeistofstroom te visualiseren met een hogesnelheidscamera en de stroomsnelheid te analyseren voor verschillende toevoersnelheden. Deze experimentele observaties werden vergeleken met de twee dimensionale numerieke simulaties van de vloeistofstroom. Verdere analyse van zowel de experimentele als de modelsimulatie resultaten hielpen het onderliggende scheidingsprincipe beter begrijpen en leidden tot een richting om de scheiding te beïnvloeden. Met deze kennis van de hydrodynamische voorwaarden is het nu mogelijk om (nog) kleine(re) deeltjes te scheiden in een verder vereenvoudigd systeem.

Het nieuwe vereenvoudigde systeem was een aangepaste kruisstroom module met een speciaal microzeef (cross-flow microsieve module) waarvan de poriën groter zijn dan de deeltjes. In *hoofdstuk 6* is dit geëvalueerd of het inderdaad deeltjes en druppeltjes kan tegenhouden die kleiner zijn dan de poriën. Numerieke simulaties werden uitgevoerd om de benodigde hydrodynamische voorwaarden te vinden. Deze hydrodynamische voorwaarden werden vergeleken met opnames van het stromingsveld die zijn verkregen met de hogesnelheidscamera. Experimenten bevestigden dat met de juiste stromingscondities, de concentratie van kleine plastic deeltjes en olie druppels veel lager is in vloeistof die door de microzeef is gegaan vergeleken met de toevoer-concentratie. Al deze resultaten lieten zien dat het mogelijk is om het microfluidische scheidingsprincipe toe te passen in een kruisstroom microzeef (cross-flow microsieve) module en dat het mogelijk is om op grote schaal deeltjes en olie druppels te scheiden die kleiner zijn dan de poriën.

De belangrijkste bevindingen en conclusies van dit werk worden beschreven in *hoofdstuk 7*. Na de belangrijkste bevindingen volgt een korte evaluatie van de haalbaarheid van het scheidingsprincipe op grote schaal vergeleken met microfiltratie. De algemene discussie wordt afgesloten met openstaande vragen nog moeten worden onderzocht. Zoals al eerder is beschreven, is het scheidingsprincipe zeer interessant om op industriële schaal te worden toegepast.

Vergeleken met microfiltratie is de drukval over de microzeef kleiner, is de kans dat de microzeef (onherstelbaar) dichtslibt kleiner, en is het mogelijk om vervormbare deeltjes en/of (olie) druppels te scheiden. Maar om de kruisstroom microzeef module op industriële schaal te gebruiken moet het worden opgeschaald om grotere volumes te verwerken. In dit proefschrift worden een aantal manieren beschreven om een kruisstroom microzeef op te schalen en daarmee deeltjes te scheiden, die kleiner zijn dan de poriën in de microzeef. Ondanks dat het beschreven systeem veel voordelen biedt ten opzichte van microfiltratie, zijn er voor dit nieuwe systeem ook nog vragen en risico's. Daarom beschrijven we meerdere aspecten die nog onderzocht moet worden, zoals bijvoorbeeld: het beste grootschalige ontwerp, de minimale deeltjesgrootte die gescheiden kan worden, het effect van de verhoogde concentratie aan het oppervlak van de microzeef en de mechanismes van vervuiling van de microzeef. Momenteel concluderen we nog dat een gevestigde techniek zoals microfiltratie een goede en veilige optie is, maar we verwachten dat de voordelen van de kruisstroom microzeef module uiteindelijk opwegen tegen de nadelen.





# One

## Introduction and outline

During the writing of this chapter I often listened to *I want to know* from *KONGOS*

## 1.1. Disperse systems

Many products we use in our daily life, and many streams in food, chemical and wastewater processing consist of dispersed particles or droplets in a fluid. Examples are milk, algae and wastewater. Milk is, for example, a product that contains fat globules (droplets) as dispersed phase. The fat concentration, however, can vary per cow, per season and per year, and is much higher than in skim milk. Therefore, the milk has to be standardized by removing a part of the fat. Algae are grown in ponds but need to be concentrated before they can be used. This concentration step is often considered the most critical step in utilizing algae. In wastewater treatment, one has to remove the sludge that is generated in the digestion of the organic components that were present in the waste water. This is typically done with sedimentation ponds; however, these are critical in the total capacity of these processes.

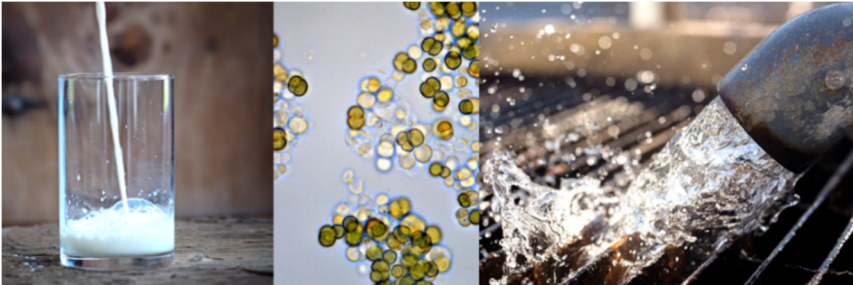


**Figure 1.1:** Examples of products and process streams that are dispersions, with milk on the left, cyanobacteria *Chlorogoeopsis fritsii* in the middle (courtesy of S. Canizales) and wastewater on the right.

Disperse systems (*Figure 1.1*) can be characterised by the physical characteristics of the dispersed and continuous phase. Typical parameters are the size distribution of the particles or droplets, the shape of the particles, the density difference between the dispersed and the continuous phase, the surface properties of the dispersed phase, and the ionic strength, surface tension and rheology of the continuous phase [1].

To separate or concentrate the dispersed phase from the liquid phase, separation techniques typically exploit one or more of these characteristics.

## 1.2. Mechanical separation technologies

A common method to separate or concentrate a dispersed phase is to exploit density differences. This can be done with for instance, settlers (sedimentation or flotation) and with centrifuges. Density based separation techniques can be used when particles or droplets have a significant density difference with the continuous phases, and when the particles or droplets are sufficiently large (*Figure 1.2*). Small particles or particles with a density practically equal to that of the liquid (neutrally buoyant) cannot easily be separated with these methods because the typical velocity between dispersed and continuous phase (terminal velocity) is too low and separation would require too much energy and/or time [2].

In those cases that the density differences and particle sizes are too small, one can use size exclusion; this is typically used with (micro)filtration, which blocks particles to pass a porous membrane with pores of a specific size. Particles with a diameter between 0.1 and 10  $\mu\text{m}$  can be separated with microfiltration on an industrial scale; however, membrane pore blocking and fouling, due to the accumulation of retained particles before and inside the membrane, generally reduce the effectiveness of the process over time. To mitigate these effects, different hydrodynamic and dynamic strategies have been developed, as was reviewed by Jaffrin et al. 2012 [3]. A different strategy to reduce (irreversible) fouling is the development of micro-engineered membranes, called microsieves.

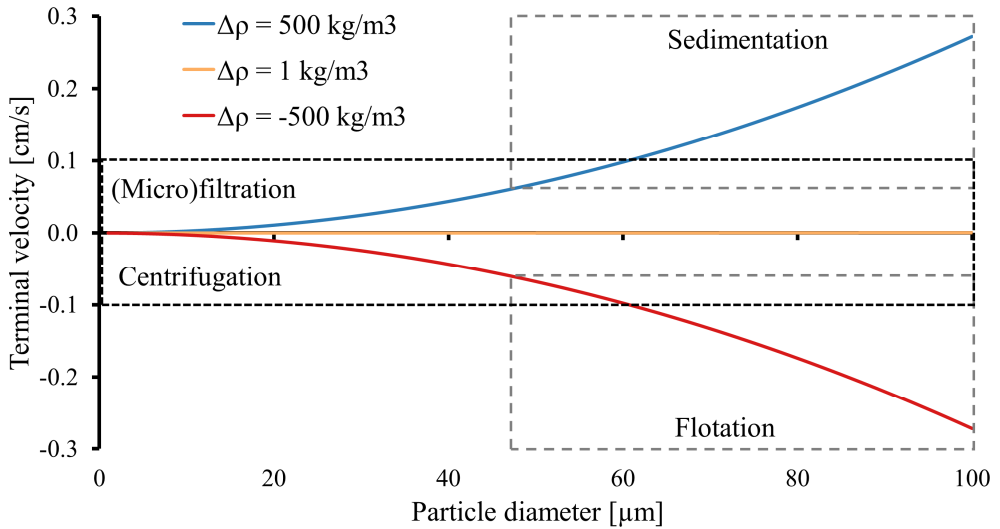


Figure 1.2: An estimation of the typical velocity between dispersed and continuous phase of particles with a size between 1 and 100 μm with a density difference of  $\pm 500 \text{ kg/m}^3$  (using general equation of the settling velocity in laminar regime). The boxes give a rough indication when density-based techniques or filtration techniques can be applied (distinctions are made based on Wakeman et al.). Microfiltration and centrifugation can be used in the same particle size range if there is a small difference in density between dispersed and continuous phase. Overlap indicates flexibility between the different techniques.

These membranes are (relatively) less sensitive to fouling because they can be operated with very low pressures, are very smooth and have great freedom in the shape of their pores [4-6]. However, even microsieves suffer from the same limitations as conventional membranes; therefore, new and/or improved separation methods are important. Because, these new/improved separation techniques are expected to recover more of our valuable resources while using less resources (e.g. energy and chemicals), and this might prove to be helpful in the future.

### 1.3. Microfluidic separation technologies

Microfluidics has emerged from the application of micro-engineering methods for preparing very small fluidic devices. It has been extensively applied in sensors, in small-scale analytic devices ('lab-on-a-chip'), and only recently has been extended to larger scale separation processes, such as with microsieves [7, 8]. Various microfluidic separation principles have been developed that do not have the same limitations as density based separation techniques or (micro)filtration, by making use of the complex designs that are possible with chip preparation methods, such as photolithography. Despite the advantages of microfluidic separation devices, their very low throughput makes direct translation of these new methods towards processing of larger streams a challenge. Processing larger volumes would be possible by mass parallelisation of microfluidic devices but because of the complex interfacing with the peripheral equipment, one traditionally scales up by increasing the throughput of a single device. Several different microfluidic separation techniques were evaluated on their potential for increasing the single unit throughput. The deterministic lateral displacement (DLD) device was identified as one of most promising microfluidic techniques for suspension separation on larger scale [9].

A DLD device is an array of obstacles placed in a specific pattern (*Figure 1.3AB*). The fluid flows in between the obstacles. The part of the fluid that meanders between two consecutive obstacles is called a flow lane (red). Only one flow lane and therefore only a small part of the total flow is shown in *Figure 1.3*; of course the rest of the system is also filled with fluid and other flow lanes. A particle that initially flows within a flow lane will at some point approach an obstacle. If the radius of the particle is larger than the width of the flow lane while passing an obstacle, it will be pushed from its initial position, out of this flow lane. This results in the particle being moved laterally into the adjacent flow lane. At a later encounter with another obstacle, the same will happen. After many of these encounters, the particles will be translated to one direction, which effectively results in macroscopic separation of the particles.

The distance between the obstacles can be larger than the size of the separated particles. Instead, the critical size of the particles that can be separated is determined by the angle in which the obstacles are placed and the size of the gap between the obstacles. This is important, as it implies that the system may be much less susceptible to fouling, than for example a microfiltration system, in which the separation rests on the existence of pores that are smaller than the particles to be separated [10], and which can therefore be clogged by these particles.

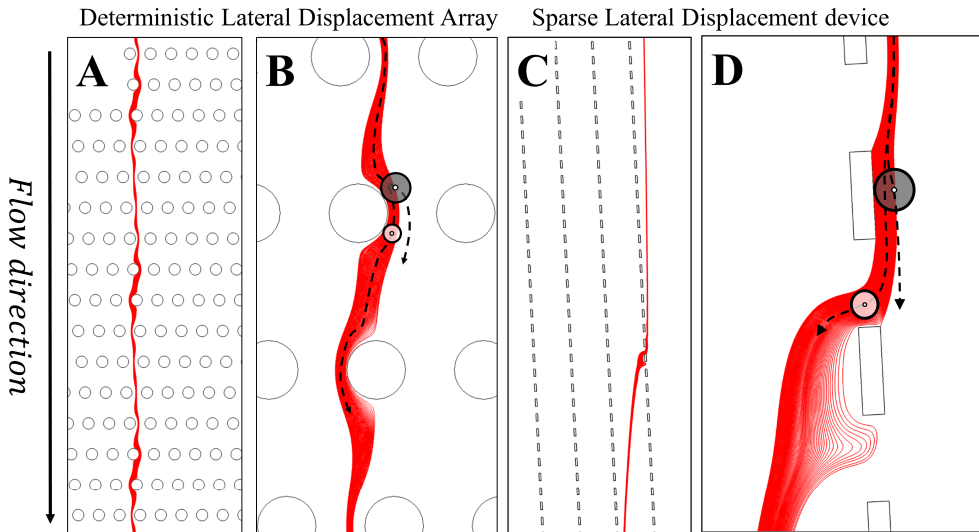


*Figure 1.3:* In (A) the original Deterministic Lateral Displacement (DLD) array. The circles are the obstacles. Only one of the many flow lanes is shown (red). (B) Close up of a flow lane and the separation principle, where particles with a radius larger (grey) than the red flow lane change direction after interacting with an obstacle. The smaller particles remain in their original trajectory and follow the flow lane. (C) shows an alternation on the original DLD device, which we call a sparse lateral displacement system. In (D) the close up of the flow lane and separation principle in a sparse lateral displacement system, where particles with a radius larger than the width of a flow lane (grey) are displaced.

While the principle of DLD is promising, direct scaling is difficult. The dense obstacle arrays become fragile when the obstacles are made longer, while larger throughputs without changing

the dimensions would result in larger pressure drops. The manufacturing of large-scale DLD with this design is a challenge that has not yet been resolved.

It was recognised by Lubbersen et al., that one does not need a complete array of obstacles for the separation of a dispersion with low volume fraction. In principle, a single column of obstacles that is tilted would be enough. In practice, however, several columns were still necessary, although with much less than the conventional fully filled DLDs. Such a sparse lateral displacement system would be much easier to construct and apply on larger scale, while it still retains the advantage of separating particles much larger than the gaps between the obstacles (*Figure 1.3CD*).

Upscaling the sparse lateral displacement device is the subject of this thesis. Just making longer obstacles with the same manufacturing techniques as are applied for microfluidic devices, leads to mechanically very fragile obstacles. Interconnecting the obstacles to their neighbours, with small connections, increases the mechanical strength of the obstacles and makes it possible to increase their length. The resulting geometry of connecting obstacles is then the same as a single microsieve, with elongated pores.

Combining microsieves into a sparse lateral displacement system, results in a hybrid system that is partly microfluidic and partly microfiltration (*Figure 1.4*). This reflects the title of this thesis, “Sieve-based deterministic particle displacement for suspension separation.”



*Figure 1.4:* On the left, normal obstacles that are only connected to the base. In the middle, interconnected obstacles that are both connected to the base as well as to other obstacles in the same obstacle column. This geometry mimics a sieve. On the right, extremely small interconnected obstacles columns which is similar to a single microsieve.

## 1.4. Research objectives and thesis outline

The objective of the study reported in this thesis was to investigate the design and performance of sparse deterministic lateral displacement systems, with the practical aim to increase the system throughput. We replaced the traditional obstacles by microsieves to create larger-scale systems, which were then compared to the traditional DLD. The influences of design and process parameters were investigated by characterising the flow field in a sparse deterministic lateral displacement system.

*Chapter 2* qualitatively compares cross-flow microfiltration and inertial microfluidics to understand their challenges for application on larger scales. The challenges of microfiltration (MF) and the existing strategies to improve MF operations are discussed. Subsequently, the upscale potential of different inertial microfluidic systems is discussed. Based on the underlying separation principles, three promising systems are identified as most promising, i.e. fluid skimming, sparse lateral displacement arrays, and inertial spiral microchannels. Finally, we propose conceptual design guidelines for large scale suspension separation.

*Chapter 3* introduces a sparse lateral displacement system that is based on sieves. This creates a hybrid “sieve-based lateral displacement” system, which is better suited for upscaling. Numerical simulations and experiments were compared and used to study particle trajectories and concentrations. The macroscopic separation was optimized by adjusting the outflow conditions.

*Chapter 4* elaborates on scaling guidelines of the sieve-based lateral displacement systems relative to the conventional deterministic lateral displacement devices. The geometry of sieve-based lateral displacement systems is asymmetric and was not expected to displace particles. Despite its asymmetric design, we could observe significant particle displacement. Analysis of the numerical simulations gives insight on the hydrodynamics and the separation mechanism.



In *Chapter 5* the flow lanes and system hydrodynamics are experimentally visualized and compared to two-dimensional numerical simulations. An in-depth analysis of the simulations shows a correlation between the ratio of the velocity components in the pores and the size of the flow lanes. This study yields understanding of the underlying requirements for deterministic lateral displacement and provides further guidance for the development devices for deterministic displacement.

*Chapter 6* describes and applies systematic system design to obtain optimal deterministic particle displacement in a cross-flow microfiltration set-up for small particles and droplets. Two-dimensional numerical simulations were used to find the specific balance of the velocity components inside the pores. Based on the simulations, an experimental module is manufactured, the velocity field visualized and compared with the 2D simulations. Concentration experiments of PMMA particles and Oil/Water emulsions confirm deterministic displacement of particles and droplets in a cross-flow microsieve module. These results demonstrate the possibility to deterministically displace particles smaller than the pores in a cross-flow microsieve module.

In *Chapter 7* we discuss the main results of this thesis. Next, the feasibility of deterministic displacement on industrial scale is evaluated and compared to microfiltration. This is followed by an outlook that describes some remaining topics for future research and an overall conclusion



# Two

## **A comparison of microfiltration and inertia-based microfluidics for large scale suspension separation**

While writing this chapter I listened frequently to *harder, better, faster, stronger*  
from *Daft Punk*

This chapter has been published as:

J.P. Dijkshoorn, M.A.I. Schutyser, R.M. Wagterveld, C.G.P.H. Schroën, R.M. Boom: A comparison of microfiltration and inertia-based microfluidics for large scale suspension separation, *Separation and purification technology* 173 (2017), 86-92.

## 2.1. Abstract

Separation of suspensions can be carried out by microfiltration and microfluidic techniques, although both rely on different principles. Conventional microfiltration involves retention of particles by a porous membrane, but is limited by (irreversible) particle accumulation and concentration polarization that can only be (partially) controlled by back pulsing that transfers particles back into the bulk. Microfluidic separation devices employ a combination of inertial forces and sometimes geometric constraints to control particle migration behaviour, which allows splitting of suspensions into concentrated and diluted streams.

Considering their effectiveness, inertia-based microfluidic separation is regarded an interesting alternative to microfiltration; therefore, this paper focusses on the use of inertial forces in suspension separation. This resulted in the selection of three concepts, which were: 1) Fluid skimming, which is a combination of microfiltration and controlled particle migration behaviour, 2) Spiral inertial microchannel separation, in which particles migrate fast towards an equilibrium position, and 3) sparse obstacle arrays, which use geometric interactions to induce particle migration. In a concluding section, the application of controlled migration behaviour in relation to scalability of inertia-based microfluidic separation techniques and the effect of suspension properties on separation are discussed in detail.

## 2.2. Introduction

Suspension separation is one of the most applied operations in for example food, water-treatment and chemical industries. It is mainly applied to either recover a valuable solid component or a fraction thereof, or to separate a valuable liquid from the solids. Since suspension separation is frequently used, a multitude of technologies exist that depending on e.g. particle size, density difference between liquid and solid, and desired concentration factor can be applied more or less successfully.

Particles with a diameter below 10 *nm* have a relatively large (Brownian) diffusion coefficient, and they are typically removed by adsorption (or depth filtration) or ultrafiltration. Particles with a diameter above 10  $\mu\text{m}$  are mostly removed by settling/creaming or by centrifugation, since their total mass is sufficient to induce significant buoyancy or settling force (given appreciable density difference). Particles between 10 *nm* and 10  $\mu\text{m}$  tend to be difficult to separate; they are too small to be separated by settling or centrifugation, yet they are too large to have significant Brownian diffusivity that is needed for adsorption, or to diffuse away from a membrane. This inherently causes a challenge, since this size range is relevant for amongst others food, pharma, chemical and waste water applications. In this paper, we specifically address techniques that target separation and fractionation of particles in the 1 to 10  $\mu\text{m}$  size range.

A mainstream technique to treat such suspensions is microfiltration. Although this technique is well developed and successfully applied at large scale, it also suffers from several drawbacks such as particle deposition, concentration polarisation, and fouling that all reduce the productivity of the system. Besides, the selectivity of fractionation processes is greatly influenced by these effects [3]. One of the strategies to increase microfiltration performance is by increasing the local shear rates near the membrane surface to reduce concentration polarization. This is usually achieved by a higher cross-flow velocity; furthermore, vibrations or the use of spacers and turbulence promoters to introduce secondary flows have been

proposed. Although various effects have been claimed, the more complex designs have some disadvantages, e.g. cleanability is influenced negatively. The interested reader is referred to a recent review that covers various aspects of dynamic flow conditions by Jaffrin and co-workers (2012).

Several microfluidic suspension separation techniques that use geometric and fluid constraints to enable ‘control’ of particle movement have been presented and compared in a review [9]. These techniques mostly make use of inertia effects that increase strongly with particle size. For example, the inertial lift in Poiseuille flow in a slit-shaped channel scales ( $Re > 1$ ) with the particle size as  $F_L \propto a^4$  for  $Re_p < 1$  and  $F_L \propto a^3$  for  $Re_p > 1$ , and the inertial force due to the proximity of a wall scales as  $F_{LW} \propto a^6$ , while a drag force due to a slip velocity would scale as  $F_D \propto a^2$ . This illustrates that, for particles, the inertial forces quickly become dominant, and are better suited to distinguish between particle sizes than drag forces. Despite the fact that microfluidic separations were found very effective, they are not applied at larger industrial scale, since these techniques cannot simply be up- or out scaled. In the current paper, we review new developments in solid-liquid separation based on microfiltration with secondary flow effects and inertia-based microfluidics. Specifically, we address the role of inertial forces in suspension separation, and identify and discuss upscaling challenges and opportunities for three novel technologies; fluid skimming, spiral inertial microchannel and sparse obstacle arrays.

## 2.3. Particle separation with microfiltration

The mainstream separation technique to treat suspensions is microfiltration, in which a porous membrane is used to separate suspended particles with a typical size between 0.1 and 10  $\mu\text{m}$  from the liquid. Microfiltration is often carried out in cross-flow-filtration mode, which improves back-transfer of retained particles near the membrane surface towards the bulk of the feed suspension, through a fluidization effect called shear induced or hydrodynamic diffusion.

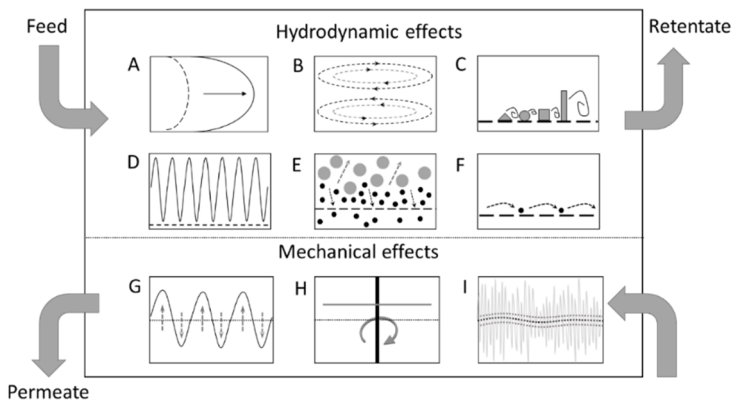


*Figure 2.1:* Overview of approaches to reduce concentration polarisation in cross-flow microfiltration. A) velocity or shear-gradient induced lift, B) Dean vortices, C) turbulence promoters, D) pulsating cross-flow, E) shear-induced diffusion, F) fluid skimming, G) back-washing or back-pulsing, H) rotating membranes or disk module and I) vibrating membranes or modules.

Although cross-flow microfiltration improves performance and is successfully used on industrial scale, it does not prevent accumulation of particles at or near the membrane surface. Therefore, many measures have been explored to further reduce concentration polarization and/or particle accumulation. In general, local fluid disturbances that reduce the concentration polarization layer are used. This can be done by redesign of the membrane modules or by introducing an external mechanical action, e.g. vibrating membranes or back-pulsating fluid as is discussed below (*Figure 2.1*).

In conventional microfiltration with spiral wound modules, spacers and high cross-flow velocity are applied therewith enhancing mixing and thus minimizing concentration polarization (*Figure 2.1AB*). Additionally, increased cross-flow velocity increases shear rate, which promotes back transport of particles from the concentration polarization layer into the bulk [11-17]. Depending on the operating parameters of the system, and the size and concentration of the particles, different hydrodynamic effects dominate the mobility of the particles (e.g. inertial lift forces, dean vortices or hydrodynamic diffusion).

The downside of a higher cross-flow velocity is an increased energy demand for the pumps to circulate the suspension, and these effects have to be weighed to achieve the most economical process setting. Another approach is to insert spacers or turbulence promoters to enhance the local shear rate near the membrane surface (*Figure 2.1C*). The drawback of such inserts is that they can be difficult to clean [15, 16]. In addition, flow instabilities can be induced by a pulsating cross-flow; the pulses create velocity and pressure gradients that may promote particles to move back into the feed (*Figure 2.1D*). This method does not need high cross-flow velocities but is difficult to use in larger systems since the velocity gradients dissipate rapidly [3, 16, 18]. Besides by means of the liquid, the membrane can be used to induce velocity gradients. Vibrating modules, rotating disk modules and rotating cylindrical membranes (*Figure 2.1HI*) are examples of dynamic systems that use moving elements to induce shear near the membrane [3, 11]. However, these moving parts lead to additional energy usage, and are more difficult to clean, which limits their application.

In most membranes, the pores are not uniform in size, but small uniform pores can be made by photolithographic etching (microsieves) [6], electroforming [19], embossing [20] and 3D printing [21]. The fluxes of these devices are typically 10-100 times higher than those of conventional membranes [6], and this also implies that the process conditions need to be controlled very carefully to prevent accumulation of particles.



In general, complete blockage occurs when particles are in the same size range as the pores. In order to prevent this, microfluidic systems have been introduced e.g. by [8, 9], as discussed in the next section.

In addition, van Dinter and co-workers successfully used large uniform pores at particle concentrations of up to 45% [22]. In their research metal sieves were used with uniform pores that were considerably larger than the particles to be separated. By control of the process parameters, particle migration is facilitated by a closed section that is used prior to the filtration area, which allowed strict control over the particle size in the permeate (*Figure 2.3A*). Through hydrodynamic interactions, larger particles migrate faster away from the membrane surface, which allows smaller particles to pass freely (*Figure 2.1E*) [23–25]. Besides shear-induced diffusion, fluid skimming can also be applied in the same system, but now for low particle concentrations  $< 5\%$  (*Figure 2.1F*) [12]. In this case, the cross-flow drags particles parallel to the membrane, while the permeate flow drags them into the pore; if these forces are balanced correctly, particles skim across the pores [14].

## 2.4. Suspension separation in microfluidic devices

Microfluidic devices are known for their precisely defined geometry, which allows accurate sorting and separation of particles from suspensions. Among the growing number of microfluidic systems there are several passive techniques that continuously sort and separate particles based on fluid inertia effects. Two main methods for lateral migration are used, namely inertial lift and Dean-like drag; in the next section we review and compare different methods.

### **Forces relevant to particle separation in microfluidic devices**

Inertial lift forces are generally dominated by; 1) a lift force that is induced by a gradient in shear rate, which drags particles away from the channel centre due to the parabolic shape of the velocity profile and 2) wall-induced lift forces which direct particles away from the wall

[26-30]. Depending on the magnitude of both forces, particles will migrate toward a stationary position, of which the location varies with the flow velocity, and the particle properties (e.g. size, density, shape and deformability).

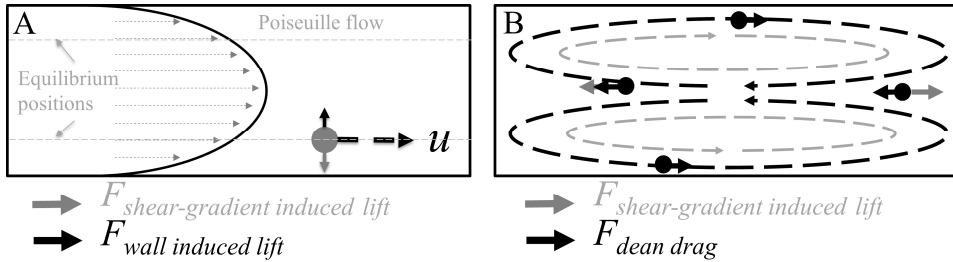








Figure 2.2: (A) side view of a channel with shear-gradient induced and wall induced lift forces with the particle residing at its equilibrium position and (B) cross-sectional view of a channel with dean vortices (motivated from [26, 31]).

Particle migration may also be influenced by the drag force of a secondary flow, which is a re-circulating flow perpendicular to the main flow direction. When the drag force of this secondary flow is combined with inertial lift forces, particle focusing can be accelerated and the equilibrium position influenced. In order to focus particles, it is crucial to match secondary flow effects with inertia through the flow velocity, the lay-out (size, shape, curvature, sequence and position of inserts) and the cross-section of the channel [32-35], as explained in the next section.

## 2.5. An overview of inertial separation techniques

The most investigated inertia-based microfluidic systems are shown in *Table 2.1*. The separation mechanism is based on at least one of the hydrodynamic forces mentioned earlier, where the deterministic lateral displacement device also makes use of geometric constraints for separation.

*Table 2.1:* Overview of inertia-based microfluidic devices suitable for suspension separation and the main forces they utilize to focus particles in equilibrium positions.

System	Hydrodynamic forces	Schematic design
Straight channel	Inertial lift forces	
Curved or spiralling channel	Inertial lift combined with secondary-flow drag force	
Serpentine channel (symmetric and asymmetric)	Inertial lift combined with secondary-flow drag force	
Multi-orifice or expansion-contraction channel	Inertial lift combined with secondary-flow drag force	
Structure-filled channels (Obstacles and herringbone)	Inertial lift combined with secondary-flow drag force	
Deterministic lateral displacement array	Inertial lift combined with secondary-flow drag force	

Straight channels are, perhaps, the ‘simplest’ designs for focusing and ordering particles based on fluid inertia. Segre and Silberberg were the first to observe lateral particle migration towards an equilibrium position in 1961, but it was not until 2007 when Di Carlo et al. used straight channels to focus, sort and separate particles [36]. This sparked the interest of many, and several straight channels with different cross-sections have been studied, each with multiple equilibrium positions from which particles can be collected [37-39].

Curved or spiralling channels are quite similar to the straight channel except for the induced secondary flow also known as ‘Dean flow’ [40, 41] that is caused by the channel curvature.

The counter-rotating vortices drag particles across streamlines and, together with inertial lift forces, cause more rapid focusing of particles towards an equilibrium position, which increases separation accuracy and decreases channel length [28, 35, 42]. As mentioned previously, these systems need to be designed carefully around the right balance between the inertial lift forces and Dean drag [26, 28]. And this is even more true for serpentine channels that have meandering curves [36] that induce alternately counter rotating vortices that focus particles faster than straight channels. Symmetric curved channels have two equilibrium positions, while asymmetric curved channels focus particles in a single equilibrium position which is favourable for particle separation [36].

Multi-orifice or expansion-contraction channels have also been suggested, as systems to separate particles [43-46]. In such systems, particles are either focussed toward their equilibrium positions using inertial lift forces and Dean-like vortices, or are trapped in vortices, or both. Trapping particles has the disadvantage that it requires an interruption of the process to remove the particles [43, 47, 48]; however, this can be circumvented by switching between continuously focussing or discontinuously trapping and siphoning off particles from outlets on the sides [49].

Besides the structure of the channel that was just discussed, inserts like micro-pillars or herringbones inspired structures can also be used to influence particle behaviour. In this case, a combination of alternating dean-like vortices and inertial lift forces lead to particle separation [32, 33, 50-52]. The use of inserts leads to more freedom in the design of the system; the shape and strength of the secondary flow can be tuned by varying the obstacle shape, size or positions [28, 32, 53]. A specific example is the deterministic lateral displacement array [54-57], in which arrays of obstacles are used, with each obstacle row slightly shifted compared to the previous row. It was found that for this system inertial hydrodynamic effects assist particle separation [55, 56].

## 2.6. Comparison of microfluidic separation techniques for large scale separation

The microfluidic suspension separation systems described in the previous section are applied on dilute small-scale suspensions (up to ml/min), usually for analytical or diagnostic purposes, with emphasis on recovery, selectivity, purity and resolution. For large scale, preparative applications, other aspects come into play such as sensitivity to disturbances and/or foulants, cleanability, energy efficiency and the ease of integration with peripheral equipment.

The low single unit throughput is a major hurdle for large scale application of the novel microfluidic separation techniques. The throughput may be increased either by upscaling or outscaling. Outscaling, or scaling by parallelization requires numerous devices to be connected either individually or to a larger feed channel. Scaling up implies increasing the dimensions of the device itself, which is economically interesting since the throughput increases with system dimensions – in laminar flow, for instance, the throughput depends on the diameter of a channel to the fourth power.

Devices with many curves, orifices or other structures in the channel are more difficult to manufacture, more susceptible to particle accumulation, and more difficult to clean. In addition, these complex structures often generate larger pressure drops compared to straight channels of similar length. The length of a channel is important as each system requires a minimal length to focus particles, and the cross-sectional diameter and channel shape play a critical role and co-determine the effectiveness of particle separation. For example, a trapezoidal cross-section was found to increase the focusing distance between different sized particles, therewith rendering easier particle collection [37]. Finally, the empirically established Confinement Ratio ( $CR = a_p/L_c$ ), where  $a_p$  is the particle diameter and  $L_c$  the characteristic length of the channel cross-section, needs to be  $\geq 0.07$  for the shear-gradient lift force to focus particles over a given channel length [36, 58, 59].

From the systems described in *Table 2.1*, three of the (in our opinion) most promising systems are selected for their scalability and other mentioned considerations. Subsequently, these systems are compared to microfiltration on important aspects for large scale use (*Table 2.2*). At this stage a qualitative comparison was preferred as lack of sufficient design data made it impossible to make a fair quantitative comparison.

*Table 2.2:* Comparison of: single unit throughput, energy efficiency, scalability and robustness (sensitivity against external fluctuations and fouling) for microfiltration, fluid skimming, sparse obstacle array and the inertial spiral microchannel.

	<b>Single unit throughput</b>	<b>Energy efficiency</b>	<b>Scalability</b>	<b>Robustness</b>
Microfiltration	++	-	++	+ *
Fluid skimming	+	+	+	+
Sparse obstacle array	+	+	+	+/-
Inertial spiral microchannel	+	++	-	+/-

*\* Only for systems with measures taken against external fluctuations/fouling*

The three selected techniques in *Table 2.2* are capable of continuously separating particles with reasonable throughput and have low risk of particle accumulation compared to conventional microfiltration, although the concentration of the suspensions investigated in these systems are still relatively low (<5v/v%).

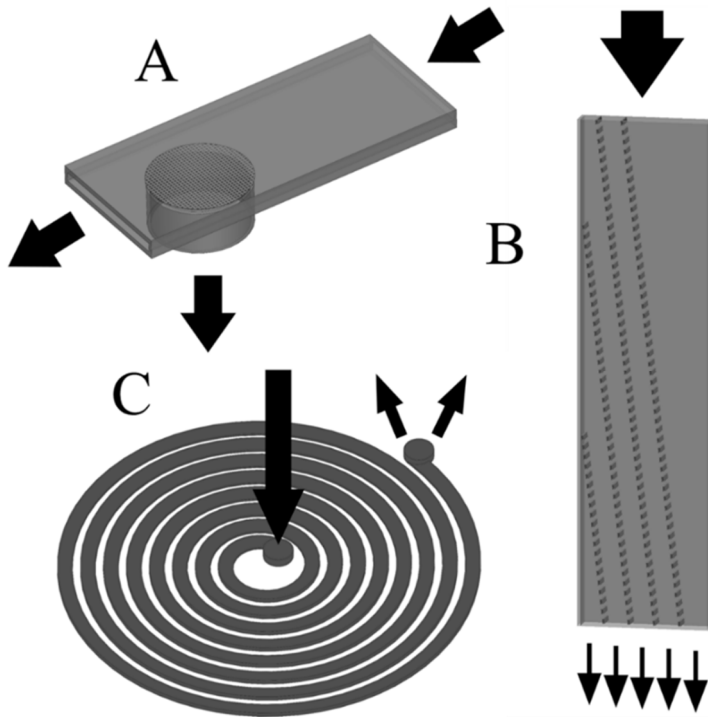


Figure 2.3: (A) a fluid skimming module with a closed channel prior to the membrane [12], (B) a sparse obstacle array [60] and (C) a spiral inertial microchannel [37].

1) Fluid skimming takes place when the cross-flow velocity and the transmembrane flux are matched in such a way that particles skim across the much larger pores of the membrane. The system module has a slightly different design as in microfiltration, with a closed section preceding the porous region (*Figure 2.3A*). This strategy facilitates particle migration without chaotically reintroducing particles in the feed stream as is customarily done in microfiltration. A fluid skimming system can be operated at a constant permeation flux that is similar to an approach often used in microfiltration, without severe fouling problems and with a lower energy consumption as the pores are considerably larger than the particles [12]. Since microfiltration is an accepted technique and broadly applied, the knowledge to implement

fluid skimming on a large scale is in principle available. 2) Sparse lateral displacement technology (*Figure 2.1B*); [60], has been used to concentrate and fractionate particles. The system uses structures inclined to the flow direction to displace particles of a critical size. Particles below the critical size will follow the flow direction. Particles above the critical size will be displaced. If fractionation is intended, the next line of structures might have a different critical size. The particles can be collected at the corresponding outlet. Geometry and number of structure lines can be adjusted according to requirements. The energy demand will be relatively low considering that the pores are larger than the particles to be separated, despite the large number of structures. The main challenge for upscaling is to precisely manufacture tall and narrow obstacles which do not break or bend. In order to achieve this, it was suggested to use a sieve type of obstacles that can be scaled up easily [10].

3) The spiral inertial microchannel (*Figure 2.3C*) has very high flux and recovery, and seems to even perform better than one would expect based on the CR. Even though there is basic understanding, the underlying aspects needed for process design are not completely understood. In spite of this, numerous papers are reporting on increased throughput of a single device [37, 61, 62]. Since the cross-section of the spiral inertial microchannel is relatively large and without structures, the energy consumption is regarded as low. Nevertheless, the current throughput is still insufficient for industrial use and needs further improvement.

The three described systems hold potential for industrial application; however, they are not investigated to the same extent. Although fluid skimming is new, the concept of microfiltration is well developed and can be easily scaled up. Deterministic lateral displacement technology and inertial microfluidics are relatively novel techniques and their upscaling has only been investigated to a limited degree. Therefore, we propose conceptual designs to apply these techniques at large scale (*Figure 2.4*). For sparse obstacle arrays, conventional upscaling is possible, whereas spiral inertial channels can be scaled out as this system is (still) limited by the CR.



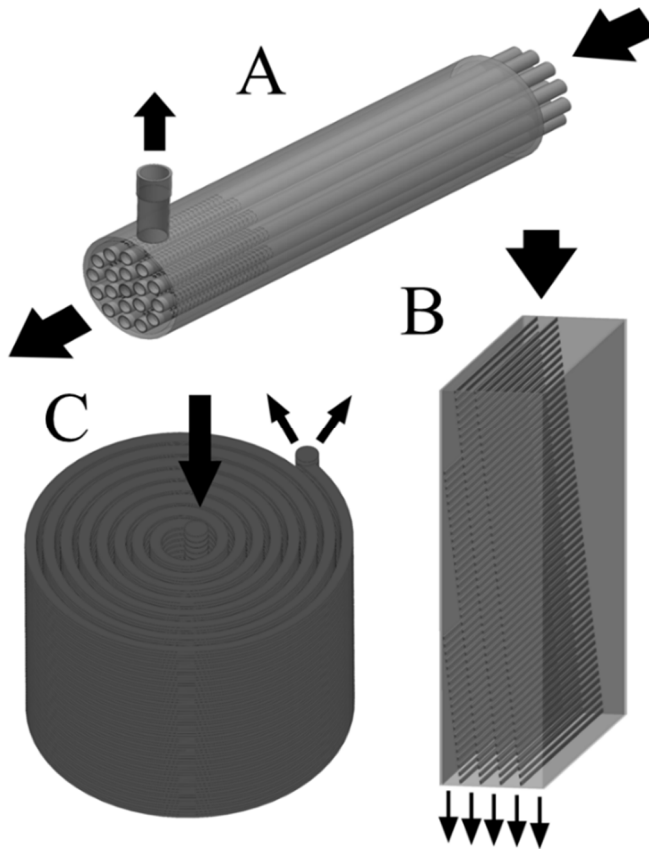


*Figure 2.4:* Concept designs of systems that could be used for larger scales. (A) Tubular/hollow fibre fluid skimming membrane module with closed channels prior to the porous area, (B) up-scaled sparse obstacle array and (C) out-scaled spiral inertial microchannels [63].

## 2.7. Influence of feed suspension characteristics on separation performance

Even though three systems are considered promising for large scale separation of suspensions, their performance can be heavily influenced by feed suspension properties. Hitherto, fluid skimming was mostly investigated for separation of yeast cells [12], and very recently for milk

fat globules. Sparse obstacle arrays were applied to separate polystyrene beads [60] while regular deterministic lateral displacement devices were also investigated for separation of blood cells [64], tumorous cells [65], bacteria [66] and parasites [67]. The spiral inertial microchannel was used for separation of polystyrene particles [35, 59, 61], yeast [63] and blood cells [68]. These evaluations in literature indicate several critical feed suspension properties for successful application such as rheological properties, deformability and shape of the particles, and particle size distribution.

Rheological properties have large influence on separation via their effect on inertial forces or the required high velocity gradients for separation. High viscous and shear-thickening fluids negatively affect maximum throughput and can render separation ineffective; on the contrary, low viscous and shear-thinning fluids can lead to higher throughput and thus enhance suspension separation [28, 69]. Conventional microfiltration is less sensitive to viscosity effects in regard to separation behaviour, but the throughput is inversely proportional to the viscosity, leading to reduced performance and/or higher energy requirements [11].

Deformable particles and/or particles with various shapes can affect separation behaviour [66, 70-72]. Depending on the system, separation of symmetric particles will rely on the maximum rotational diameter. In case of a sparse obstacle array it depends on the smallest diameter. Deformability of the particles can lead to additional lift forces or can influence the physical interactions needed for separation [28, 71, 72]. In specific cases, shape and/or deformability are used to induce separation [70, 72, 73].

Suspensions with a large particle size distribution are likely to have a cut-off diameter below which particles are no longer separated. Higher recovery of the smaller particles requires smaller cross-sections or multiple systems in series, at the expense of energy cost [63]. In such situations the sparse obstacle array can fractionate particles of different size in a single system [60, 74].

## 2.8. Conclusions

Various methods to enhance microfiltration revolve around redistributing particles that have accumulated near the membrane surface. Unlike membrane filtration, in microfluidic applications, geometric constraints and inertia are used to direct particles to positions from which they can be harvested easily. Both methods differ greatly in the scale at which they have been applied; as microfluidic techniques are still in their early stages of development, microfiltration is the current method of choice.

Three microfluidic techniques were identified as promising for out- or upscaling. Spiral inertial microchannels have been successfully mass parallelized but are restricted in confinement ratio that can be used, which limits upscaling. Sparse obstacle arrays allow high flux at relatively low pressure drop, but still need to be developed for particles in the 1-10 micrometre range. Fluid skimming exploits well-defined sieves in combination with control over the feed and permeate flows. This last technique employs a specific microfiltration configuration and is thus expected to be easier scalable, although this requires further confirmation. Finally, despite the potential of all discussed systems for large scale separation their effectiveness will also depend on feed suspension properties. This needs to be topic of further research before successful industrial application.



# Three

## **Sieve-based lateral displacement technology for suspension separation**

During the writing of this chapter I listened a lot to *Lane Boy* from *Twenty one pilots*

This chapter has been published as:

J.P. Dijkshoorn, R.M. Wagterveld, R.M. Boom, M.A.I. Schutyser: Sieve-based lateral displacement technology for suspension separation, *Separation and purification technology* 175 (2017), 384-390.

### 3.1. Abstract

Sparse lateral displacement arrays are easier to scale up than full deterministic lateral displacement arrays or deterministic ratchets, because they require lower pressure drop and simplify the construction of the device. However, the asymmetry of sparse arrays leads to a non-homogeneous pressure distribution with as a consequence an uneven flow field and limited separation performance. Furthermore, the construction of high throughput sparse obstacle arrays that allow separation of small particles is challenging. Therefore, in this study we investigated the use of sieves to replace obstacles in sparse systems. Moreover, we investigated a strategy to optimize the separation performance by adjusting the internal pressure distribution. Our experiments showed in first instance that the introduction of sieves negatively affects separation performance, which was explained by the lower porosity of the sieves. However, via fluid flow calculations and high-speed camera analyses we found that pressure distribution can be optimized by adapting the flow rates of the different outlets preventing high pressure drop across the obstacles arrays near the bottom of the device. Experimental separation data for adjusted outlet flow conditions indeed showed better particle displacement, especially in the bottom region, and as a result improved separation behavior. These findings demonstrate the potential of the scalable sieve-based lateral displacement device to effectively separate particles.

## 3.2. Introduction

A deterministic lateral displacement device or deterministic ratchet is a microfluidic device to separate or fractionate particles from suspensions [54]. The separation principle involves arrays of obstacles to displace and separate particles based on their size. Fluid flows through the openings between individual obstacles, which are arranged in rows that are tilted relative to the overall average flow direction of the fluid.

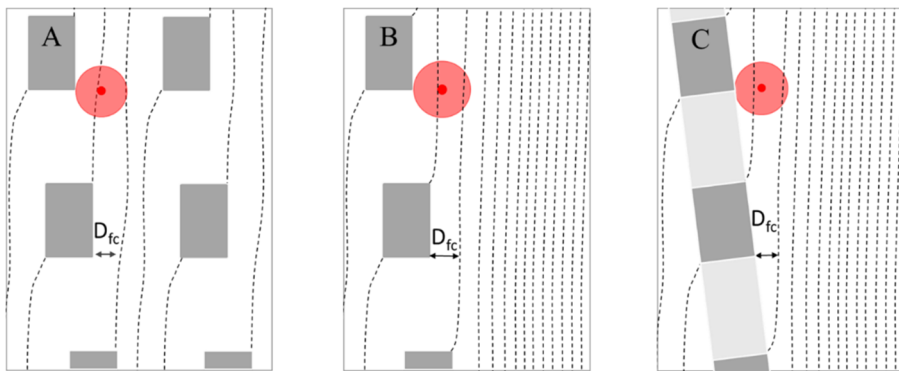


*Figure 3.1:* Schematic diagram of the deterministic lateral displacement separation principle with in (A) the initial obstacle array, in (B) the sparse lateral displacement array and in (C) the sieve-based deterministic lateral displacement device. The fluid through the system can be divided into flow lanes indicated by the dotted lines. Particles with a diameter  $\geq 2D_{fc}$  are displaced by each obstacle into the adjacent flow lane. Forcing larger particles to follow the direction of the obstacles instead of the flow direction. When particles  $< 2D_{fc}$ , they are not displaced laterally, stay in their flow lanes and follow the flow direction.

In a laminar flow field, the fluid that will flow through a particular opening is bounded by two flow lines, which comprise the so-called flow lane (dotted lines in *Figure 3.1*). If particles, that are suspended in the fluid, have a diameter that is larger than two times the typical width of the flow lane, ( $D_{fc}$ ), lateral displacement occurs after steric interaction of the particle with an obstacle (*Figure 3.1A*). When the particle is smaller it stays within its flow lane (dotted lines) and follows the fluid [75]. Thus, larger particles are shifted unidirectionally from their flow

lanes, which after many such events results in macroscopic separation. All particles that are smaller than the flow lane width will follow the fluid and therefore will less likely cause obstruction and fouling of the structure, compared to membrane filtration, in which all particles accumulate before a single sieve. This is one of the reasons why the deterministic lateral displacement separation principle has been considered promising to separate suspensions at a larger scale [9, 76, 77].

It is often suggested to scale up microfluidic systems through outscaling or massive parallelization [63, 65, 74], but this requires a large number of connected devices, requiring large investment in the peripheral structure, which would also compromise its robustness in operation. It would be economically more interesting to follow the classical laws of scale-up and increase the dimensions of the device [76]. However, increasing the dimensions of deterministic lateral displacement devices is challenging from a construction perspective. Especially the construction of tall obstacles with enough mechanical strength is difficult and expensive, and therefore the throughput is limited by the cross-section of the channel [74]. A possible solution to increase the throughput of the deterministic lateral displacement technology is to use sieves to replace obstacles (sieve frame) and gaps (pores) as shown in *Figure 3.1C*. In contrast to the construction of individual obstacles, there are multiple available manufacturing techniques to create sieves with small and uniform pores (e.g. photolithographic etching [6], electroforming [19], embossing [20] and 3D printing [21]). Another challenge, besides increasing the single unit throughput, is to apply deterministic lateral displacement system to process of industrial relevant suspensions. Such suspensions usually consist of deformable and/or irregular-shaped particles which may increase the risk of clogging, even though different properties may be used to enhance separation in deterministic lateral displacement devices [70].



Recently, Lubbersen et al. introduced the sparse lateral displacement concept with a reduced number of obstacles (*Figure 3.1B*). This geometry works, because for dilute suspensions, the separation principle requires only a single obstacle array to displace particles [60]. Fewer obstacles further reduces the risk of particle accumulation, which decreases the pressure drop and lowers the construction costs [60]. However, the asymmetric design of sparse lateral displacement device creates an inhomogeneous pressure distribution, which negatively affects the separation [60, 78]. Nevertheless, a large scale sparse lateral displacement design that employs sieves to separate particles is anticipated to be less challenging to produce and to use, compared to mass-parallelized conventional deterministic lateral displacement devices.

In this work, we investigate the use of sieves to separate particle suspensions in a sparse lateral displacement geometry. Using sieves instead of obstacles will create the possibility to increase the single unit throughput of a deterministic lateral displacement system and thus better facilitates larger scale operation. Here, the effect of sieves on suspension separation and on the fluid flow are described for the sparse lateral displacement design. Subsequently, the changes on fluid flow caused by the asymmetric design are examined and optimized to improve suspension separation.

### 3.3. Materials and methods

#### **Device**

Experiments were carried out using a flow device (*Figure 3.2A*) as previously described by Lubbersen and co-workers; the flow enters at the top and leaves at the bottom at five different outlets [55, 56, 79].

In this device the array designs are placed (top view in *Figure 3.2B*). Three sparse lateral displacement arrays with different obstacle designs were used, the original (*Figure 3.2C*) was milled from PEEK. The other two designs consisted of a base plate, which is milled from

PEEK and sieve structures which are 3D printed with nylon (*Figure 3.2DE*). The design of the sparse lateral displacement devices (*Figure 3.2B*) remained the same and only the obstacles were changed (*Figure 3.2CDE*). The obstacle and gap parameters can be found in *Table 3.1*. Note that the size of the gaps in the flow direction (gap length) remained unchanged.

## Materials

For concentration experiments, 1 v/v% suspensions of neutrally buoyant particles were prepared using polystyrene particles with a density of  $1.05 \text{ g/cm}^3$  (Maxiblast, USA), 79.5% water, 20% glycerol (VWR BDH Prolabo, France) and 0.5% surfactant (SDS, obtained from VWR BDH Prolabo). The particle size distribution was measured with a Mastersizer 2000 (Malvern, UK) and a D50 of  $785 \mu\text{m}$  was obtained with D10 of  $568 \mu\text{m}$  and a D90 of  $1103 \mu\text{m}$ . For high speed camera imaging a suspension of demi water, Tween-80 (Merck, Germany) and polyethylene particles of  $425\text{-}500 \mu\text{m}$  (Cospheric, USA) with a density  $0.98\text{-}1.00 \text{ g/ml}$  were used.

*Table 3.1:* Design parameters of the obstacles and gaps for the 3 designs.

Design	Angle °	Obstacle width [mm]	Obstacle height [mm]	Obstacle length [mm]	Gap height [mm]	Gap length [mm]	Porosity %
1	5.9	0.8	2.5	1.8	2.5	1.6	~50
2	5.9	0.8	5	1.8	4	1.6	~40
3	5.9	0.8	5	1.8	1.5 (2x)	1.6	~30

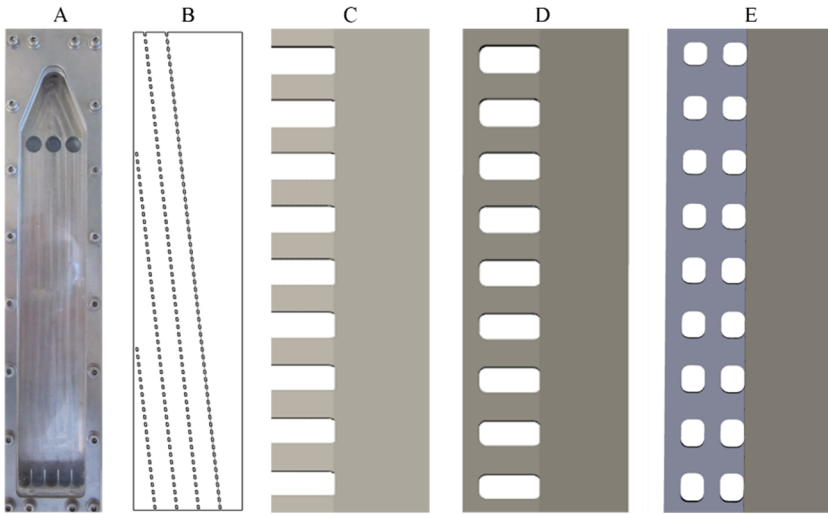


Figure 3.2: (A) The module that holds the sparse lateral displacement designs, (B) top view of a sparse obstacle array (adapted from [60]), (C) side view of a sparse obstacle array (*Table 3.1*: design 1), (D) side view of a sparse lateral displacement system employing sieves with a single pore band (*Table 3.1*: design 2), (E) side view of a sparse lateral displacement system employing sieves with a double pore band (*Table 3.1*: design 3).

## Experiments

The sieve-based lateral displacement designs were positioned in the module (*Figure 3.2A*) and employed by pumping the suspension vertically from the top down to the 5 outlets where the particles can be collected [55]. The inlet flow rate was adjusted in order to obtain a fixed fluid velocity of 0.06 m/s in the channel cross-section before the sieves. The volume concentration at the inlet is calculated using the outlet volume concentrations and respective flow rates of the 5 outlets, which varied slightly per experiment. For ease of comparison between different experiments, the outlet concentrations are normalized using the inlet concentration. Initial experiments were performed with the outflow equally divided over the outlets. At a later stage, experiments were conducted with optimized outflow conditions. For these experiments the volumetric flow rate per outlet was adjusted according the results obtained from the numerical simulations (*Table 3.2*). Experiments with different outflows were only performed with design

3, since it shows most resemblance with sieves. The concentration, in case of ideal separation (when all particles are above the critical particle diameter and therefore are displaced) is calculated by assuming a homogeneous distributed suspension at the top of the system.

*Table 3.2:* Outlet conditions (volume percentages) for the equal outflow and optimized outflow found using numerical simulations.

Design 3	Outlet 1	Outlet 2	Outlet 3	Outlet 4	Outlet 5
<b>Equal outflow conditions</b>	20%	20%	20%	20%	20%
<b>Optimized outflow conditions</b>	16%	16%	16%	16%	36%

### Flow visualization

Tracer particles were recorded in design 3 using a high speed camera (Fastcam SA 1.1, Photron, USA) for several inlet velocities. Recorded images are stacked using ImageJ (Z-project) to create a single image that shows the path lines (trajectories of particles) over time. Time between two particles is 7 milliseconds.

A 3D drawing of Design 3 is created in COMSOL Multiphysics 5.0 and the system is simulated assuming stationary laminar flow using a FEM approach [80]. The fluid is assumed to be incompressible and the basic properties of water at 293.15 K are used. For all boundaries, other than the inlet and outlet, no-slip conditions are used. Normal inlet velocity was swept from 0.01 to 0.2 m/s and outlet 1-4 are fixed to the desired outflow volume fractions, outlet 5 is pressure based. Using stream lines, which are lines tangent to the instantaneous velocity vector, the fluid flow is visualized in the system. The model was mesh independent.

## 3.4. Results and discussion

First, the effect of replacing conventional obstacles with sieve-structures in an open, asymmetric sparse obstacle design on particle concentration is presented and discussed. Then, the fluid flow in the device is analyzed by high speed camera imaging using particle trajectories and compared to numerical simulations. These simulations are used to visualize stream lines and the transmembrane pressure difference. Finally, the separation performance is evaluated for adjusted outflow conditions.

### **Separation performance for different sparse deterministic designs**

*Figure 3.3* gives the outlet concentrations for three different designs which can be compared with the maximum achievable concentration. The experimentally obtained particle concentrations for all designs are relatively equally distributed over all outlets, indicating poor separation. The distribution that could be achieved is sketched as number 4 in *Figure 3.3*. Design 1 performed best and obtained the highest concentration in outlet 4, but not in the targeted outlet (outlet 5). The other two designs performed substantially less compared to design 1, and relatively similar to each other. We explain this by the fact that designs 2 and 3 have a lower porosity (higher resistance against flow), which leads to a change in the pressure distribution in the device and thus to the observed reduced separation performance. An interesting notion is that the differences between design 2 and 3 is small while there is quite some difference in design and porosity.

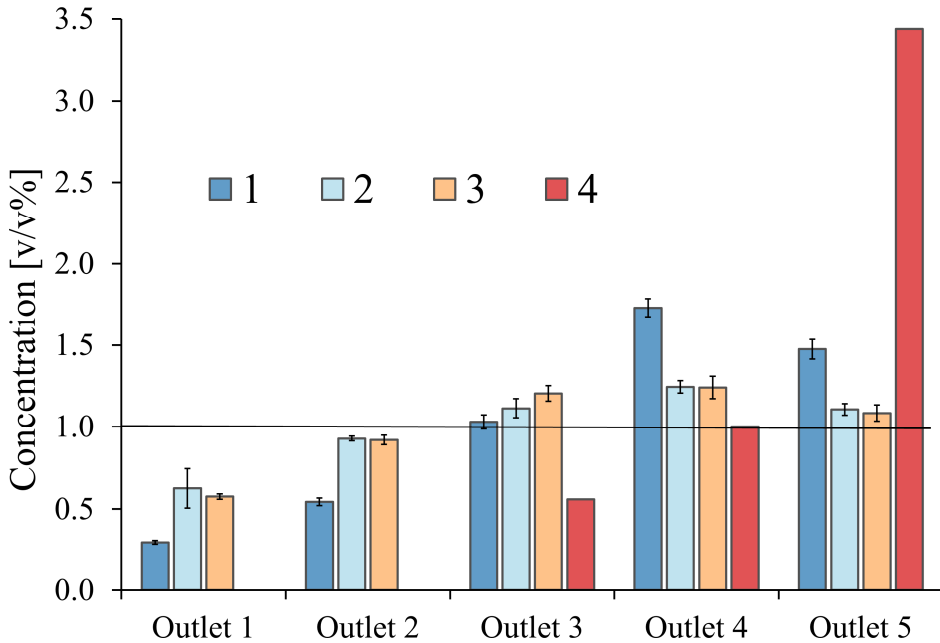


Figure 3.3: Particle concentration per outlet for the 3 designs under equal outflow conditions and ideal separation (1, 2 and 3 correspond to the designs in *Tabel 3.1* respectively, ideal separation is 4). The average inflow velocity is 0.06 m/s and the particles D50 is 2.3 times smaller than the pores. The black line indicates the inlet concentration. Error bars show standard deviation.

### Visualizing flow and pressure distribution for improved particle separation

For improved understanding of the effects of different obstacle-structures on particle separation, particle trajectories and stream lines were visualized for design 3. *Figure 3.4A* shows the trajectories of tracer particles, which give an impression of the flow direction and velocity. The tracer particles traverse with a curve towards the sieve, especially near the outlets. Furthermore, some trajectories pass two sieves within a short time frame, indicating lateral flow of the fluid. In *Figure 3.4B*, stream lines are shown that were obtained by numerical simulation. Similar flow behavior and velocity can be observed as compared to the high speed camera imaging data of the tracer particles in *Figure 3.4*.

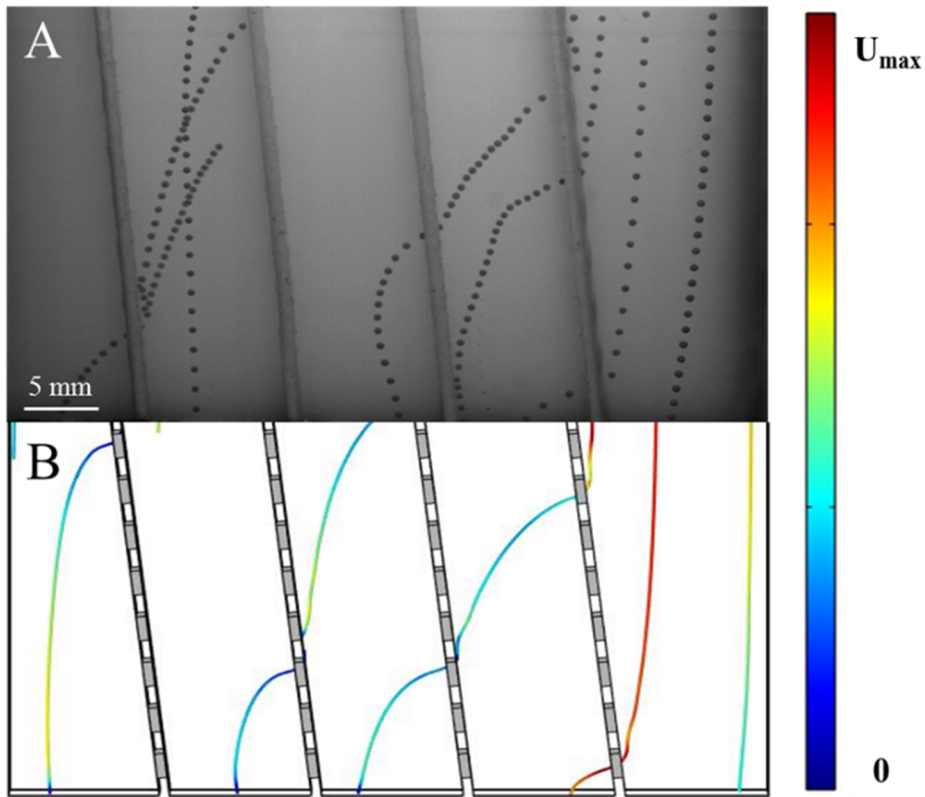


Figure 3.4: (A) Path lines of tracer particles ( $\sim 0.21$  m/s) in the experimental setup (interval between two dots of the same path line is 7 milliseconds) and (B) 3D CFD simulated stream lines where the velocity is indicated by the colour legend ( $U_{\max} = 0.28$  m/s). Results shown are near the outlets at the bottom of the system.

A result of the lateral flow is a larger angle between the flow lanes and the sieves. As a consequence, the critical particle diameter for displacement is strongly increased and particle separation is adversely affected. This explains the observations of Lubbersen et al. and the results found in Figure 3.3, where the particle concentrations in the outlets other than outlet 5, especially outlet 4, are higher than expected [60].

The poor particle separation in the sparse obstacle array is explained by thus the influence of the lateral flow through the openings as it drags particles along through the obstacle lines [60].

Zeming et al. [78] also discussed the influence of the lateral flow resistance between neighboring obstacle rows on the critical particle diameter. In their system, anisotropic resistance is caused by the different dimensions of the gaps in lateral and downstream direction. However, by both previous studies the magnitude and the impact of this effect were not investigated any further.

While for regular deterministic lateral displacement systems the pressure distribution is homogeneous, it is not in a sparse obstacle arrays due to its asymmetric design. Therefore, the pressure difference along the far right sieve (red line) from top (0) to bottom (1) was simulated (Figure 3.5). The pressure difference on the right (upstream) and left (downstream) side of the sieves slowly increases especially near the bottom of the sieve. The increased pressure difference creates an extra driving force for the fluid to flow through the sieve, causing strong lateral flow and strongly increases the size of the flow lanes.

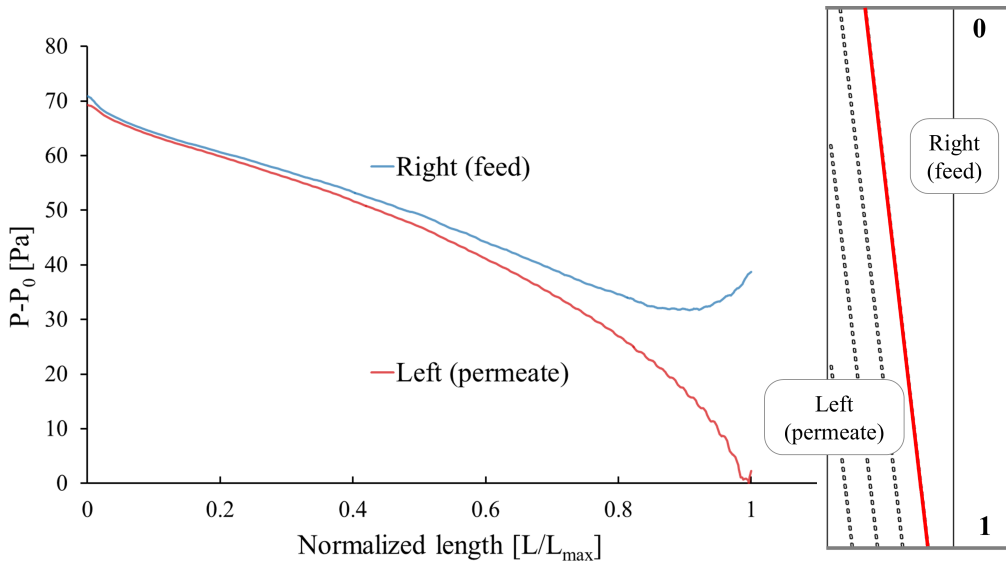
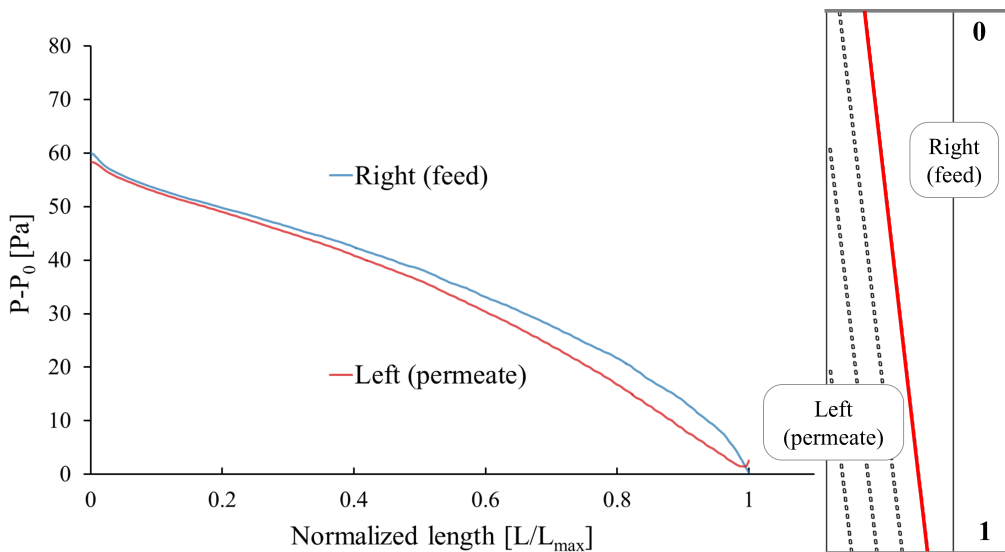


Figure 3.5: Simulated pressure difference along the normalized length of sieve (redline) on both the right (feed) side (black) and on the permeate (left) side (gray). From 0.8 the pressure difference over the sieve rapidly segregates; changing the flow and causing part the fluid to flow through the sieve.



Minimizing the pressure difference along the length of the sieve would improve the separation performance. To achieve this while keeping the geometry intact, the flow conditions of the outlets were changed (*Table 3.1*). 3D simulations were carried out to identify which outflow conditions would minimize the pressure difference across the sieve. The flow rate of outlet 5 was increased up to 36% by throttling of the channels, while the flow rates of all other 4 outlets were decreased to 16%. This adjusted flow distribution resulted in the pressure distribution over the sieve on the right hand side as shown in *Figure 3.6*.



*Figure 3.6:* Simulated pressure along the normalized length of sieve (redline) on both the right (feed) side (black) and on the permeate (left) side (gray). The pressure difference on both sides is kept to a minimum.

The pressure difference across the sieve slightly increases along the length of the sieve, but even near the outlets (approaching a normalized length of 1). By minimizing the pressure difference across the (right) sieve, the flow direction and thus magnitude of the flow lanes should remain unaffected. We hypothesize that this keeps the flow lane width  $D_{fc}$  consistent over the length of the system.

This hypothesis was confirmed with new particle tracking experiments with the adapted flow distribution as can be observed in *Figure 3.7A*. The stream lines no longer bend towards the sieves compared to the stream lines shown in *Figure 3.4B*, but are now relatively straight from top (0) to bottom (1) and no longer show much lateral motion (only directly behind the sieves). The outflow conditions found with the numerical simulations were used to adapt the experimental setup, and tracer particles were recorded (*Figure 3.7B*). The observed experimental particle trajectories confirm the model predictions (*Figure 3.7A*).

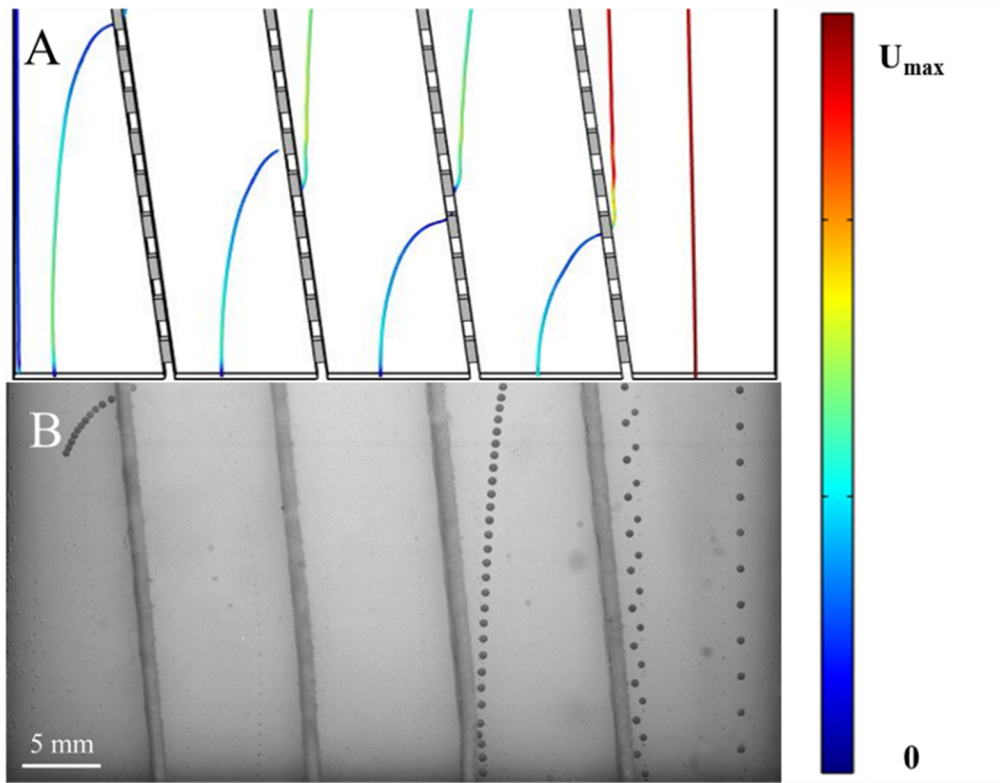


*Figure 3.7:* (A) 3D CFD simulation with optimized outflow conditions were stream lines gives an indication of fluid flow; the velocity is indicated by the colour legend ( $U_{max} = 0.29$  [m/s]) and (B) particle trajectories indicate fluid flow and velocity ( $\sim 0.27$  [m/s]) in the experimental setup with adjusted outflow conditions (interval between two dots of the same path line is 7 milliseconds). Results shown are near the outlets at the bottom of the system.

### Evaluation of the separation performance with adapted outflow rates

New separation experiments were carried out using the new conditions. In *Figure 3.8A* the experimental particle concentrations per outlet for the adjusted outflow condition are compared to the separation predicted by the flow lane theory. The particle concentration in outlet 5 for adjusted outflow conditions is now close to the maximum possible concentration, which indeed shows the importance of the pressure distribution for particle separation. Therefore, sieves can indeed be used in a sparse lateral displacement array to displace particles.

Design 3 in *Figure 3.3* yielded a concentration in outlet 5 that was three times lower (1.1%) than maximum possible predicts (3.4%), and in fact was similar to the inlet concentration (black line). *Figure 3.8A* shows that with optimized outflow conditions (case 5), the concentration in outlet 5 increases only slightly from 1.1 to 1.5 v/v%; nevertheless, it does approach the maximum reachable concentration (1.9%) for these conditions as indicated by data case 6. The adapted flow conditions required an increase of the flow in outlet 5 from 20% to 36% (see *Table 3.2*); the consequence is a lower particle concentration of the collected suspension in outlet 5. Therefore, despite the relatively low concentration, outlet 5 contains 54% of the total particles. This represents an improvement of 33% compared to the results obtained with equal outflow conditions, but it is still 15% (volume basis) lower than the maximum reachable in case of the ideal situation (*Figure 3.8B*). This difference may be explained by the particle size distribution (D10 is 568 $\mu\text{m}$  and D90 is 1103 $\mu\text{m}$ ) of the polystyrene particles. If the particle size distribution is considered, it can be approximated that 15% of the particles are smaller than the critical particle diameter ( $\sim 600\mu\text{m}$ ). This means that the maximum reachable concentration decreases from 1.9 to 1.7%. In *Figure 3.8A*, case 7 shows the separation results taking into account the particle size distribution and it can be seen that it is more in line with the experimental results. It is noted that a critical particle diameter of  $\sim 600\mu\text{m}$  is reasonable for this system, since this implies that it is 3 times smaller than the downstream pore size.

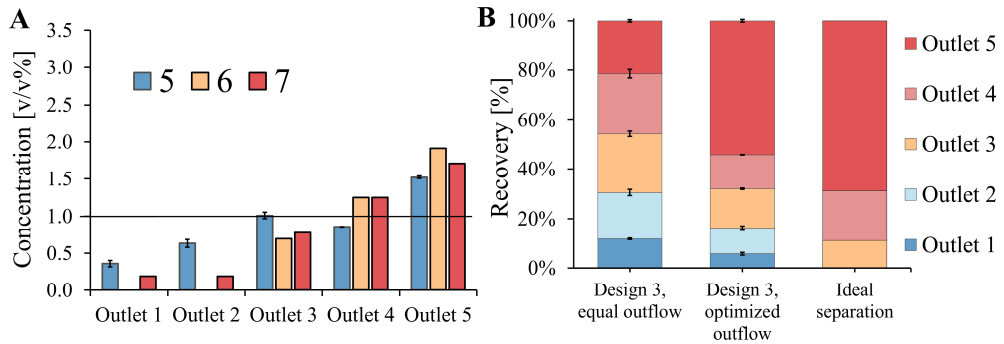
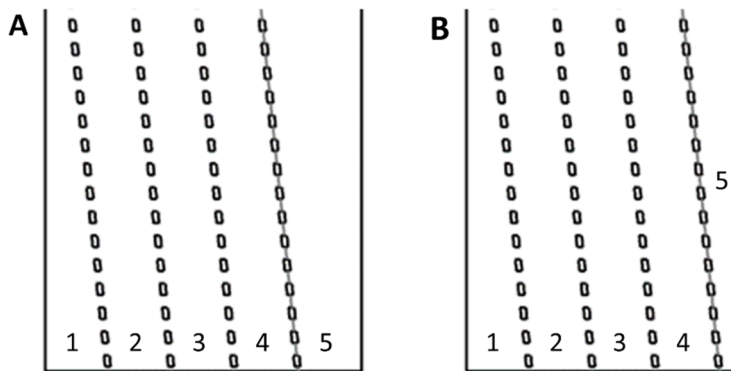


Figure 3.8: (A) Particle concentration ( $v/v\%$ ) per outlet for design 3 (5 represents the experimental data, 6 the ideal situation (assuming perfect displacement) for optimized outflow conditions, and 7 the ideal displacement except for particles smaller than the critical diameter). (B) Percentage recovered particles per outlet for design 3 with equal outflow conditions, optimized outflow conditions and ideal separation. At the inlet, the suspension had average velocity of 0.06 m/s and a concentration of 1  $v/v\%$  (black line in A), the particles  $D_{50}$  is 2.3 times smaller than the gaps (pores) in flow direction. Error bars show standard deviation.

The separation performance found for the sieved-based lateral displacement device with adjusted flow conditions is found equal to that of the sparse obstacle array reported by Lubbersen *et al.* (2015) without adjusted flow conditions. This can be concluded by comparison of the outlet concentration of outlet 5, which is  $\sim 1.5 v/v\%$  for both case 1 (Figure 3.3) and case 7 (Figure 3.8). It is noted that the sparse obstacle array was not optimized by adjusting flow rates as it is impossible to scale this device other than by massive parallelization. Important is that with these results we demonstrate the possibility to use sieves to replace obstacles, with the potential to reach much higher single unit throughput while still displacing particles. The next step is to translate the results of this study to separate smaller micron-sized particles with a diameter smaller than 100  $\mu\text{m}$  with the sieve-based lateral displacement system as their separation is more industrially relevant.

### Alternative strategies to optimize the pressure distribution

Other strategies may be followed to improve the pressure distribution without increasing the outflow in outlet 5. For example, a strategy could involve an adaptation to the sieves, where the pores near the top of the sieve are larger and gradually decrease in size towards the bottom of the device. Another strategy (confirmed by CFD) that may be followed is to decrease the width of outlet 5 compared to outlet 1-4 (*Figure 3.9B*).



*Figure 3.9:* Lower parts of sparse lateral displacement arrays with the 5 outlets are shown. In (A) the current design where the obstacles at the outlets are placed at equal distance from each other and in (B) a conceptual design where the size of outlet 5 is decreased compared to outlet 1-4 in order to improve the pressure distribution without changing the flow rates

This adjustment results in a lower volumetric outflow in outlet 5 (possibly below the outflow of outlet 1-4) and subsequently improves the pressure distribution. However, decreasing the width of outlet 5 as shown in *Figure 3.9B* will increase the risk of blockage.

### 3.5. Conclusions

We investigated the use of sieves instead of individual obstacles to construct sparse deterministic lateral displacement device for suspension separation. This was successful, if the internal pressure distribution is optimized for it. Experiments and numerical simulations show that the asymmetric design of our system leads to an inhomogeneous pressure distribution inside. The pressure difference increases along the entire sieve length and leads to lateral flows towards the sieves at the bottom of the device, which explains the poor particle displacement. Numerical simulations were carried out to find the optimal outflow conditions to maintain the pressure difference along the sieves practically constant. Experiments with these optimized outlet flow conditions showed improved particle separation, indicating that more particles are displaced. These findings confirm the feasibility of large, up-scaled sieve-based deterministic lateral displacement systems for processing of suspensions with micrometer sized particles.







# Four

## **Reducing the critical particle diameter in (highly) asymmetric sieve-based lateral displacement devices**

I listened to *Friction* from *Imagine Dragons* many times while writing this chapter

This chapter has been published as:

J.P. Dijkshoorn, M.A.I. Schutyser, R.M. Boom, R.M. Wagterveld: Reducing the critical particle diameter in (highly) asymmetric sieve-based lateral displacement devices, *Scientific Reports* 7 (2017), 14162.

## 4.1. Abstract

Deterministic lateral displacement technology was originally developed in the realm of microfluidics, but has potential for larger scale separation as well. In our previous studies, we proposed a sieve-based lateral displacement device inspired on the principle of deterministic lateral displacement technology. The advantages of this new device is that it gives a lower pressure drop, lower risk of particle accumulation, higher throughput and is simpler to manufacture. However, until now this device has only been investigated for its separation of large particles of around 785  $\mu\text{m}$  diameter. To separate smaller particles, we investigate several design parameters for their influence on the critical particle diameter. In a dimensionless evaluation, device designs with different geometry and dimensions were compared. It was found that sieve-based lateral displacement devices are able to displace particles due to the crucial role of the flow profile, despite their unusual asymmetric design. These results demonstrate the possibility to actively steer the velocity profile in order to reduce the critical diameter in deterministic lateral displacement devices, which makes this separation principle more accessible for large-scale, high throughput applications.

## 4.2. Introduction:

Deterministic lateral displacement technology is originally a microfluidic suspension separation technique that holds potential for large scale separation of suspensions: it features low pressure drop and low risk of particle accumulation while the design and operation is simple [9, 74, 77, 78, 81-83]. Deterministic lateral displacement devices exploit arrays of obstacles in which each row is slightly displaced relative to the previous row. The fluid that flows between two obstacles in subsequent rows, is called a flow lane (*Figure 4.1*). When the radius of a particle is larger than the width of its flow lane ( $D_c$ ), the particle will be displaced laterally. Due to its hydrodynamic interaction with the obstacle it moves into the next flow lane (*Figure 4.1B*). Particles having a diameter smaller than the critical diameter ( $D_c$ ) are not displaced. Instead they follow the direction of the fluid flow (*Figure 4.1C*) and pass through the array of obstacles along with the fluid [54]. Eventually this leads to separation or fractionation of particles that are different in size.

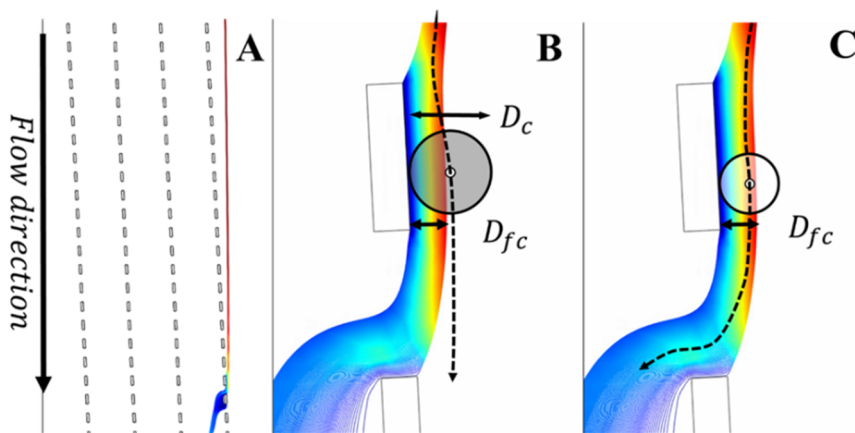


*Figure 4.1:* Visual representation of a fluid flow lane through a gap between white obstacles, derived from a 2D simulation. The blue colour represents low velocity; red colour a high velocity. The layout of a device having 4 obstacle columns is shown in (A). In (B) the gray circle represents a particle larger than the critical diameter being displaced and in (C) the white circle represents a small particle that stays in the flow lane and follows the flow direction.

The highest reported throughput for microfluidic separation in a single deterministic lateral displacement device is approximately 2 mL/min [84]. For analytical purposes this is large enough, but it is far too small for large-scale industrial separation applications [82]. To enable larger-scale separation, sparse obstacle array designs with lower numbers of obstacles (up to 90% less) have been proposed [60]. The sparse designs are characterised by a lower pressure drop, reduced risk of fouling and easier scale-up [60]. Another advantage of the sparse design is simpler construction of obstacles by applying sieves instead of manufacturing individual pillars (*Figure 4.2*). In previous research we reported on particle displacement of relatively large particles with a D50 of 785 $\mu\text{m}$  with sparse and sieve-based lateral displacement devices [60, 85].

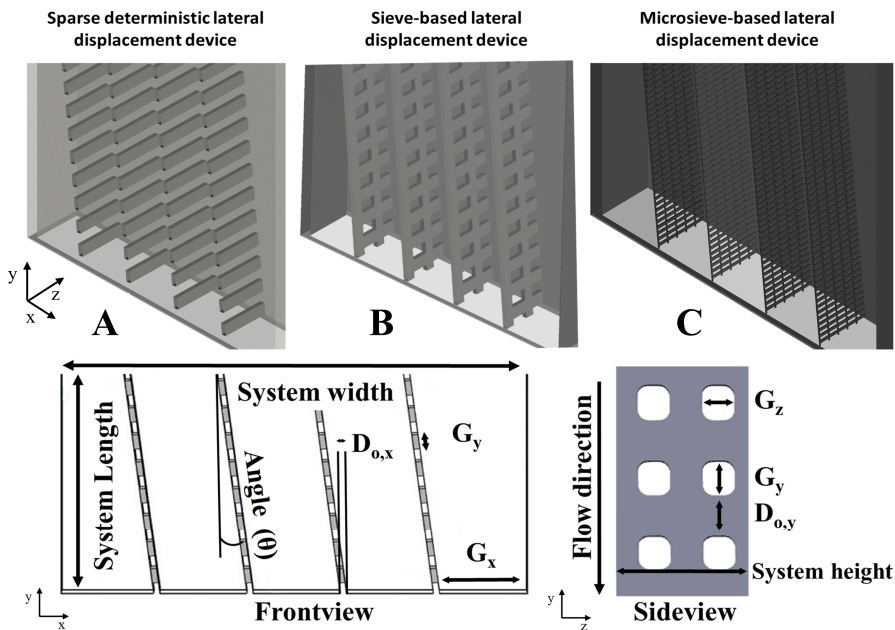


*Figure 4.2:* 3D representation of (A) a sparse deterministic lateral displacement device [60], (B) a sieve-based lateral displacement device [85] and (C) a sieve-based lateral displacement device that employs micro sieves for separation of smaller particles. In (D) an overview of important geometric parameters in these devices. The exact parameter values for each system are shown in *Table 4.2*.

Here, we aim to decrease the size of particles that can be separated while maximizing the throughput using the sieve-based lateral displacement devices. The concept is to employ micro-sieves in order to separate small particles that are closer to industrially relevant suspensions. Eventually the ambition is to separate cells, algae or starch granules with a size between 5 and 20  $\mu\text{m}$ , although in this study the smallest particles have a diameter between 70 and 140  $\mu\text{m}$ . To effectively separate small particles the critical particle diameter and thus flow lane needs to be small. The size of the flow lanes does not only depend on the size of the pores in the sieves but depends on more (geometrical) parameters. For this reason the deterministic lateral displacement theory (*equation 1*) was analysed [75, 78].

$$D_c = 2\alpha \sin \theta \frac{(G_y + D_o, y)}{G_x + D_o, x} G_x \quad (1)$$

Where  $D_c$  is the critical particle diameter,  $\alpha$  is a dimensionless correction factor for a non-uniform flow profile,  $\theta$  is the angle in which the sieves are placed,  $G_y$  is the gap in downstream direction,  $G_x$  is the lateral gap and  $D_o$  the obstacle size in x or y direction. Note that the geometric parameters and operational conditions of the sieve-based systems used in this study vary (open design and unequal outflow). This results in varying  $G_x$  and  $\alpha$  along the length (y) of the device and a critical diameter that depends on location. Moreover, because  $\alpha$  might not be completely independent of other parameters, it is not possible to estimate the critical diameter with theory described above and thus should be derived from experiments or numerical simulations. Nonetheless, *equation 1* introduces crucial parameters to scale down the critical diameter in full deterministic lateral displacement arrays, namely  $\alpha$ ,  $\theta$ ,  $G_y$ ,  $G_x$  and  $D_o$ . Accordingly, we study these parameters for their influence on the critical particle diameter in sieve-based lateral displacement devices (except for  $D_o$  because of practical reasons). The influence of these parameters on suspension separation provides guidelines towards a system design in which the dimensions are specifically adjusted for high throughput separation purposes.

## 4.3. Materials and methods

### Materials

Particle suspensions were prepared with demineralized water, 0.1 w/v% Tween-80 (Merck, Germany) and 0.04 v/v% polyethylene particles (Cospheric, USA). These particles have a density of 0.98-1.00 g/ml. The particle size distribution was measured with a Mastersizer 2000 (Malvern, UK), shown in *Table 4.1*.

*Table 4.1:* Particle size distribution in  $\mu\text{m}$ .

Particles	D10	D50	D90
<b>Small</b>	54	73	98
<b>Medium</b>	76	102	137
<b>Large</b>	104	140	189

### Devices

The influence of  $\theta$ ,  $G_y$  and  $G_x$  was investigated using three different sized flow devices (*Figure 4.3A*), with system 1 being the largest and system 3 the smallest. The design and parameters of all used devices are given in *Figure 4.2*, *Figure 4.3* and *Table 4.2*. Systems 1 and 2 were previously used by Lubbersen and co-workers and also employed for this study [79]. Both systems 1 and 2 (*Figure 4.3A*) have a base plate with grooves of 2mm depth (fine milled polyoxymethylene) in which the sieves are positioned. In these two systems the two rightmost sieves do not touch the left wall. System 3 was constructed from polylactic acid (PLA) with a 3D printer (Ultimaker 2+, The Netherlands). The five outlets are constructed with injection needles with an outer diameter of 0.7 mm for outlet 1 to 4 and 1.3 mm for outlet 5. In order to investigate  $\theta$ , four versions of system 3 were constructed with varying sieve configurations (*Table 4.2*). This was done because the sieves in this system are permanently fixed. For all systems, the suspension is introduced (Masterflex L/S, Cole-Palmer, Chicago, IL) from the top and collected at the five outlets at the bottom.

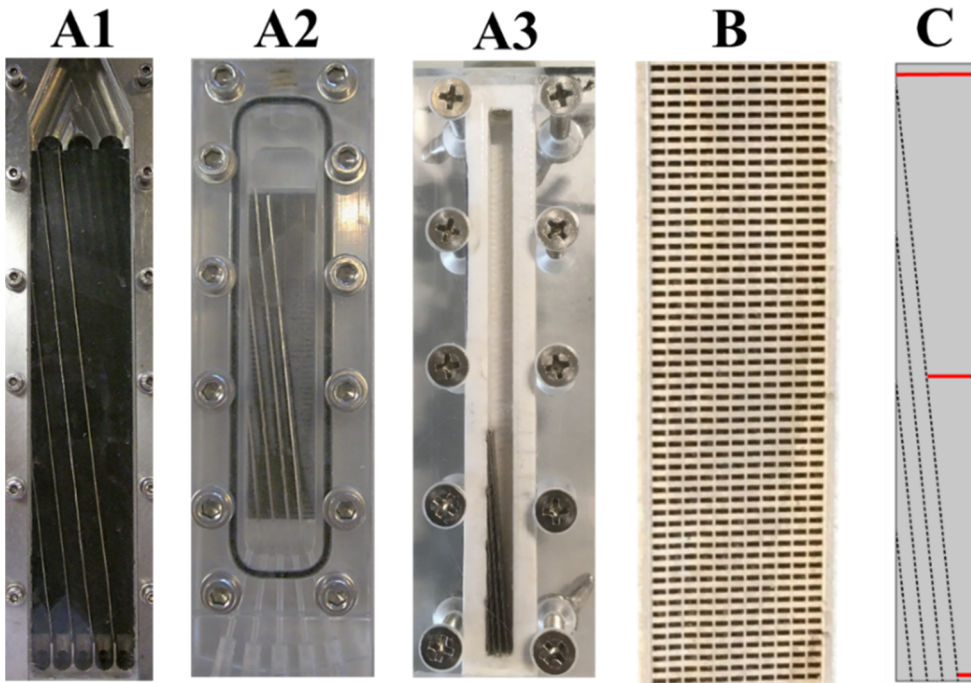


*Figure 4.3:* (A) System 1 is the largest flow cell [55, 56] , System 2 is an intermediate sized flow cell previously used by Lubbersen et al. (2014) and system 3 the smallest flow cell. (B) shows the sieve (nickel) used to serve as obstacles inside the devices (pores are black). (C) shows the geometry of system 3 only, system 1 and 2 are shorter and therefore the sieves do not start on the left hand sidewall. The red lines at the top middle and bottom are the locations where the velocity profiles are taken (*Figure 4.7*). The geometrical parameters are given in *Table 4.2*.

*Figure 4.3B* shows one of the sieves used, where the pores (black) are 200 by 500 $\mu\text{m}$  and the support structures between the pores (nickel) are 200 $\mu\text{m}$  in vertical direction and 50 $\mu\text{m}$  in horizontal direction. The sieves have post aspect ratios of 25 (system 1 and 2) and 35 (system 3), which is about 4 to 17 times larger than reported previously [74, 79].

*Table 4.2:* Geometrical parameters of the systems all given in mm. The number of pores in depth of the system (sieve) is indicated behind the depth of an individual gap in brackets. The lateral gap size is variable and therefore the smallest lateral gap is indicated for comparison. The W stands for Width, H for Height and L for the length.

	Angle ° [ $\theta$ ]	G <sub>y</sub>	G <sub>x</sub>	G <sub>z</sub>	D <sub>o,x</sub>	D <sub>o,y</sub>	W	H	L	Porosity [%]
<b>System 1</b>	5.9	0.2	8.9	0.5 (9x)	0.05	0.2	44.8	5	216	~45
<b>System 2</b>	5.9	0.2	2.2	0.5 (9x)	0.05	0.2	11.2	5	5.4	~45
<b>System 3</b>	2.9-5.9	0.2	1	0.5 (11x)	0.05	0.2	5	7	10	~45

### Experimental procedures

Experiments with varying geometrical parameters were performed with the three systems described in *Figure 4.3*. For the experiments, suspensions with three different size particles sizes (*Table 4.1*) were used to determine the critical diameter. All experiments were conducted in triplicate ( $n=3$ ) with an average inlet flow velocity of 0.12 m/s. In addition, these systems are operated with adjusted outflow conditions to ensure the optimal pressure distribution (*Table 4.3*) [85]. These conditions were selected based on experimental observations of particle trajectories. The inlet concentration was calculated using the weighted average of the outlet concentrations and volumetric outflow rates [85]. To enable comparison between the different experiments, the outlet concentrations are normalized with the measured inlet concentration (0.04 v/v%), because the inlet concentration may vary slightly per experiment. The experimental concentrations are presented as mean  $\pm$  standard deviation (SD) and were analysed using one-way analysis of variance (ANOVA) and Welch's t-test.

*Table 4.3:* Experimental outlet conditions in percentages used while operating the different systems. System 3 was investigated for four different angles (5.9°, 4.9°, 3.9° and 2.9°) with the same outflow conditions.

	Outlet 1	Outlet 2	Outlet 3	Outlet 4	Outlet 5
<b>System 1</b>	16%	16%	16%	16%	36%
<b>System 2</b>	16%	16%	16%	16%	36%
<b>System 3</b>	18%	18%	18%	18%	28%



### Numerical simulations

COMSOL Multiphysics 5.2a was used to create 2D models of the 3 systems described in *Figure 4.3A* [80]. *Figure 4.3C* shows an example of one of the devices and the locations where the velocity profile are taken. The fluid was considered to be incompressible, stationary in the laminar regime and had the physical properties of water at 293.15 K. The laminar inlet flow was parabolic with an average velocity of 0.12 m/s. Outlets 1 to 4 were fixed at specific outflow conditions and the outflow from outlet 5 was based on pressure. A no-slip boundary condition was applied. A mesh dependency study was performed and the results were independent of mesh size.

## 4.4. Results and discussion

### Separation with varying sieve angle ( $\theta$ )

First we describe the influence of the sieve angle ( $\theta$ ) on separation. For this investigation four systems were prepared, in each system the sieves are placed at a different angle. The white bar indicates the maximum reachable concentration, when all particles are displaced and end up in outlet 5. The results presented in *Figure 4.4* show two suspensions with large (A) and medium (B) sized particles (*Table 4.1*) and demonstrate an increasing particle concentration in outlet 5 with decreasing angle. The mean concentrations measured in outlet 5 are significantly influenced by changing the sieve angle (one-way ANOVA:  $p < 0.005$ ), which holds for both particle sizes. These results agree with observations done for conventional full deterministic lateral displacement systems [64, 75].

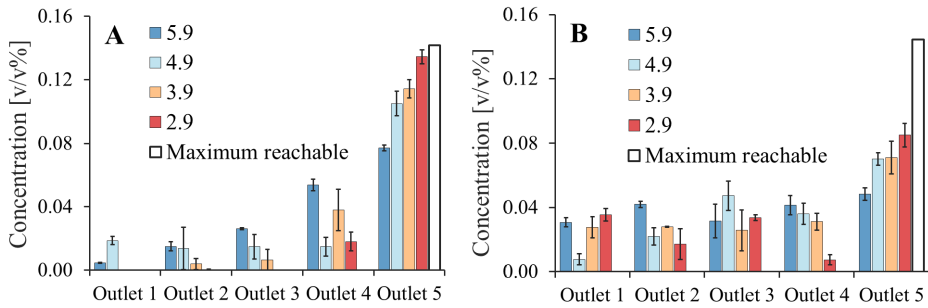


Figure 4.4: Comparison of experimental concentration (mean  $\pm$  1 SD) with variable sieve angle ( $\theta$ ) in system 3 and the maximal concentration that can be reached in theory (white). For all experiments the average inlet velocity was 0.12 m/s and the inlet suspension contained 0.04 v/v% particles. In (A) the results of large particles with a D50 of 140 $\mu$ m are shown and in (B) the results of small particles with D50 of 102  $\mu$ m.

The results in *Figure 4.4A* show that the system with sieves placed at an angle of 2.9°, recovers 95% of all large particles in the targeted outlet. A very low angle may cause practical limitations, since systems with considerable displacement will have to be relatively long [75]. Longer systems usually also exhibit a larger pressure drop, but in case of open sparse systems this is of less concern.

Additional experiments were carried out with medium sized particles (*Figure 4.4B*). The smaller particles show a similar trend compared to the larger particles in *Figure 4.4A*. The separation improves with decreasing angle, but the concentrations in outlet 5 are lower compared to the experiment with larger size range. A decreasing angle leads to a reduction in the critical diameter and thus an increase in concentration of outlet 5 could be expected: the system with an angle of 2.9 concentrates 57% of all particles in outlet 5.

When the results presented in *Figure 4.4* are combined with the particle size distributions (*Table 4.1*) the critical diameter can be estimated to be between 100-140 $\mu\text{m}$  for angles between 2.9 $^\circ$  and 5.9 $^\circ$ . This can be derived from the observation that the system with an angle of 5.9 $^\circ$  separates around half of the particles with a D50 of 140 $\mu\text{m}$ , but hardly any particles with a D90 of 137 $\mu\text{m}$ . When the angle is 2.9 $^\circ$  nearly all particles with a D10 of 104 $\mu\text{m}$  are separated and about 57% of the particles with a D50 of 102 $\mu\text{m}$ . These results illustrate the influence of the sieve angle on the critical diameter in sieve-based lateral displacement systems.

### Gap in downstream direction ( $G_y$ ) and system overview

The  $G_y$  size is known to influence successful separation as well [78]. Because different system designs (*Table 4.4*) and particle sizes are compared here, the  $G_y$  is made dimensionless by relating it to  $G_x$  and the mean particle diameter of the suspension ( $D_p$ ). In this work, the  $D_p$  is related to the  $G_y$  instead of the usually used  $G_x$  [75]. The reason is that for the discussed systems  $G_y$  is the smallest gap and determines whether particles are displaced or filtered; while for most deterministic lateral displacement systems  $G_x$  is limiting. For the overview in *Figure 4.5*, several systems of Zeming et al. (2016) as well as the sparse and sieve-based systems are analysed. The geometrical parameters of the sparse and sieve-based systems are described in *Table 4.4*.

*Table 4.4:* Geometrical parameters of the systems shown in *Figure 4.5* in mm. The number of pores in depth of the system (sieve) is indicated behind the depth of an individual gap in brackets. The W stands for Width, H for Height and L for the length.

	Angle [ $\theta$ ]	$G_y$	$G_x$	$G_z$	$D_{o,y}$	$D_{o,x}$	W	H	L	Porosity [%]
<b>System 1</b>	5.9 $^\circ$	1.8	8.3	1.5 (2x)	1.6	0.8	44.8	5	216	~50
	5.9 $^\circ$	1.1	8.4	2.5	0.68	0.68	44.8	2.5	216	~62
	5.9 $^\circ$	0.2	8.9	0.5 (9x)	0.2	0.05	44.8	5	216	~45
<b>System 2</b>	5.9 $^\circ$	0.2	2.2	0.5 (9x)	0.2	0.05	11.2	5	5.4	~45
<b>System 3</b>	5.9 $^\circ$	0.2	1	0.5 (11x)	0.2	0.05	5	7	10	~45
	5.9 $^\circ$	0.1	1	0.5 (11x)	0.1	0.05	5	7	10	~45

The results in *Figure 4.5* give an impression of the differences between the devices with regards to particle displacement as a function of the systems geometry. The criterion used for the data points to distinguish whether particles were displaced or not is based on the mean particle diameter and the particle concentration in the target outlet (outlet 5), which must be significantly higher than the inlet concentration (one sample Welch's t-test:  $p < 0.05$ ).

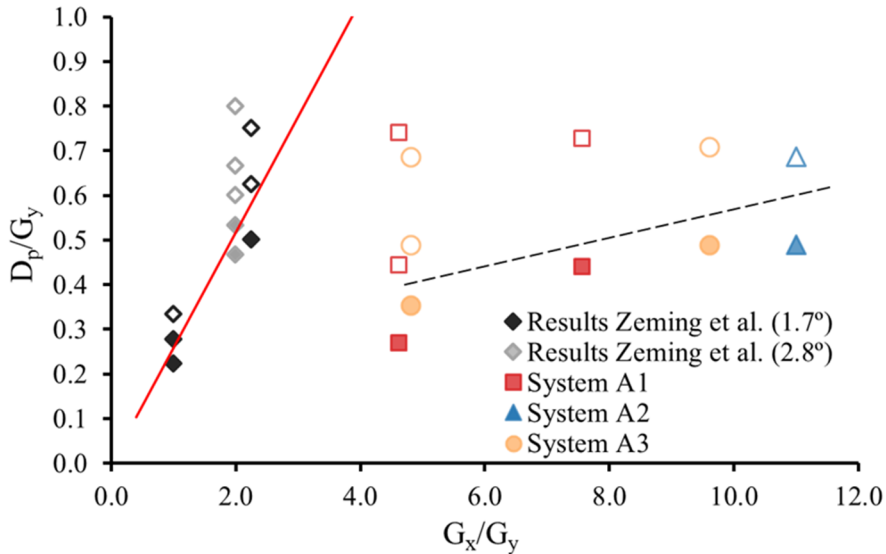


*Figure 4.5:* Fraction of filtration limit versus system asymmetry; dimensionless comparison of  $G_y$  relative to  $G_x$  and  $D_p$ . The experimental results are obtained with different (sized) sparse, sieve-based systems and deterministic lateral displacement devices [11, 81, 88]. The open marks indicate particle displacement, this implies that these systems led to a significantly higher concentration in outlet 5 compared to the inlet concentration (one sample Welch's t-test:  $p < 0.05$ ). The filled marks indicate that particles were not displaced, which means no significant difference was observed between the inlet concentration and the concentration in outlet 5 (one sample Welch's t-test:  $p > 0.05$ ). The black and grey diamonds illustrate the results of a full obstacle array with an  $\theta$  of  $1.7^\circ$  and  $2.8^\circ$  respectively [81]. The red line indicates the estimated critical diameter for the full deterministic lateral displacement devices with a  $\theta$  of  $1.7^\circ$ , using the empirical model of Davis et al. [89]. The black dotted line guides the eye and shows the distinction between separation and no separation for the sparse systems with different proportions, an angle of  $5.9^\circ$  and an average inlet velocity of 0.12 m/s.

The ratio of  $G_x/G_y$  describes the asymmetry of the designs. Asymmetry ( $G_x/G_y > 1$ ) is desired since it reduces the pressure drop, the risk of particle accumulation and allows for effective upscaling [78, 85]. However, in *Figure 4.5* and *Figure 4.6* it can be observed that for fixed operational conditions the degree of asymmetry ( $G_x/G_y$ ) is limiting and should not exceed a critical value specific for these conditions. If this critical value is crossed,  $D_p$  equals  $G_y$  which means that particles can no longer move through the gap and will cause obstruction and internal fouling. In the best situation, the  $D_p$  is much smaller than the  $G_y$  while it is still being displaced.

One should bear in mind that the systems of Zeming et al. are very different from the asymmetric systems described here. Not only the open design but also the obstacle shape/size, the inlet velocity and outflow conditions are different and thus can only be compared qualitatively. Regardless, all these systems are able to displace particles and it gives a perspective of the possibilities of using asymmetric systems.

The differences between the designs of the full deterministic lateral displacement devices and sparse lateral displacement devices are illustrated in *Figure 4.5*. Full obstacle arrays are generally symmetric or moderately asymmetric and have a  $G_y$  that is 1 to 2.5 times as smaller as the  $G_x$ . Asymmetric systems where  $G_y$  is bigger than  $G_x$  (ratio smaller than 1) have a larger pressure drop and a higher risk of clogging [78], therefore they are not suitable for large scale and not taken into account. These full obstacle arrays are able to displace particles 2 to 3 times smaller than the downstream gap [78].

Sparse or sieve-based lateral displacement systems are very asymmetric and have a  $G_y$  that is 4 to 11 times as smaller as the  $G_x$  but are still able to displace particles ~2 times smaller than the  $G_y$ . That these systems, despite the extreme geometry are able to displace particles is possible because of the adjusted outflow conditions as was described earlier by Dijkshoorn et al (2017). It is hypothesized that by changing the outflow conditions the uniformity of the flow profile is affected ( $\alpha$  in *equation 1*) such that it becomes possible to displace particles in systems with

extreme geometry. However, the consequence of adjusting the outflow conditions, is a lower maximum attainable concentration in the target outlet [85].

### **Influencing $\alpha$ by varying the lateral gap ( $G_x$ )**

For a better understanding of  $\alpha$  (the flow profile correction factor) and how it influences particle separation, the deterministic lateral displacement theory was applied to sparse and sieve-based lateral displacement systems. From this theory (*equation 1*) it can be derived that when the geometry is very asymmetric ( $D_{o,x} \ll G_x$ ); the influence of  $G_x$  (and  $D_{o,x}$ ) on the critical diameter becomes very small and can be neglected. This leads to *equation 2*:

$$D_c = 2\alpha \sin \theta (G_y + D_{o,y}) \quad (2)$$

On the basis of *equation 2*, it is possible to change  $G_x$  without affecting  $D_c$ . However, the results in *Figure 4.5* indicate that there is an effect of changing  $G_x$  relative to  $G_y$  (e.g. a higher ratio of  $D_p/G_y$  can be observed with increasing  $G_x/G_y$ ). It is hypothesized that  $G_x$  affects the flow or velocity profile ( $\alpha$ ), which is known to influence the critical particle diameter and thus separation [69, 75, 86].

The velocity profile was investigated by systematically varying  $G_x$  in three different sized system designs (described in *Figure 4.3* and *Table 4.2*). These were operated with same sieve configuration and pore sizes (*Figure 4.3B*), equal particle suspension ( $D_{50}$  of 140 $\mu\text{m}$ ) and equal average inlet velocity. The experimental results are shown in *Figure 4.6*.

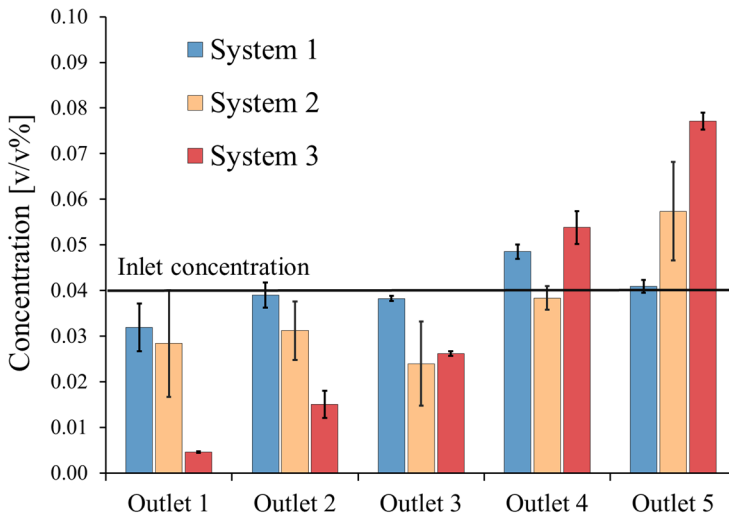


Figure 4.6: Particle concentrations (mean  $\pm$  1 SD) are shown per outlet for the three systems with varying size and  $G_x$ . System 3 has different design compared to system 1 and system 2 (Figure 4.3A). The sieves (Figure 4.3B) are identical and positioned at an angle of  $5.9^\circ$  in all three systems. The average inlet velocity was 0.12 m/s and the suspension contained 0.04 v/v% particles with a D50 of  $140\mu\text{m}$ .

A significant increase in concentration can be observed for outlet 5 with decreasing system width or  $G_x$  (one-way ANOVA:  $p < 0.005$ ). For the largest system 1, a somewhat higher concentration in outlet 4 was observed compared to the concentration in outlet 5. Overall however, limited particle displacement was observed for this system (supplementary movie). System 2 that has a width  $\sim 4$  times smaller than system 1 reached a concentration of 0.057 v/v% in outlet 5. System 3, which is about two times narrower than system 2 obtained a mean concentration of 0.077v/v%. A remark here is that the sieves in system 3 continue until the left border, unlike system 1 and 2 where the sieves stop short (Figure 4.3A). As a result, more particles are available for outlet 5 in system 3, which makes it difficult to compare system 3 with system 1 and 2. Moreover, system 3 was operated with different outflow conditions, which were selected after experimental observations because these conditions were found to improve pressure distribution for system 3. Despite these differences, system 1 does not show

separation but both systems 2 and 3 do show elevated concentrations in outlet 5. System 3 shows better depletion of outlet 1 and the highest concentration in outlet 5. This gives the impression that separation indeed is influenced by differences in  $G_x$  and possibly affects the velocity profile. For confirmation, two-dimensional numerical flow simulations of the three systems (*Figure 4.3A*) were created to illustrate the differences in the velocity profiles in the normalized lateral gap, and to visualize the changes in velocity profile along the length of the system at three locations (top, middle and bottom, *Figure 4.3C*). Two-dimensional numerical simulations were chosen to reduce the computational requirements. The velocity profiles (*Figure 4.7ABC*) were set to start with the same parabolic shape. Progressing along the length of the system, the velocity profiles become more non-uniform under influence of a receding  $G_x$ . Clear differences can be observed in the development of the velocity profile for the different systems.

*Figure 4.7DEF* show the velocity profiles for the first 100 $\mu\text{m}$  from the sieve towards the channel centre. Only the first 100 $\mu\text{m}$  is shown because the gap in the downstream direction is 200 $\mu\text{m}$  and a flow lane larger than 100  $\mu\text{m}$  would result in a critical diameter larger than the gap. The velocity profile close to the sieve for the three systems (*Figure 4.7DEF*) differ most at the top of the systems (D), where the smallest system shows the highest velocity gradient. In the middle of the systems (E) the differences in the velocity gradients have become smaller where system 2 and 3 became practically equal to each other. Near the bottom of the system (F) the velocity profiles close to the sieve are equal for all systems. A sharper velocity gradient will result in a somewhat smaller critical diameter assuming that the flow lanes carry equal flux, explaining the better performance of smaller systems [69, 75, 86]. Surprisingly, the velocity profile at the bottom and near the sieves become equal for all systems, which means that the smaller systems lose their advantage.



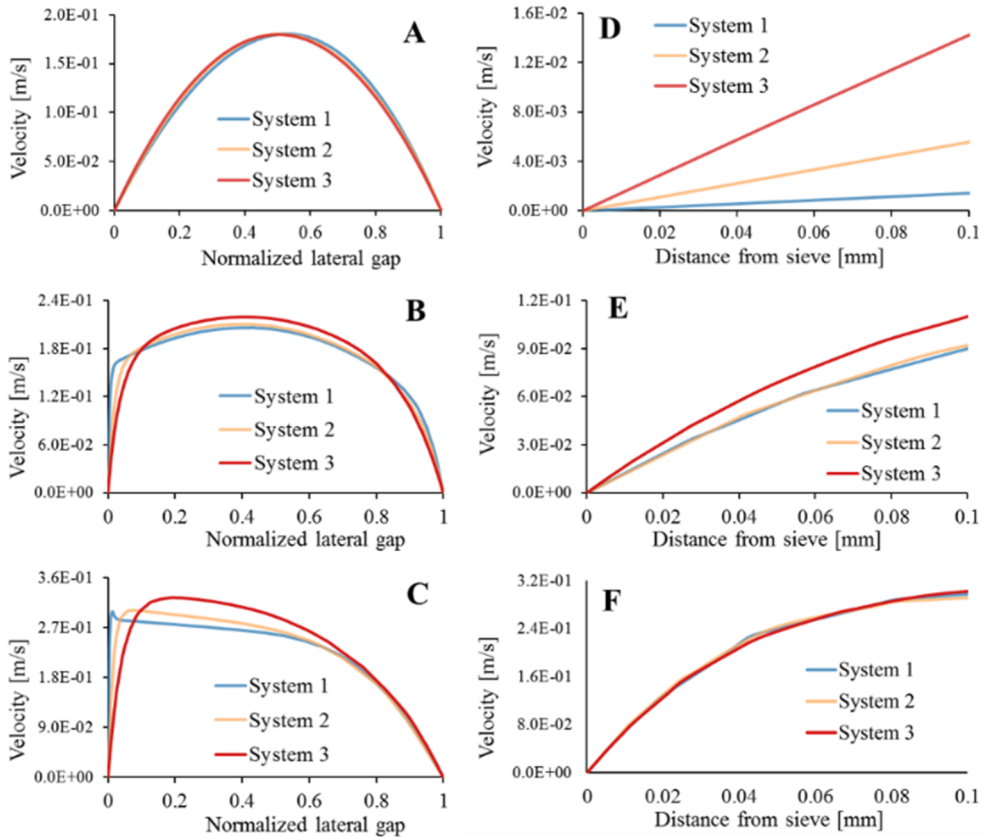


Figure 4.7: 2D numerical simulations show the horizontal velocity profile at the top (AD), in the middle (BE) and at the bottom (CF, near outlet 5) of the three systems. ABC show the velocity profile over the normalized lateral gap and DEF show the first 100 $\mu$ m starting from the sieve towards the channel centre. The results presented in were obtained by assuming similar outlet conditions for all systems with 36% in outlet 5 and 16% in the other outlets.

A possible explanation is that the flow lanes do not carry equal flux along the length of the sieve and that flux of the flow lanes is larger for larger systems. Therefore, the same 2D models were used to verify the flux through the gaps over the entire length of the three systems (Figure 4.8).

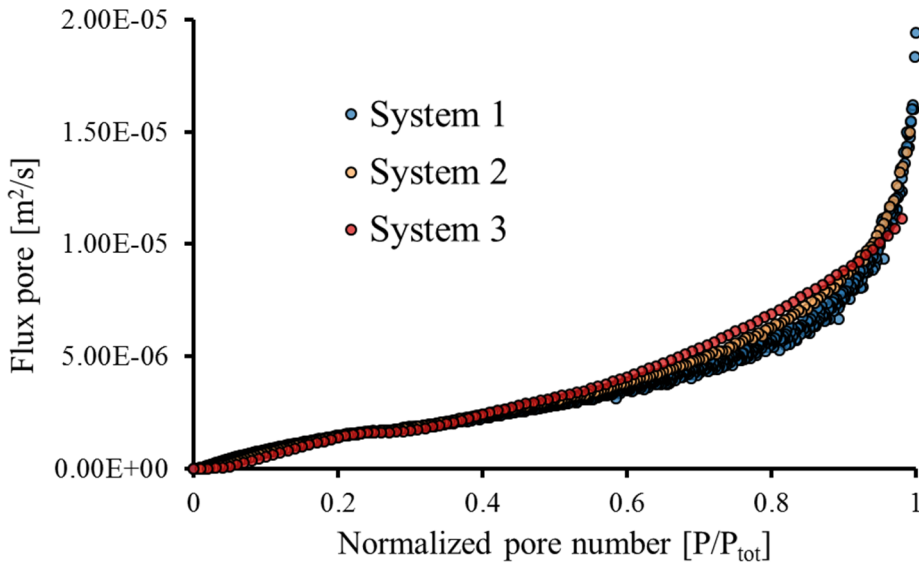


Figure 4.8: Numerically calculated fluxes through all pores for the three systems, where each marker represents the flux in a single pore. For these results the same outflow conditions were used in all systems (outlet 1-4 at 16% and outlet 5 36%). The blue markers (system 1) have a larger spread because the mesh relative to the pores was larger compared to the other systems. However, improving the mesh did not affect the overall trend of the flux through the pores.

The calculations shown in *Figure 4.8* nicely illustrates that the flux through the gaps increases in the flow direction for all systems. This is different from conventional deterministic lateral displacement devices, where it is assumed that the flow lanes carry equal flux [54, 75]. This assumption, however, is not valid for this system and not necessarily valid for systems with anisotropic permeability [87-90]. From the flux through the gaps (*Figure 4.8*) and the partial area of the velocity profiles at these specific locations (*Figure 4.8DEF*) it is possible to calculate the width of the flow lanes. These estimated flow lanes are shown in *Table 4.5* and are in good agreement with the radius of the experimentally used particles (*Table 4.1*).

The flow lanes in the upper part of all systems are 22-50 times smaller than the gaps and become larger in the downstream direction. In system 1 and 2 the flow lanes become larger

and their sizes ultimately increase up to  $96\mu\text{m}$  and  $81\mu\text{m}$  respectively. This increase is caused by the strong increase of the flux through the pores near the end of these systems (*Figure 4.8*), which can be a result of the outflow conditions. The flow lanes in system 3 seem to stabilize around  $66\mu\text{m}$  in the middle and the bottom part which indicates a well-adjusted outflow condition. It is noted that the flow distribution results derived from the simulations do not correspond to the experimental results, where in systems 1 and 2 similar outlet flow conditions lead to optimal for flow distribution and surprisingly in system 3 even different outlet flow conditions were found optimal for flow distribution. These remarkable differences may be explained by the different flow distribution in a 2D simulation compared to flow in a 3D device in practice.

*Table 4.5:* Width of the flow lanes calculated by integrating the areal velocity profiles given in *Figure 4.7DEF* and equalize it with the flux through the gaps (*Figure 4.8*).

	Top	Middle	Bottom
<b>System 1</b>	$6.7\mu\text{m}$	$75.0\mu\text{m}$	$96.2\mu\text{m}$
<b>System 2</b>	$8.7\mu\text{m}$	$72.3\mu\text{m}$	$81.0\mu\text{m}$
<b>System 3</b>	$3.9\mu\text{m}$	$65.9\mu\text{m}$	$66.3\mu\text{m}$

Extensive analysis shows that the velocity profile in these systems change substantially along the length of the axis, both in magnitude and in shape (*Figure 4.7*). These changes in turn, affect the size of the flow lanes and determine the change in critical diameter along the length of the system. This uncertainty makes it impossible to obtain a single description for the critical particle diameter. However, the critical particle diameter might be estimated by considering the separation data in a dimensionless diagram for this specific angle (*Figure 4.5*). Or alternatively, the minimum required  $G_x$  may be estimated for a chosen  $D_p$  and  $G_y$  for the specific inlet velocity. For example, to separate particles of  $10\mu\text{m}$  with a  $G_y$  of  $20\mu\text{m}$ , an angle of  $5.9^\circ$  and an average inlet velocity of  $0.12\text{ m/s}$ , the smallest  $G_x$  should not be more than  $\sim 8$  times the  $G_y$ , i.e.  $160\mu\text{m}$ . These dimensions were cross-checked using COMSOL and found to be in good agreement.

## 4.5. Conclusions

Design parameters of sparse and sieve-based lateral displacement systems were investigated for their influence on the critical particle diameter; with perspective of applying these systems for practically relevant large-scale application. The design and operation conditions of these systems are different from those of the full deterministic lateral displacement devices. For a better understanding of the interrelation between critical device parameters on the particles that can be separated, the parameters were varied systematically. The angle in which the sieves are placed influences the critical diameter in sparse obstacle arrays, which is in agreement with previous findings based on the existing deterministic lateral displacement technology. Highly asymmetric lateral displacement systems with a much smaller downstream gap ( $G_y$ ) than the lateral gap ( $G_x$ ) proved to be able to displace particles  $\sim 2$  times smaller than the downstream gap ( $G_y$ ). Based on theory it might be expected that in highly asymmetric systems the lateral gap ( $G_x$ ) has little influence on the critical diameter; however, it was found that  $G_x$  has indirect influence on the critical diameter by influencing the hydrodynamics in these systems. Moreover, asymmetric lateral displacement systems are only able to displace particles, because the velocity profile becomes increasingly non-uniform ( $\alpha$ ) and stabilizes with increasing flux through the pores. These results show the possibilities to use the deterministic lateral displacement separation principle by actively governing the hydrodynamics instead of being restricted by the geometry. Because of the geometric and hydrodynamic differences compared to the full deterministic lateral displacement devices, it is not possible to estimate an overall critical particle diameter. However, it is possible to make a dimensionless comparison of different systems to approximate the required dimensions (e.g. lateral gap ( $G_x$ ) and downstream gap ( $G_y$ )) for the specific operation conditions and particle diameter.





# Five

## Visualizing the hydrodynamics in sieve-based lateral displacement systems

I wrote this chapter while often listening to *Modern way* from *Kaiser Chiefs*

This chapter has been published as:

J.P. Dijkshoorn, J.C. de Valença, R.M. Wagterveld, R.M. Boom, M.A.I. Schutyser: Visualizing the hydrodynamics in sieve-based lateral displacement systems, *Scientific Reports* 8 (2018), 12861.

## 5.1. Abstract

Deterministic lateral displacement (DLD) systems structure suspension flow in so called flow lanes. The width of these flow lanes is crucial for separation of particles and determines whether particles with certain size are displaced or not. In previous research, separation was observed in simplified DLD systems that did not meet the established DLD geometric design criteria, by adjusting the outflow conditions. We here investigate why these simplified DLD systems are able to displace particles, by experimentally investigating the hydrodynamics in the device. Flow lanes were visualized and the local flow velocities were measured using  $\mu$ PIV and compared with 2D fluid dynamics simulations. The size of the flow lanes strongly correlates with the *local* flow velocity ( $V_y$  and  $V_x$ ), which depends on the hydrodynamics. Therefore, the geometric design criteria of DLD devices is in fact just one method to control the local hydrodynamics, which may also be influenced by other means. These findings give a new perspective on the separation principle, which makes the technique more flexible and easier to translate to industrial scale.



## 5.2. Introduction

Separating neutrally buoyant suspensions of micron-sized particles (1-10 $\mu\text{m}$ ) is not a trivial operation. An effective technique to separate large volumes of these particle suspensions is microfiltration, but even this technique suffers from drawbacks like concentration polarization, cake layer formation, pore blocking and internal pore fouling [3, 6, 82]. Therefore, alternative separation techniques have been proposed that make use of microfluidic separation principles [8, 9, 83, 91]. Many of these microfluidic separation principles may show potential, but they need significant redesign to enable upscaling to larger volumes. Adaptation of the design may render these systems more suited for processing large volumes, but this makes it essential to characterise the hydrodynamics of the redesigned system. This can be done by combining visualization methodologies, such as Particle Image Velocimetry (PIV) with Computational Fluid Dynamics (CFD) [92-94].

Deterministic lateral displacement (DLD) systems are promising for (large-scale) suspension separation, because it can separate particles that are smaller than the gaps or pores in the system, limiting the risk of blockage. As a consequence, the systems are expected to be less sensitive to fouling than a microfiltration system, while the required pressure drop is lower and the design of the peripheral system is simpler, lowering the capital and operational costs. However, DLD devices in their microfluidic design are difficult to scale up and not yet suitable for processing large volumes. Asymmetric DLD systems such as a sieve-based lateral displacement (SLD) system are more promising for scale-up (*Figure 5.1A* vs. *Figure 5.1C*) because they (1) are less prone to foul, (2) have an even lower pressure drop, and (3) are easier to manufacture and can be constructed with existing microsieves [9, 60, 78, 82, 85, 95].

Separation in DLD systems relies on particle-obstacle interactions that laterally displace particles in the fluid from their streamlines, out of the critical flow lane [54]. A flow lane (red lane in *Figure 5.1*) is defined as the set of streamlines that passes between two subsequent (longitudinally adjacent) obstacles. Each gap possesses a flow lane. When a particle is larger

than twice the width of the flow lane at the location when it is about to flow between two obstacles, particle-structure interaction will laterally displace this particle (grey) from its initial flow lane into the next (*Figure 5.1BD*). If the particle radius is smaller than the flow lane width, this particle (white) may still be displaced but not sufficiently to cross over to the next flow lane and therefore will stay in its initial flow lane (*Figure 5.1BD*). This means that the critical particle diameter is controlled by the width of the flow lanes, which makes precise control of the flow essential. In most previous published studies the flow is controlled by (periodic) geometric design constraints (e.g., angle, gap sizes, obstacle size/shape) by adjusting inlet velocity [55] and/or outflow conditions [85]. In systems meant for large-scale separations, one wishes to minimise the presence of obstacles, while the system should not be too dependent on the precise local velocity and outflow conditions (e.g. a SLD system). In addition, the influence of particle-particle interactions and the influence of particles on the flow are neglected and we assume that separation only depends on the flow lane width. This is not valid for separations with a significant volume fraction of particles to separate.

The influence of the geometric design criteria on the critical particle diameter has been thoroughly investigated. The hydrodynamics in such systems have however not yet received much attention, although it is known to influence the size of the flow lanes. Improved control of the hydrodynamics for instance by adjusting the outflow conditions can provide more design freedom and make production easier and cheaper [85, 95]. Specifically, we address the hydrodynamics in asymmetric DLD systems.

The objective of the study reported here is to characterize the hydrodynamics and its influence on flow lane size. The flow lanes were experimentally visualized and the local velocities were measured in a sieve-based lateral displacement device with different inlet flow rates. These measurements were compared with 2D numerical simulations. Subsequently, this model was used to correlate the size of the flow lanes with the local velocity.

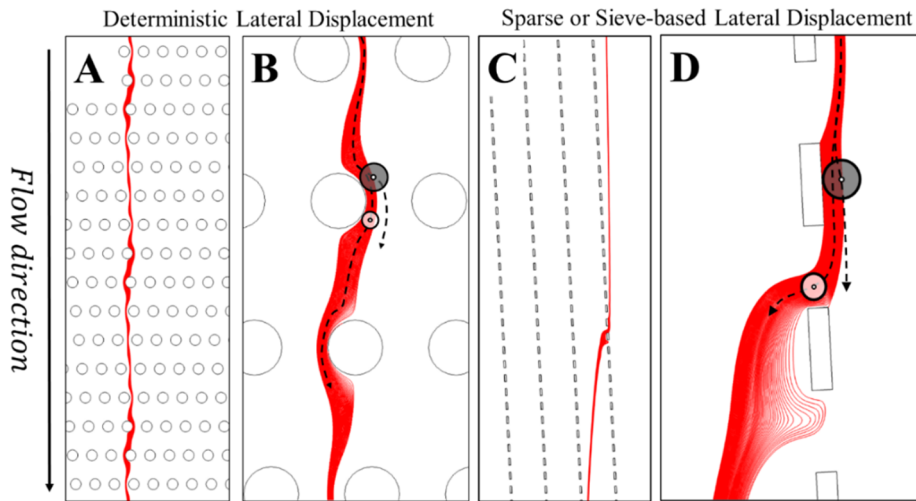


Figure 5.1: Flow lanes (red) in a part of the DLD array (AB) and in the (bottom) part of the sieve-based lateral displacement (SLD) system (CD). (AC) shows the flow lanes in a larger part of the device. (BD) Shows a close up of the same flow lanes with the trajectories of two particles. Particles larger than twice the critical flow lane diameter (grey) are displaced and follow the angle of the obstacle column. Particles smaller than this critical diameter (white) follow the flow lane and flow through the gap.

### 5.3. Materials and Methods

#### Experimental setup

A sieve-based lateral displacement system was constructed with optical access from two sides (Figure 5.4). The main frame was 3D printed from Polylactic acid (Ultimaker 2+, The Netherlands) and two transparent Polymethylmethacrylate (PMMA) plates were attached to the front and at right side frame's exterior. Inside, four nickel sieves (Veco, The Netherlands) were placed with 1 mm space between them at an average angle of  $2.9^\circ$  with respect to the channel walls ( $y$ -direction). The pores at the front of the sieves are  $200 \pm 10 \mu\text{m} \times 500 \pm 30 \mu\text{m}$  every  $200 \pm 10 \mu\text{m}$  in  $y$ -direction and every  $50 \pm 5 \mu\text{m}$  in  $z$ -direction (Figure 5.2). Because of the electroforming production process, the pores at back of the sieves are slightly smaller than at the front. The channel length ( $y$ ) was 100 mm, the width ( $x$ ) 5 mm and the depth ( $z$ ) 7 mm.

The inlet was at the top and five outlets were at the bottom. The outlet tubes were used to fix specific outflow conditions of the five channels, outlets 1 to 4 were fixed at 16% of the inflow and outlet 5 at 36% [85]. The outlet suspension was collected in a collection vessel (1 L) and pumped (Masterflex L/S, Cole Parmer, US) to a pressure vessel (1 L) to dampen the pumping pulsations. The suspension was continuously recirculated through the system at the selected volumetric flow rate until the flow stabilized.

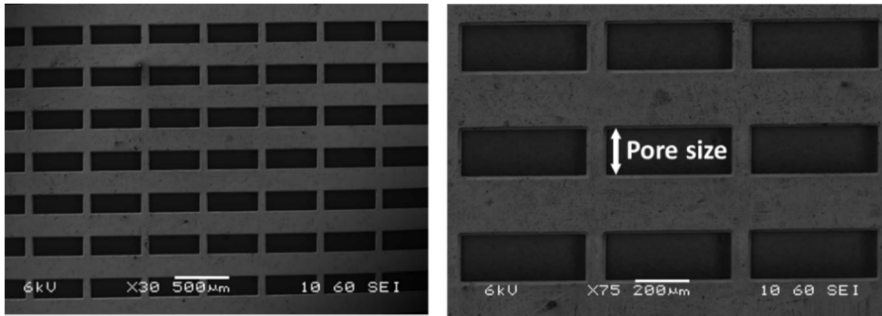


Figure 5.2: SEM images of a representative example of the microsieves used in our device with different magnification (x30 and x75). The pore size we discussed in this paper is indicated and is  $200\pm 10\ \mu\text{m}$ .

### Image recording

The flow was monitored with a camera at three positions in the system: the top section (0.1 normalized length) where the suspension enters, slightly above the middle section (0.4 normalized length) and the bottom section (0.8 normalized length) (Figure 5.4). The motion of the fluid was visualized by seeding deionized water (milliQ) with 0.1 wt% red polystyrene tracer particles ( $d=2\ \mu\text{m}$ ,  $\rho=1.05\ \text{g/cm}^3$ , Microparticles GmbH) and 0.1wt% non-ionic surfactant (Tween80) to prevent the particles from aggregating. The particles were illuminated with a thin ( $0.4\pm 0.1\ \text{mm}$ ) laser sheet (808 nm, Firefly, Oxford lasers) positioned in the middle of the channel at a depth of 3 mm. The reflected light was captured through a long distance magnifying lens (Navitar 1-14x) on a high speed camera ( $1024 \times 1024$  pixels,  $20 \times 20\ \mu\text{m}^2/\text{pixel}$ , Photron, SA1.1). The desired magnification ( $M$ ), appropriate recording frequency and pulse length were chosen depending on the particle velocity. The recording frequency varied

between 1-10 kHz and the pulse duration between 2-10  $\mu\text{s}$  with a pulse power of 0.03-0.15 mJ/pulse. An overview of the full channel was taken with a magnification of  $M=4$ , with the resolution of 1 pixel = 5  $\mu\text{m}$ . Detailed images that focused on the pores of the largest sieve were taken at  $M=10$ , with a resolution of 1 pixel = 2  $\mu\text{m}$ .

### **Flow lane determination using image analysis**

The particle pathlines were visualized by superimposing 100 consecutively recorded images (*Figure 5.3*). This new superimposed image only shows the maximum intensity of the all 100 images for each pixel position (z-stack, IMAGEJ, NIH). The flow lane width was defined as the distance between the sieve at the boundary transition of an obstacle and gap, and the most outward pathline that enters this gap (red line in *Figure 5.3*). Using IMAGEJ, 45 flow lanes were measured in 15 superimposed images for each velocity at locations 0.4 and 0.8.

### **Flow velocity calculation with Particle Image Velocimetry (PIV)**

The image recordings were used to calculate full vector flow fields, which were calculated from the displacement of particles groups between two consecutive images by using commercial PIV software (DaVis, LaVision, Germany). A multigrid cross correlation method was chosen with decreasing window size. The first interrogation window was 98 x 98 pixels, followed by a second calculation where the window size was 16 x 16 pixels when  $M=4$  and 32 x 32 pixels when  $M=10$ . The flow fields derived from the recordings made of the whole channel ( $M=4$ ) had a higher resolution because the interrogation windows had a 50% overlap. The boundary of the vector field was defined using a geometrical mask to distinguish between regions where vector field should or should not be calculated. Following the vector field calculation, a post-processing algorithm was used to eliminate erroneous vectors and outlier detection was used based on the median value of the nearest neighbouring vectors [96].

If some vectors were rejected, they were interpolated or extrapolated from the accepted, neighbouring vectors. The percentage of rejected vectors from the obtained vector field was around  $3\pm 2\%$ . The final vector field was made by averaging the orthogonal components of nine consecutive vector fields (sliding averages).

### **Experimental determination of $V_y$ and $V_x$**

A line profile was made in the middle of the vector fields and in the middle the pores (e.g. the white line in *Figure 5.4*). This line profile illustrates the average velocity in a volume of 0.08 mm thick when  $M=4$  and 0.06 mm when  $M=10$ . The average velocity at the top (0.1) was calculated from 1500 PIV vector fields because the flow was turbulent. The flow at the middle and the bottom was observed to be stable (laminar) and the average velocity was determined from three sets of nine vector fields, each set was inconsistently taken at the beginning, in middle and at the end of the recording.

### **2D numerical simulations**

Laminar fluid flow (NS equation) was numerically simulated in a 2D system with the same geometry as our experimental setup using COMSOL Multiphysics 5.3 [80]. The fluid (water at 293.15 K) was assumed incompressible and the flow stationary. The flow was calculated for following average inlet velocities: 0.02 m/s ( $Re\sim 100$ ), 0.04 m/s ( $Re\sim 200$ ), 0.06 m/s ( $Re\sim 300$ ), 0.075 m/s ( $Re\sim 375$ ) and 0.12 m/s ( $Re\sim 600$ ). The outlets were fixed to specific outflow conditions, where outlets 1 to 4 were fixed at 16% of the inflow and outlet 5 at 36% [85]. The no-slip wall condition was applied and the mesh was refined until results were independent on the mesh ( $\sim 200000$  elements). The simulations were performed with the finite element method with 2nd order elements for velocity and 1st order elements for pressure.  $V_y$  and  $V_x$  were integrated over a cutline through each pore and the flow lanes were manually measured at the boundary transition of an obstacle and gap. Afterwards, three additional models were made with slightly varying geometry: two different angles ( $5.9^\circ$  and  $2.9^\circ$ ) and two different pore sizes (200 $\mu\text{m}$  and 100 $\mu\text{m}$ ). All other conditions remained the same.

## 5.4. Results & Discussion

We first visualized the flow lanes with a high speed camera. Second, we used micro-particle image velocimetry ( $\mu$ PIV) to measure the local flow velocities and compare these with the 2D simulations. These 2D simulations were then used to correlate the width of the flow lanes with the flow velocity.

### **Visualization of the flow lane in a sieve-based lateral displacement device**

Critical flow lanes were experimentally visualized in a sieve-based lateral displacement device on three locations and with three inlet velocities (*Figure 5.4*). The flow lane width was visualized using the trajectories of individual tracer particles and the most outward pathline that enters or exits this gap is outlined by a red line. These flow lanes were then compared with the flow lanes obtained from the 2D fluid model, which did not contain particles.

Near the entrance of the system, the experimental flow pattern deviated from the 2D fluid simulations. This was caused by the inlet configuration which induced a jet and resulted in some turbulence entrance region in the experimental setup. The turbulence resulted in flow instability over time, and the suspension intermittently flowed into and out of some of the pores at the top of the system. These variations made it impossible to measure stable flow lanes. For the 2D simulations, the entrance flow was assumed to be laminar and stable over time, which allowed us to derive the flow lane width. These simulated flow lane widths were smaller at lower inlet velocity, and gradually grew larger with increasing inlet velocity. Furthermore, the simulated flow lanes in the top section were narrower compared to the flow lanes in the bottom section. Though, the experimental results and simulations at the top of the system are not alike, separation has yet to take place. The bottom region is more important because at this location significant particle displacement should have taken place. Because the experimental observed flow lanes and simulated flow lanes are similar at the bottom of the system we used these simulations for further analysis.

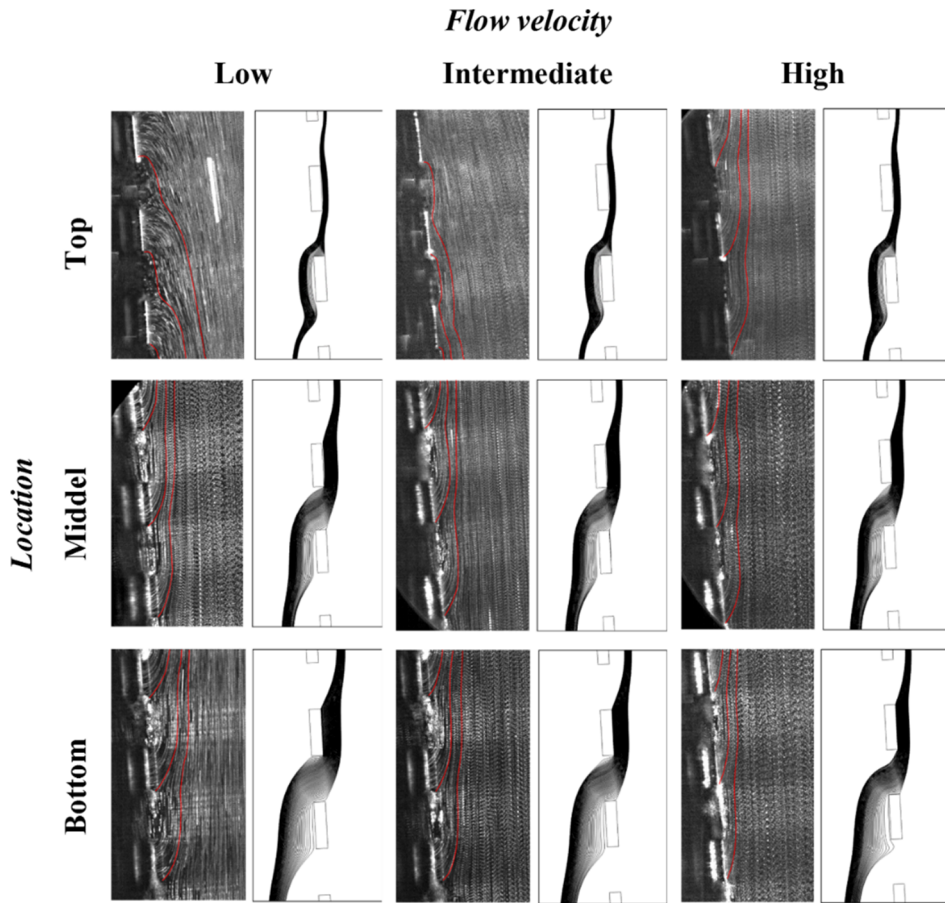


Figure 5.3: Experimental and numerical visualization of the flow lanes in a sieve-based lateral displacement device. From left to right, the inlet velocities increases (between 0.1 and 0.12 m/s), from top to bottom are three locations along the right sieve (Figure 5.4). The red lines are introduced to distinguish between the pathlines that will flow into the pore and that will go straight, the pathlines clustered together that flow into a pore are considered a flow lane. The flow lanes at the top are not steady because the flow in this region was turbulent (supplementary video). The 2D numerical simulations assume laminar inflow.



Flow lanes were visualized in all locations but only measured in the middle and bottom sections of the device, because here the flow had stabilized and became independent from the inlet disturbances (*Figure 5.3* and *Table 5.1*). In general, the width of the flow lanes varies depending on the location and the inlet velocity. A higher inlet velocity reduces the width of the flow lanes. The widest observed flow lane was 106  $\mu\text{m}$ , which means that the cut-off particle size is equal to the pore size; particles in this flow lane that have a diameter smaller than that of a pore (200 $\mu\text{m}$ ) will always flow into this pore and larger particles will be excluded. Wide flow lanes are, therefore, not desired.

*Table 5.1:* Size of the flow lanes (*Figure 5.3*) are given in  $\mu\text{m}$ . Experimental obtained flow lane sizes (mean  $\pm$  standard deviation) are measured for 3 pores in 15 stacks of 100 frames (45 measurements per flow lane) and obtained using 2D numerical simulations in COMSOL.

	Low velocity		Intermediate velocity		High velocity	
	<i>PIV</i>	<i>Simulation</i>	<i>PIV</i>	<i>Simulation</i>	<i>PIV</i>	<i>Simulation</i>
<b>Top</b>	NA	25	NA	27	NA	30
<b>Middle</b>	71 $\pm$ 7	64	64 $\pm$ 5	61	63 $\pm$ 5	56
<b>Bottom</b>	106 $\pm$ 8	77	81 $\pm$ 6	65	61 $\pm$ 5	55

The flow lane width is known to be influenced by the velocity profile [69, 75, 95]; an asymmetric velocity profile is beneficial for separation because it reduces the width of the flow lanes [86]. This, however, is only true if the flow lanes through all gaps carry equal flux, which is assumed in (periodic) DLD systems [54, 75]. This assumption is not valid in case of sparse or sieve-based lateral displacement systems and is expected to also not to hold for systems with anisotropic permeability [87, 89, 95, 97]. A highly asymmetric velocity profile does not by definition reduce the width of the flow lanes. We hypothesize that there is a balance between the vertical velocity component ( $V_y$ ) due to the inlet flow, and the horizontal velocity component ( $V_x$ ) of the fluid, due to the flow into the gaps. When  $V_y$  and  $V_x$  are balanced over the entire length of a system, the flow lanes will have the same width throughout the system. And if  $V_y$  grows with respect to  $V_x$  the flow lane should become narrower and vice versa. To

confirm this hypothesis, the velocity field was measured at the same locations where the flow lanes were visualized. The  $V_y$  and  $V_x$  components were analysed from the acquired data. The velocity profiles obtained with these  $\mu$ PIV measurements are compared with the velocity profiles calculated with the 2D numerical simulations.

### **Velocity profile obtained with $\mu$ PIV and 2D numerical simulations**

The flow velocity profile was measured for three different inlet velocities and at three locations in the device (*Figure 5.4*). Two sets of recordings were made for each location: a recording of the entire channel width (light green squares) and a detailed recording of the largest sieve (dark green squares). The recordings were translated into an average vector field by using PIV software (*Figure 5.4*). The vectors indicate the size and direction of the composite velocity; the background colour indicates the magnitude of the transverse velocity component  $V_x$ . These average vector fields were used to collect  $V_y$  and  $V_x$  profiles along a line that passes through the centre of a pore, for example the white horizontal line in *Figure 5.4*.  $V_y$  was acquired from the entire channel (light green square), which also allowed us to determine the flow velocity behind the sieves. For an accurate estimation of  $V_x$  near a pore gap it was necessary to zoom in onto the sieve (dark green square), which allowed the observation of tracer particles flowing towards the pores.

The measured and simulated velocity profiles are shown in *Figure 5.5* for the three locations and three inlet velocities. The velocity profiles increase (negative direction) towards the bottom of the device. The actual inlet flow velocities during the experiments were estimated with the 2D simulations because the flow rate of the pump was influenced by the pressure drop at higher flow rates. The low inlet velocity was  $\sim 0.02$  m/s ( $Re \sim 100$ ), the intermediate inlet velocity was  $\sim 0.04$  m/s ( $Re \sim 200$ ) and the high inlet velocity was  $\sim 0.075$  m/s ( $Re \sim 375$ ). Slight differences in channel width can be observed between the experimental system and the 2D simulations, which may be caused by irregularities in the construction (e.g. sieves and channel surface) or by inaccuracies in the imaging (e.g. camera position and/or lighting).

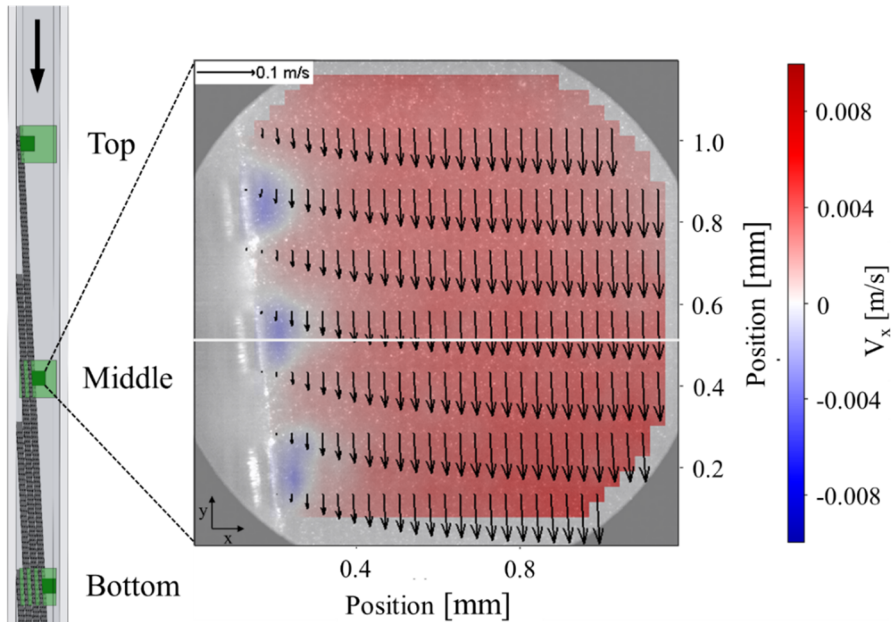


*Figure 5.4:* Schematic overview of the experimental setup and the recording locations: top, middle and bottom for both the entire channel (light green square) and the pores (dark green square). The vector field shown (every fourth vector row is taken near the pores and is recorded at the middle of the device, where the colour indicates the  $V_x$  (blue is left and red is right). The white line gives an example of a measurement location for the average velocity profile (*Figure 5.5DF*). The vector field shows the absolute velocity and the colour indicates only  $V_x$ .

The velocities measured in the top section of the device are presented in *Figure 5.5A*. At this location the flow was turbulent due to a jet created at the entrance of the device. Therefore the results were averaged over  $\sim 1500$  images; because the standard deviation (SD) was  $\pm 0.04$  m/s it is not shown. We do not show the experimental  $V_x$  profile in *Figure 5.5B* because of strong flow instabilities. Only a small amount of fluid flows through the pores (negative velocity), while most of the fluid flows away from the sieves (positive velocity).

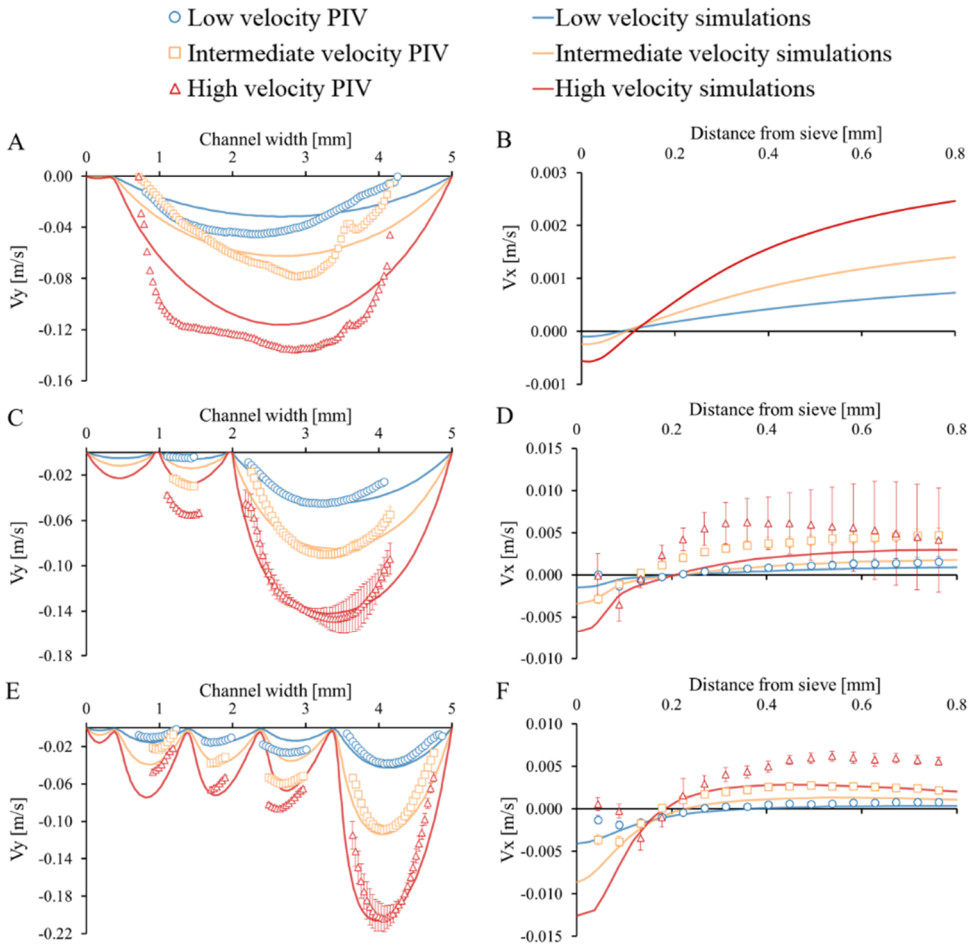


Figure 5.5: Velocity profiles ( $V_y$  in ACE and  $V_x$  in BDF) at three locations in the device (AB at the top, CD in the middle and EF at the bottom) for three average inlet velocities (low is 0.02 m/s, intermediate is 0.04 m/s and high is 0.075 m/s). The experimental data shows the mean velocity and SD and the y-axes are not equal. The data points of (A) are an average  $V_y$  of 1500 images and the SD is not shown. The measured  $V_x$  is not shown in (B) because the flow was not stable.

The velocities measured in the middle section are shown in *Figure 5.5CD*. At this location the flow had become laminar, and  $V_y$  could be measured both in front and behind the sieve (*Figure 5.5C*). The experimental  $V_x$  component was negative near the sieves indicating that the fluid indeed flowed towards the sieves and through the pores. While this is qualitatively in line with

the simulations, the magnitudes of the velocities were somewhat different (*Figure 5.5D*). Towards the channel centre, the direction of  $V_x$  reverses and the fluid started to flow away from the sieves.

*Figure 5.5E* presents values for the  $V_y$  component between multiple sieves in the bottom section of the device for both simulations and experiments. The  $V_x$  component is shown in *Figure 5.5F*. The agreement between experiment and simulation is acceptable. The flow could not be visualized inside the pores and consequently, the experimental measurements cannot be used to find a correlation between the size of the flow lanes and the flow velocity ( $V_y$  and  $V_x$ ) inside the gap. Therefore, the 2D simulations are used instead for this.

### **The balance between $V_y$ and $V_x$ , and its influence on the flow lanes**

A two dimensional model was made of our experimental setup, which was used to correlate the velocity components ( $V_y$  and  $V_x$ ) with the flow lanes. These flow velocity components were integrated over a cutline in the entrance region of each pore, the ratio of these components ( $V_y/V_x$ ) is shown in *Figure 5.6*. This velocity ratio is presented as function of the number of pores relative to the total number of pores along the sieve ( $P_i/P_n$ ), where  $P_1/P_n \approx 0$  indicates the first pore at the top and  $P_n/P_n = 1$  the last pore in the sieve at the bottom. This number therefore represents a spatial coordinate along the sieve. Due to the design of the system, the  $V_x$  component at the top was near zero and therefore, the ratio of the velocity components was very high between  $P_i/P_n = 0 - 0.1$ . The  $V_x$  component quickly increased in the downstream direction but  $V_y$  increased as well (*Figure 5.5ACE*). The velocity ratio ( $V_y/V_x$ ) eventually stabilized around a value of 2 (*Figure 5.6A*), but this ratio was not completely stable and fluctuated somewhat near  $P_i/P_n = 0.3$ , which corresponds to the start of a new parallel sieve (see also *Figure 5.4*). This parallel sieve locally decreases the  $V_x$  and thus results in a small increase of  $V_y/V_x$ . This effect is apparent at 0.3 and is repeated to a smaller extent around  $P_i/P_n = 0.55$ , where a third sieve starts. The final ratio is slightly different for the three inlet velocities, which means that depending on the inlet velocity,  $V_y$  changes relative to  $V_x$  (*Figure 5.5A*).

Correlation of the width of the flow lanes (*Table 5.1*) with the corresponding velocity ratios, shows that a lower  $V_y/V_x$  resulted in wider flow lanes, and thus separation of larger particles. This effect was visualized for three locations and three inlet velocities in four different system designs (*Figure 5.6B*). *Figure 5.6B* illustrates the same trend observed in *Figure 5.6A*, where a higher  $V_y/V_x$  results in smaller flow lanes. The sizes of the flow lanes were normalized with the size of the pores ( $D_{fc}/D_{pore}$ ), which are shown as function of the  $V_y/V_x$  ratios. The circular symbols in *Figure 5.6B* represent the same nine flow lanes (three velocities and three locations) as described in *Figure 5.6A*. The influence of  $V_y/V_x$  on  $D_{fc}/D_{pore}$  was investigated for three additional designs with varying angles ( $5.9^\circ$  and  $2.9^\circ$ ) and pore size ( $100\mu\text{m}$  and  $200\mu\text{m}$ ) to compare the effect of the geometry. Similarly shaped curves were obtained, with slightly different values per geometry. This is expected as the flow does not always behave linearly to changes in the geometry. Therefore, there is no unified description of  $V_y/V_x$  for a specific flow lane size in devices with a different design.

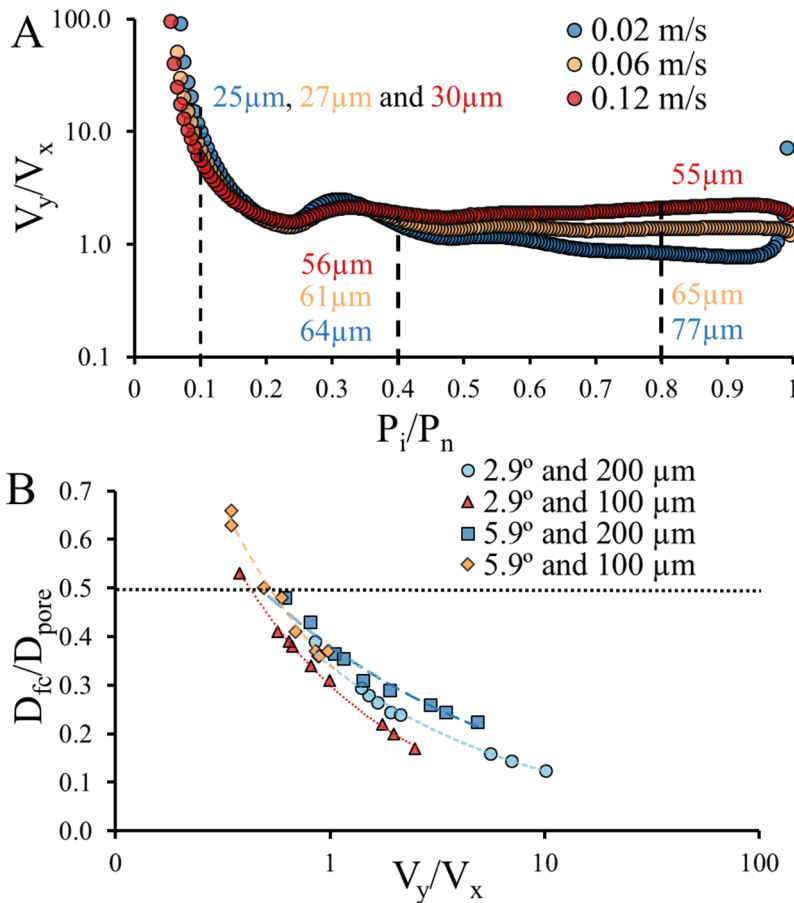


Figure 5.6: (A) For this system the ratio of velocity components ( $V_y/V_x$ ) in each pore was plotted on a logarithmic scale for the three inlet velocities. The pores were normalized by the total number of pores. The size of the numerically simulated flow lanes (Figure 5.3 and Table 5.1) were indicated at top (0.1), middle (0.4) and bottom (0.8). A model was used with the same geometry as our experimental system, where the sieves were placed at an angle of 2.9° and had pores of 200 $\mu\text{m}$ . (B) The size of nine flow lanes ( $D_{fc}$ ) relative to the pore size ( $D_{pore}$ ) were plotted against the  $V_y/V_x$  ratio, where each marker represents one location and one inlet velocity. This was done for four systems with varying angle and pore size. A higher  $V_y/V_x$  ratio decreased the flow lane width relative to the size of the pores. A minimum  $V_y/V_x$  is required to displace particles because if  $D_{fc} \geq 0.5 * D_{pore}$ , particles will not be displaced but filtered instead (dotted line).

Using the results in *Figure 5.6B*, the performance of the four designs can be discussed. Displacement of the smallest possible particles with the largest possible pores requires flow lanes that are much smaller than the pores and thus,  $D_{fc}/D_{pore}$  should be as low as possible. In contrast, with  $D_{fc}/D_{pore} \geq 0.5$ , the width of the flow lane is equal or larger than half the size of a pore and particles are no longer displaced but will either flow through the pore or are physically blocked instead. This limit is indicated by the black dotted line in *Figure 5.6B*. A low  $D_{fc}/D_{pore}$  requires a high  $V_y/V_x$  (*Figure 5.6*) but in practice it is difficult to reach a  $V_y/V_x > 10$ , except for a small region at the top of the systems (between 0 and 0.1 in *Figure 5.6A*). The effort needed to maintain a high  $V_y/V_x$  throughout the system limits the possibilities to create small flow lanes in the entire system. Characterizing the influence of  $V_y/V_x$  on the  $D_{fc}/D_{pore}$  is essential to evaluate the performance of a specific device and/or operating conditions.

Overall, the results summarized in *Figure 5.6* show the correlation between the velocity of the fluid that flows in downstream direction ( $V_y$ ) and the fluid that flows into the pore ( $V_x$ ) with the size of the flow lanes. We expect that this balance also holds for conventional DLD devices. But unlike sparse or sieve-based systems, conventional DLD devices use geometric criteria to obtain stable (and periodic)  $V_y/V_x$  to form flow lanes for displacing particles. Small changes in the geometry and/or inflow velocity of DLD devices can influence the stability and the periodicity of this balance, which may result in anisotropic permeability and different migration directions [56, 87, 89, 90, 97].



## 5.5. Conclusions

An in-depth characterization was done on the flow lane sizes in asymmetric, sieve-based deterministic lateral displacement devices. CFD and  $\mu$ PIV were used to quantify the flow lanes, in addition to their flow velocities at different locations and at four different inlet velocities. The flow lanes width varies with the ratio of velocity components ( $V_y/V_x$ ) and these velocity components ( $V_y$  and  $V_x$ ) vary depending on location and inlet velocity. The ratio of the longitudinal and transversal velocity components ( $V_y$  and  $V_x$ ) stabilized along the sieve towards the outlets. A good correlation was observed between the velocity ratio and the width of the flow lanes: a high  $V_y/V_x$  ratio results in a smaller flow lane and vice versa. This implies that particles can also be displaced by accurate control of the hydrodynamics instead of only applying geometric design constraints. This insight may help application of this separation principle to larger-scale separation operation.



# Six

## **Deterministic displacement of particles and oil droplets in a cross-flow microsieve module**

This chapter was written while playing *Panic Station* from *Muse* many times

This chapter has been accepted as:

J.P. Dijkshoorn, R.M. Wagterveld, R.M. Boom, M.A.I. Schutyser: Deterministic displacement of particles and oil droplets in a cross-flow microsieve module, *Journal of Membrane Science* (2018).

## 6.1. Abstract

Our investigation aims to apply Deterministic Lateral Displacement (DLD) to separate (deformable) particles or droplets from dispersions on industrial scale. DLD is a promising technique because it can separate particles smaller than the pores. Previous work shows how to manipulate the critical particle diameter in a sieve-based lateral displacement system by modifying the hydrodynamics. In this study, we apply this fundamental understanding of the DLD separation principle to deterministically displace particles in a cross-flow microsieve module. First, two dimensional simulations of the fluid dynamics in this cross-flow module were performed to investigate the hydrodynamic conditions required for particle displacement. Next, these simulations were compared with the flow fields visualized in the experimental setup. In addition, high speed recordings confirmed deterministic displacement of particles and oil droplets over the microsieve surface. Last, the systems performance was evaluated by measuring the transmission of rigid PMMA particles and deformable hexadecane droplets and the particle size distribution for different operation conditions. These results clearly demonstrate that the DLD principle can be effectively applied in a cross-flow microsieve module. With this, the application of this microfluidic separation principle to separate particles or droplets (1 to 20 micrometer) from dispersions on industrial scale has become realistic.

## 6.2. Introduction

Separation of dispersed particles is important in many sectors: for example, in medical laboratories, in water treatment plants or in the food industry. While dispersions of particles that are larger than 20  $\mu\text{m}$  are generally separated with centrifuges or decanters, this is more difficult with smaller particles, especially when the particles are near neutrally buoyant and/or easily deformed [2, 82, 83]. One cannot use gravity based techniques for these dispersions (e.g. centrifugation) or (micro)filtration, because the particles block the pores or deform and pass the membrane pores [98].

This study focuses on deterministic lateral displacement (DLD) system, which uses tilted obstacle arrays to separate particles smaller than the gaps or pores between the pillars [54, 75]. To be separated, particles require to have a radius larger than the width of the stream that is about to flow into the next pore (*Figure 6.1*). These streams are called flow lanes. When the radii of the particles are larger than the width of the flow lanes, particle-obstacle interactions will displace these particles laterally and push their centre of mass just outside the flow lanes. Because particles are physically excluded from the flow lanes, they cannot be dragged into the gaps or pores and are guided laterally by the obstacle columns. These larger particles are laterally displaced and can be collected at the end of the obstacle column on one side of the system.

Application of the DLD separation principle has especially potential in biotechnological and food industries because process streams often contain deformable and neutrally buoyant particles. The DLD technology was evaluated as promising to separate such dispersions on larger scale [9, 64, 67, 99, 100]. While the principle was discovered in microfluidic devices, the volumetric throughput of a single device has been increased to scale this microfluidic separation principle towards larger applications [55, 56]. In these studies, it was shown that particles can be displaced by particle-obstacle interactions without using the classical DLD obstacle arrays, but instead applying simplified sparse obstacle arrays. These sparse lateral

displacement designs are constructed with only a small number of rows of obstacles, which could be translated in a configuration of a set of parallel sieves that were placed at a small angle to the flow direction [60, 85]. Particle displacement could be achieved by adjusting the hydrodynamic conditions to obtain flow lanes with a specific width in the sieve-based lateral displacement (SLD) design (*Figure 6.1B*) [85, 95, 101]. The flow should be laminar and such that the axial velocity of the fluid just above the pores ( $V_y$ ) is larger but in balance with the transversal flow velocity into the pores ( $V_x$ ). If both flows ( $V_y$  and  $V_x$ ) are controlled well, the width of the stream that flows into a pore can be defined (i). Preferably, the flow lanes and thus the critical particle diameter, have the same size along the length of the microsieve [101]. If all flow lanes are of equal size, a clear critical diameter defines whether a particle is displaced or not. In other words, to deterministically displace particles with the same diameter in the entire system, the hydrodynamic conditions ( $V_y/V_x$ ) must be balanced.

The influence of hydrodynamic conditions on displacement of suspended particles has been previously described when for example studying particle screening during shear flow across a wall with suction via side branch channels [102]. In this study the phenomenon of particle displacement or particle screening was subscribed to the deviation of the particle trajectory from the fluid streamlines of the fluid entering the side branch channel because of interaction with the pore entrance. This is slightly different from the fluid skimming mechanism that removes the particle-free layer [103]. Moreover, it appeared that the ratio of the magnitudes of the cross and the shear flows influenced the screened particle size. In yet another microfluidic study it was observed that if specific hydrodynamic conditions are applied during suspension flow in a system with side channels, a portion of fluid near the wall is withdrawn from the main stream into the side stream [104]. These conditions could be adjusted such that particles whose diameter is larger than a critical value would not enter the side channels, even if a particle is located close to the wall and it is smaller than the cross section of the side channel. Both Wu et al. and Yamada et al. describe very similar conditions that prevent particles from entering a side channel, like also was described for SLD technology [101].

However, these two examples focus on controlling individual side streams for a single pore, which can be placed in series. Only Van Dinster et al. employed a similar principle to facilitate higher throughputs [12]. They investigated cross-flow microfiltration with balanced cross-flow and permeate flow to enable particle separation in dilute suspensions. Yeast cells ( $\sim 5 \mu\text{m}$ ) were successfully separated from a dilute suspension using a microsieve with pores of  $20 \mu\text{m}$ . While successful separation was achieved, the operation of the device was not optimised.

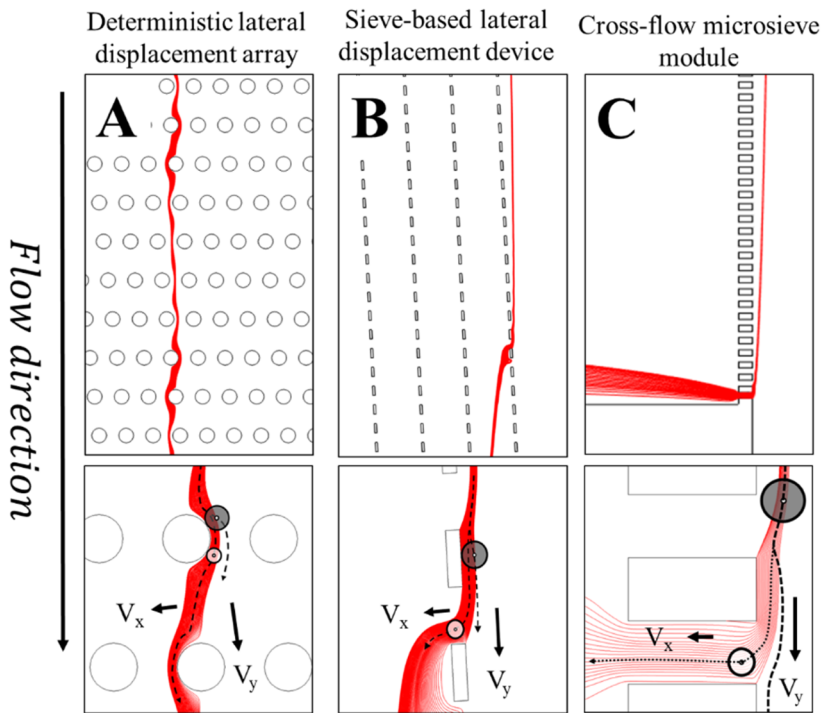


*Figure 6.1:* Three geometries with flow lanes (red) are shown that allow deterministic displacement of particles. In (A) the original deterministic lateral displacement (DLD) array, in (B) a sieve-based lateral displacement (SLD) device and in (C) a cross-flow microsieve (CFM) module. In the close-up figures the flow lanes and separation principle is illustrated for each system. Particles with a radius larger than the flow lanes (grey) are physically excluded from the flow lane by particle-structure interactions, the smaller particles (white) cannot be physically excluded and are dragged into the pore by the flow lane. The width of the flow lane can be changed by influencing the velocity components ( $V_y$  and  $V_x$ ).

Based on our previous work and literature, we formulated a new hypothesis that particle displacement does *not* require a distinct DLD design (e.g. angle, size of the gaps or obstacle size (*Figure 6.1*)), but can be achieved by control of the hydrodynamic conditions [22, 101, 102, 104]. More specifically, by controlling the ratio of the axial and transversal velocities ( $V_y/V_x$ ), it is possible to separate particles with the DLD principle in unconventional DLD designs, such as a cross-flow microsieve module, in which the microsieve is not placed in an angle with respect to the flow direction (*Figure 6.1*).

This study therefore aims at resolving the local hydrodynamics in a cross-flow microsieve device and subsequently use this to displace (deformable) particles that are smaller than the pores. Firstly, numerical simulations of the fluid dynamics in this cross-flow module were performed to investigate the hydrodynamic conditions required for particle displacement. Subsequently, these simulations were compared with the flow fields visualized by high speed recordings in the experimental setup. In addition, we recorded and confirmed deterministic displacement of particles and oil droplets ( $25\pm 5\mu\text{m}$ ) over the microsieve surface (supplementary videos). Lastly, the systems performance was evaluated by measuring the transmission of rigid PMMA particles and deformable hexadecane droplets (Stokes number  $\ll 1$  if the particles are in the proximity of the microsieve) and the particle size distribution for a cross-flow velocity of 0.6 m/s ( $\sim 1$  L/min and  $\text{Re}: \sim 2400$ ) with varying permeate flow velocities 0.4-7.9 mm/s (2-50 mL/min).



## 6.3. Materials and methods

### 2D CFD simulations

The NS-equation was solved for a complete 2D geometry similar to that of the constructed flat plate cross-flow microsieve module (Figure 6.2). The simulations were performed using the finite element method (2<sup>nd</sup> order elements for velocity and 1<sup>st</sup> order elements for pressure) in COMSOL Multiphysics 5.3 [80]. The microsieve was 150 mm long and 100  $\mu\text{m}$  thick. The pores in the microsieve were 50  $\mu\text{m}$  wide, 100  $\mu\text{m}$  deep and the spacing between the pores was 50  $\mu\text{m}$ . The simulated water flow (at 293.15 K) through the system was assumed to be laminar, incompressible and stationary. Three average inlet velocities were calculated:  $\sim 0.3$  m/s,  $\sim 0.6$  m/s and  $\sim 0.9$  m/s. The permeate outlet was swept for multiple outflow velocities ( $\bar{V}_x$ ) in relation to the cross-flow velocities ( $\bar{V}_y$ ). The outlet in the main channel was pressure based. A no-slip wall condition was applied and the results were checked for mesh dependency (selected mesh had  $\sim 125,000$  elements). The  $V_y$  and the  $V_x$  were integrated over a cutline in each pore and three flow lanes were manually measured at the transition of an obstacle and gap [101].

### Image recording

A high speed camera (1024 x 1024 pixels, 20x20  $\mu\text{m}^2/\text{pixel}$ , Photron, SA1.1) and a magnifying lens (OPTEM ZOOM 125 1-13x) were used to record the motion of red polystyrene tracer particles ( $d=2$   $\mu\text{m}$ ,  $\rho=1.05$  g/cm<sup>3</sup>, Microparticles GmbH) in milliQ water with 0.1wt% non-ionic surfactant (Triton X-100, Sigma Aldrich 9284) to prevent particles from aggregating. The tracer particles were illuminated with a thin (0.4 $\pm$ 0.1 mm) laser sheet (808 nm, Firefly, Oxford lasers) positioned in the middle of the membrane at a depth ( $z$ ) of 3.5 mm. The desired magnification ( $M$ ), appropriate recording frequency and pulse length were chosen depending on the particle velocity. A magnification of  $M=1$  was used to record the entire membrane, with the resolution of 1 pixel = 20  $\mu\text{m}$ . Particle screening or displacement of PMMA particles and

hexadecane oil in water emulsions were recorded on top of the microsieve (supplementary videos). For these more detailed videos that focused on the pores, a magnification of  $M=9$  was used with a resolution of 1 pixel = 2.3  $\mu\text{m}$ . The recording frequency varied between 0.5-2 kHz and the pulse duration between 2-20  $\mu\text{s}$  with a pulse power of 0.03-0.30 mJ/pulse.

### **Flow field visualization**

The pathlines were visualized by superimposing 200 consecutively recorded images. This new superimposed image only shows the maximum intensity of the all 200 images for each pixel position (z-stack, IMAGEJ 1.51S, NIH).

### **Dispersion preparation**

The model suspension was prepared with MilliQ water, 0.1wt% non-ionic surfactant (Triton X-100, Sigma Aldrich 9284) and 0.1 v/v% PMMA microspheres with an average diameter of 27  $\mu\text{m}$  (Cospheric, USA). The density of these particles was around 1.2 g/ml. The 0.1 v/v% oil in water emulsion was prepared with hexadecane (Sigma Aldrich 6703), 0.5 w/v% BiPRO Whey Protein Isolate (Davisco Foods, USA) and MilliQ water and was homogenised at 8000 RPM for 15 minutes using an Ultra-turrax digital T25 (IKA, USA). The 1 v/v% and 5 v/v% oil in water emulsions were prepared with hexadecane (Sigma Aldrich 6703), 1w/v% BiPRO WPI (Davisco Foods, USA) and MilliQ water and was homogenised at 9000 RPM for 15 minutes using an Ultra-turrax digital T25 (IKA, USA). Particles and droplets in the proximity of the microsieve have a  $Re_p = \rho V d^2 / \mu H \ll 1$  and  $Stk = \tau V / l \ll 1$ . Here  $\rho$  is the density of the fluid with a viscosity  $\mu$  flowing at a velocity  $V$ ,  $d$  is the particle diameter and  $H$  is the channel height (4 mm). The relaxation time is depicted by  $\tau$  and  $l$  is the length of a pore in flow direction (50  $\mu\text{m}$ ). The particle size distributions used for the concentration distributions in *Figure 6.7* were measured with the EyeTech particle size analyser (Ankersmid, The Netherlands).

## Experimental setup

A cross-flow microsieve module was manufactured as is shown in *Figure 6.2*. The channels were milled into transparent Poly methyl methacrylate (PMMA) plate. The main channel was 150 mm (y) by 4 mm (x) by 7 mm (z) and the side channel was 15 mm (y) by 40 mm (x) by 7 mm (z) with a microsieve (Veco B.V., The Netherlands) in between. This sieve was 15 mm long, 7 mm wide and 0.05 mm thick and had pores of  $55\pm 2\ \mu\text{m}$  by  $500\pm 5\ \mu\text{m}$  placed with a spacing of  $45\pm 2\ \mu\text{m}$  from each other in all directions on the top side. The pores at the bottom, however, were smaller because of the production process; they were  $30\pm 2\ \mu\text{m}$  by  $475\pm 2\ \mu\text{m}$  with a spacing between the pores of  $70\pm 2\ \mu\text{m}$  in all directions. The dispersed system was collected in a collection vessel and pumped (Masterflex L/S, Cole Parmer, US) to a pressure vessel to dampen the pulsations. The suspension was continuously recirculated through the system at the selected volumetric flow rate until the flow stabilized. The permeate flow rate was controlled by a needle valve.

## 6.4. Results and discussion

### Numerical simulation of deterministic displacement in the cross-flow module

A cross-flow microsieve module (CFM) was numerically simulated in 2D, with COMSOL 5.3. A range of inlet and outlet flow velocities was simulated to find the best balance between the velocity of the bulk flow across the microsieve ( $V_y$ ) and the velocity of the fluid flowing through pores of  $50\ \mu\text{m}$  ( $V_x$ ) [101].

We show three different operating conditions and how these affect the  $V_y/V_x$  ratio along the microsieve (*Figure 6.3*): one where the permeate flow, relative to the cross flow, is too low (B); one where the permeate flow and cross flow velocity are in balance (C); and one where the permeate flow relative to the cross flow is too high (D). If the permeate flow is low, the  $V_y/V_x$  ratio becomes negative at the end of the channel: the direction of the flow reverses and fluid

flows back into the main channel (*Figure 6.3AB*). This happens when the pressure drop in the main channel is larger than the pressure drop over the microsieve and limits the length of a single microsieve. In the situation that the permeate flow (and pressure difference over them membrane) is too high,  $V_y/V_x$  decreases across the length of the sieve (*Figure 6.3AD*); as a result, the flow lanes gradually become larger and particles may no longer be separated (*Figure 6.4*). For separation, one should therefore balance the cross-flow velocity ( $V_y$ ) with the velocity of the fluid flowing through the pores ( $V_x$ ) (*Figure 6.3AC*). The size of the flow lanes for the three situations illustrated in *Figure 6.3* are shown in *Figure 6.4*.

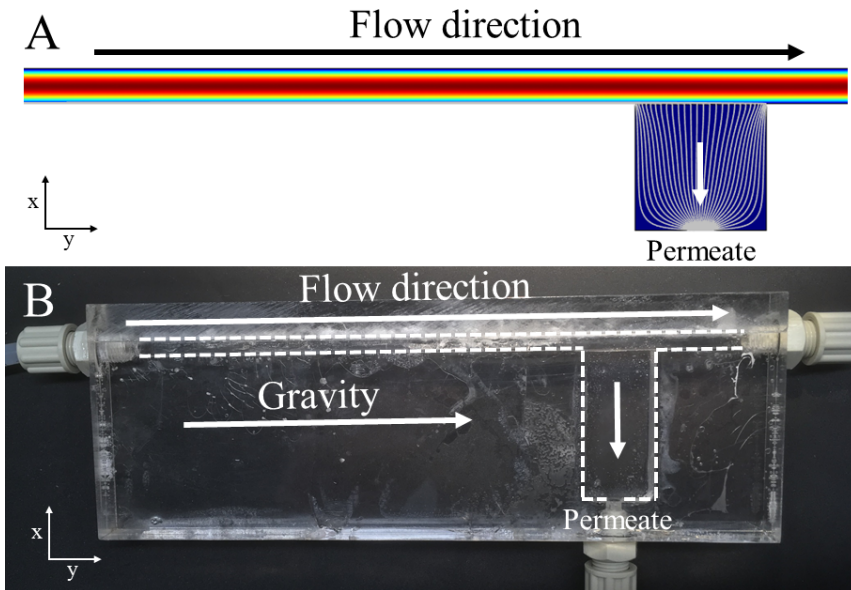


*Figure 6.2:* A) 2D model of microsieve module with the main channel at the top (fluid flowing from left to right), and a side channel with in between a microsieve. The colour indicates the velocity magnitude (from red to blue indicates from high to low) and the stream lines are shown in grey. (B) The cross flow microsieve module used for the experiments (white dotted lines are drawn to guide the eye). The microsieve module was placed such that the flow direction was from top to bottom ( $y$ ) and the permeate flow to the side ( $x$ ).

These simulations suggest that it is possible to create uniform flow lanes within the cross-flow microsieve module by adjusting the hydrodynamic conditions. Particles will be displaced when their radius is larger than the width of a flow lane implying that their centre of mass falls outside the flow lane. Because flow lanes are smaller for low permeate flows (*Figure 6.4*), these conditions can separate the smallest particles (diameter of  $\sim 30 \mu\text{m}$ ), while the pores are  $50 \mu\text{m}$ . However, the overall permeate flow is small and a reversed flow is observed. A too high permeate flow relative to the cross-flow will increase the size of the flow lanes (*Figure 6.4*) and therefore the critical particle diameter will also be larger ( $\sim 60 \mu\text{m}$ ). This means that the only particles that are separated are particles larger than the pores ( $50 \mu\text{m}$ ) or in other words, they are filtered.

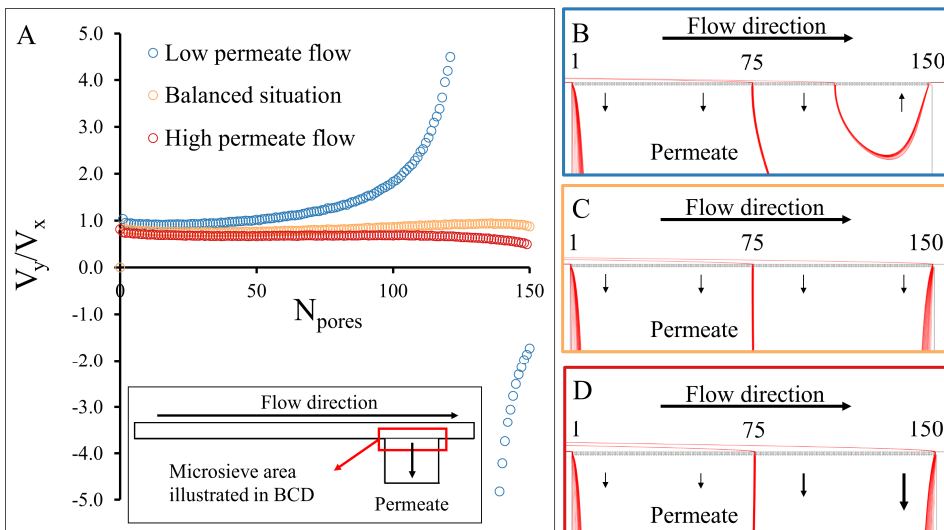


*Figure 6.3:* (A) The ratio between  $V_y$  and  $V_x$  (velocity on the boundary of the pores and main channel) for three different situations over the microsieve. (BCD) Flow lanes in red are shown in a cross-flow microsieve module (the location of BCD is indicated by the red box in A) with the feed fluid flowing from left to right over 150 pores, a microsieve in the middle and on the bottom the permeate. Three flow lanes (red) visualize the flow field for three situations with equal inlet flow velocity (0.3 m/s): (B) a low permeate flow velocity (0.5 mm/s), (C) the balanced situation (1.0 mm/s) and (D) a higher permeate flow (1.3 mm/s).

In the intermediate situation (*Figure 6.4*) where the cross flow ( $V_y$ ) and the permeate flow ( $V_x$ ) are balanced, the flow lanes are of equal size ( $17 \mu\text{m}$ ) over the entire sieve. This balanced situation can separate particles with a diameter of  $\sim 34 \mu\text{m}$ , which is smaller than the pore size ( $50 \mu\text{m}$ ).

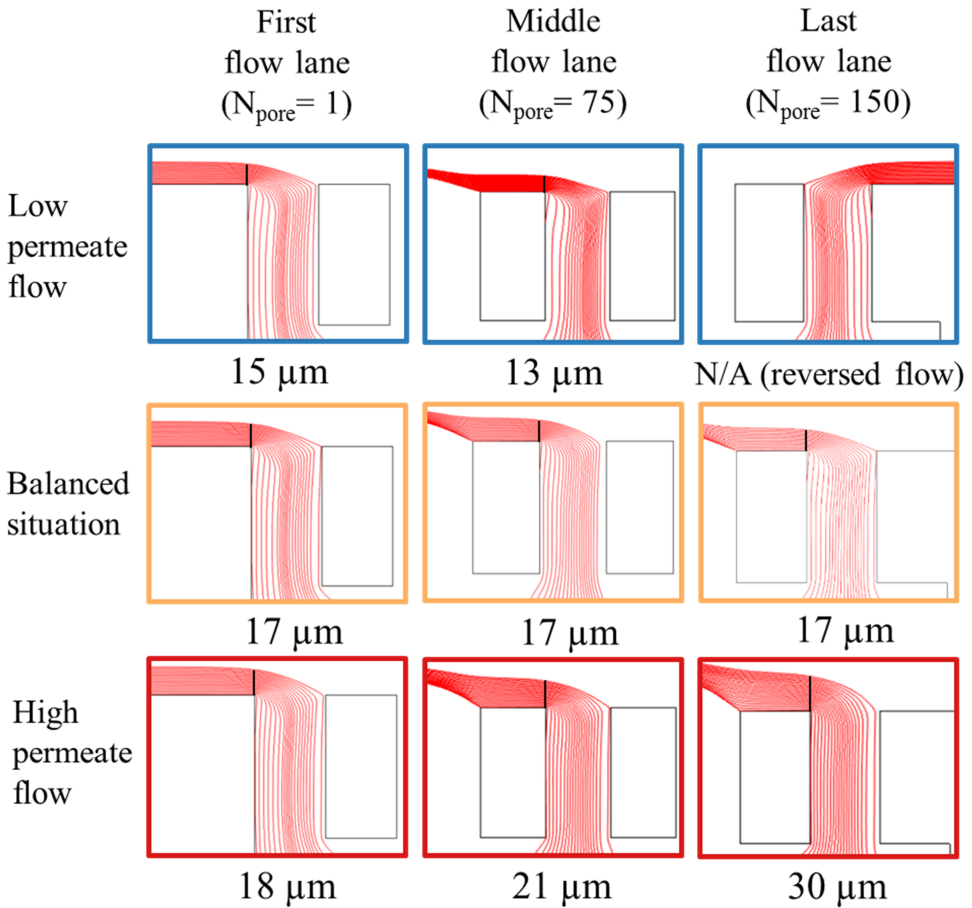


*Figure 6.4:* Close up of the flow lanes shown in *Figure 6.3*, indicating the flow lane width at the start ( $N_{\text{pore}}=1$ ), in the middle ( $N_{\text{pore}}=75$ ) and at the end ( $N_{\text{pore}}=150$ ) of the microsieve for different operation conditions. Streamlines are shown in red and the little black lines indicate the width of the flow lanes. The width of the pores is  $50 \mu\text{m}$ .

### High speed imaging of the fluid flow for model validation

A cross-flow module with a microsieve was constructed to validate the numerical simulations (*Figure 6.2*). Small tracer particles (2  $\mu\text{m}$ ), that were not retained, were introduced and recorded to visualize the flow field. The system was operated with an average cross-flow velocity ( $\bar{V}_y$ ) of 0.3 m/s (500 ml/min and Re of  $\sim 1200$ ) and three different average permeate flow velocities ( $\bar{V}_x$ ). The experimental recordings of the high speed camera were superimposed to visualize the path lines of particles flowing through the sieve, subsequently these were overlaid with the simulated streamlines (*Figure 6.5*). Similar to the simulations, a reversed flow was observed with a permeate flow velocity of  $\sim 0.6$  mm/s (4 ml/min). The reversed flow disappeared after increasing the permeate flow velocity to  $\sim 1.1$  mm/s (7 ml/min) and with these conditions the cross-flow velocity and the permeate flow velocity appeared to be balanced. Further increasing the permeate flow velocity to an extreme permeate flow velocity of  $\sim 28.6$  mm/s (180 ml/min) led to a situation with very large flow lanes which will drag particles that are smaller than the pores through the microsieve. The experimental pathlines were qualitatively similar to those simulated with the 2D model. Following these results, we established hydrodynamic conditions that would enable displacement of particles targeted for separation, which are larger than the tracer particles but smaller than the pores in the microsieve.

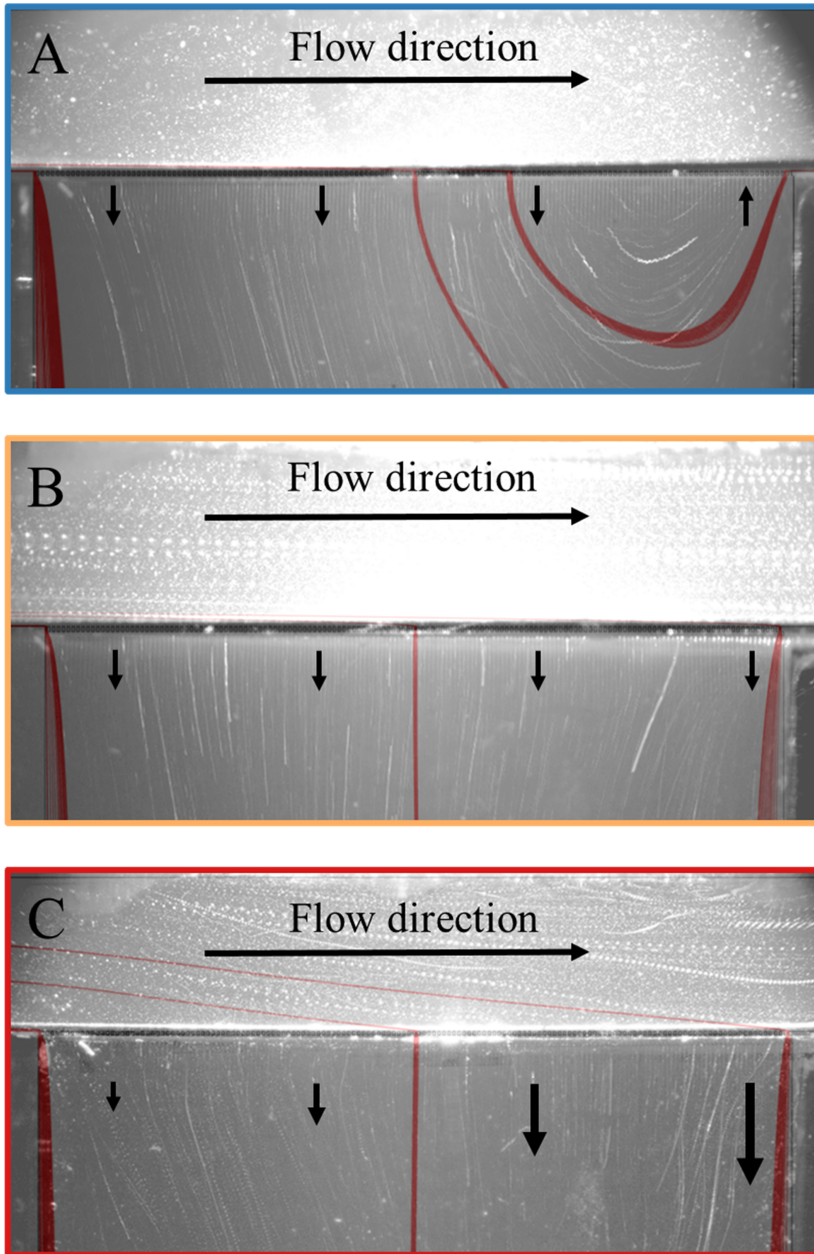


Figure 6.5: Experimental visualized flow field in CFM module with an average inlet flow velocity of 0.3 m/s and three different average permeate flow velocities: (A) a low average permeate flow velocity (~0.6 mm/s), (B) a balanced situation (~1.1 mm/s) and (C) an extreme average permeate flow velocity (~28.6 mm/s).



### Particle and droplet displacement in the cross-flow device

Experiments were conducted to investigate to what extent particles can be displaced in the module with varying conditions. Because we could not measure the local velocity components ( $V_y$  and  $V_x$ ) in the pores as in the numerical simulations, the experimental operation conditions are described using the average cross-flow velocity ( $\bar{V}_y$ ) in the channel and the average permeate flow velocity ( $\bar{V}_x$ ) flowing through the microsieve. The experimental velocity ratio ( $\bar{V}_y/\bar{V}_x$ ) was, therefore, much higher than the local velocity ratio ( $V_y/V_x$ ) obtained from the numerical simulations. The system was operated with an average cross-flow velocity of 0.6 m/s (~1000 ml/min Re of ~2400, which is in the transition regime) and the average permeate flow velocity was varied ranging between 0.4 mm/s (~2 ml/min) and 7.9 mm/s (~50 ml/min), which is equivalent to a permeate flux of 1480 L/m<sup>2</sup>/h and 22860 L/m<sup>2</sup>/h with a transmembrane pressure of 15±5 mbar. The permeate flux in the balanced situation was close to 4000 L/m<sup>2</sup>/h (Figure 6.5). The fluxes applied in this study are of similar magnitude compared to those used by others that used microsieves for cross-flow microfiltration [5, 12, 105, 106]. However, the flux is several times higher compared to the fluxes reported in other studies for conventional membrane microfiltration of oil-in-water emulsions (50-1200 L/m<sup>2</sup>/h) [107-109].

First, we performed concentration experiments using a model suspension of 0.1 v/v% rigid PMMA particles. Subsequently, we investigated the displacement of deformable hexadecane droplets in an oil in water emulsion with different concentrations (~0.1v/v%, ~1v/v% and 5v/v%) (Figure 6.6). The transmission is a measure of the separation; it is the ratio of the concentration of particles or droplets in the permeate over their concentration in the feed. The transmission is expected to vary with the flow conditions described by the ratio between  $\bar{V}_y/\bar{V}_x$ . The x-axis shows the applied velocity ratio and the y-axis transmission. To highlight the regions of the three operational conditions (discussed above), the graph is subdivided in three sections: a high permeate flow velocity (red), a balanced situation (orange) and a low permeate flow velocity (blue) (Figure 6.6). A high permeate flow velocity would be desired to make

effective use of the total microsieve surface area, however particles will not be displaced in that situation and will be transmitted through the microsieve. Alternatively, a low transmission at a low permeate flow velocity would be desired for optimal recovery, but then the microsieve surface area is not used effectively because the flow reverses near the end of the microsieve. The optimal condition for this microsieve module is therefore the balanced flow situation where transmission and operation conditions lead to high displacement at still reasonable permeate flux.

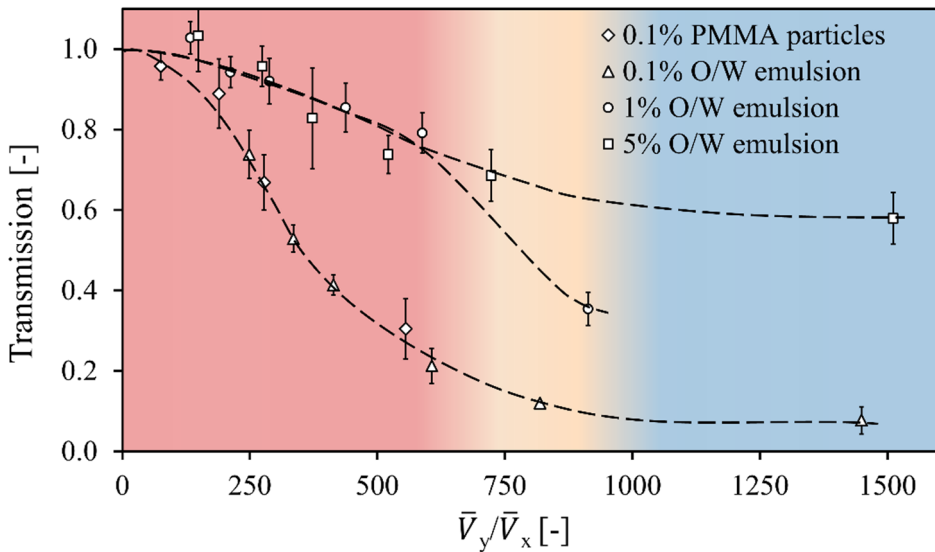


Figure 6.6: Displacement of PMMA particles and Hexadecane oil droplets in water for three concentrations. The transmission decreases for an increasing velocity ratio ( $\bar{V}_y/\bar{V}_x$ ). The red section indicates the region where  $\bar{V}_x$  is too high for particle displacement, the blue section indicates the region where  $\bar{V}_x$  is too low and reversed flow is observed. The orange region shows the situation where  $\bar{V}_y$  and  $\bar{V}_x$  are balanced and particles or oil droplets are displaced using the DLD separation principle. The black dashed lines are drawn to guide the eye.

The transmission indeed decreases with an increasing velocity ratio ( $\bar{V}_y/\bar{V}_x$ ). The trend observed for the dispersions with concentration of 0.1 v/v% is similar to the situation described by Dinther et al., although with a different interpretation [12]. The rigid PMMA particles

behave quite similar to the hexadecane droplets and suggests that separation is not significantly influenced by possible deformation of the droplets at these low concentrations. The stresses exerted by the flow ( $V = 0.1$  m/s) on the hexadecane droplets ( $\sigma = 53.5$  mN/m and  $d = 25$   $\mu\text{m}$ ) near the microsieve surface are insufficient to deform the droplets ( $Ca = \mu V/\sigma \ll 1$  and  $We = \rho V^2 d/\sigma \ll 1$ ). However, droplet-microsieve collisions can deform (flatten) the droplets and have a negative impact on separation. In the supplementary videos some deformation can be observed if looked at closely. The limited effect of deformability on separation is very interesting for separation of applications with particles or droplets of  $0.1$   $\mu\text{m}$  to  $10$   $\mu\text{m}$  that have a density close to that of the liquid phase, like many emulsions and cells. It should be noted that the data of the rigid PMMA particles are limited to low concentrations and low  $\bar{V}_y/\bar{V}_x$  (red region); therefore, we are cautious with conclusions about the limited effect of deformability on separation. For higher concentrations (1v/v% and 5 v/v%) one can observe that separation is less effective and that the transmission declines at higher velocity ratio ( $\bar{V}_y/\bar{V}_x$ ) compared to the low concentration (0.1v/v%). The initial decline of 1v/v% and 5v/v% is similar but they diverge at higher  $\bar{V}_y/\bar{V}_x$ . For additional information on the results in Figure 6, the particle size distributions was measured of the particles that transmitted the microsieve and multiplied with the corresponding concentration (Figure 6.7).

Figure 6.7A shows the particle concentration distribution of the PMMA particles (feed concentration of 0.1 v/v%) for several velocity ratios. Figure 6.7BCD show the particle concentration distribution of the hexadecane droplets in water, with a feed concentration of 0.1 v/v% in B, 1 v/v% in C and a concentration of 5 v/v% in D. The reduction in transmission for a low feed concentration (0.1 v/v%) shown in Figure 6.6 can also be observed in the concentration distribution (Figure 6.7AB). The concentration distribution decreases with increasing  $\bar{V}_y/\bar{V}_x$  and Figure 6.7B shows that the average particle size in the permeate becomes smaller. Figure 6.7CD shows the particle concentration distributions of the permeate stream for experiments with a feed concentration of 1 v/v% and 5 v/v%. The concentration

distributions in *Figure 6.7CD* do not shift towards smaller droplets as is clear for the lower concentration in *Figure 6.7B*; even though a minor shift can be observed for the highest  $\bar{V}_y/\bar{V}_x$  values. *Figure 6.7BCD* underpins the results shown in *Figure 6.6* that separation becomes less effective with increasing feed concentration. The influence of the feed concentration on the separation and particle concentration distribution can be a result of particle-particle interactions (in this case droplet-droplet interaction). The frequency of these interactions depends on the square of the concentration of the particles. However, presence of a concentrated layer of particles or droplets will affect the hydrodynamics in the system and influence the hydrodynamic balance and the flow lanes [34, 110, 111]. This can affect the hydrodynamic regions (the red, orange and blue sections) in which particles can be displaced and reduce the effectiveness of the separation principle.

*Figure 6.7E* shows scanning electron microscopic (SEM) images of the microsieves. The dimensions of the pores at the top surface of the microsieves were  $55\pm 2\ \mu\text{m}$  by  $500\pm 5\ \mu\text{m}$ , but the dimensions of the pores at the bottom surface of the microsieves were  $30\pm 2\ \mu\text{m}$  by  $475\pm 5\ \mu\text{m}$ , which is a consequence of the electroforming process. The influence of the tapered pore shape on the flow lanes was inspected using numerical simulation. Minor effects were observed on the pressure drop across the membrane at the highest cross-flow velocities, which stabilized the pressure distribution along the microsieve and the flow lane size. The size of the pores at the bottom of the microsieves ( $30\ \mu\text{m}$ ) does not affect separation because particle displacement only occurs at the top surface of the microsieve (supplementary videos). If a particle or droplet enters a pore they either get stuck in the pore or leave via the permeate flow. The smaller pore size at the bottom did not affect our results because it can be observed that for a low  $\bar{V}_y/\bar{V}_x$  ratio (range where conventional sieving takes place), also droplets larger than  $30\ \mu\text{m}$  were found in the permeate flow (*Figure 6.7BCD*). These oil droplets were exposed to enough stress for them to deform and pass the lower, narrower end of the pores.

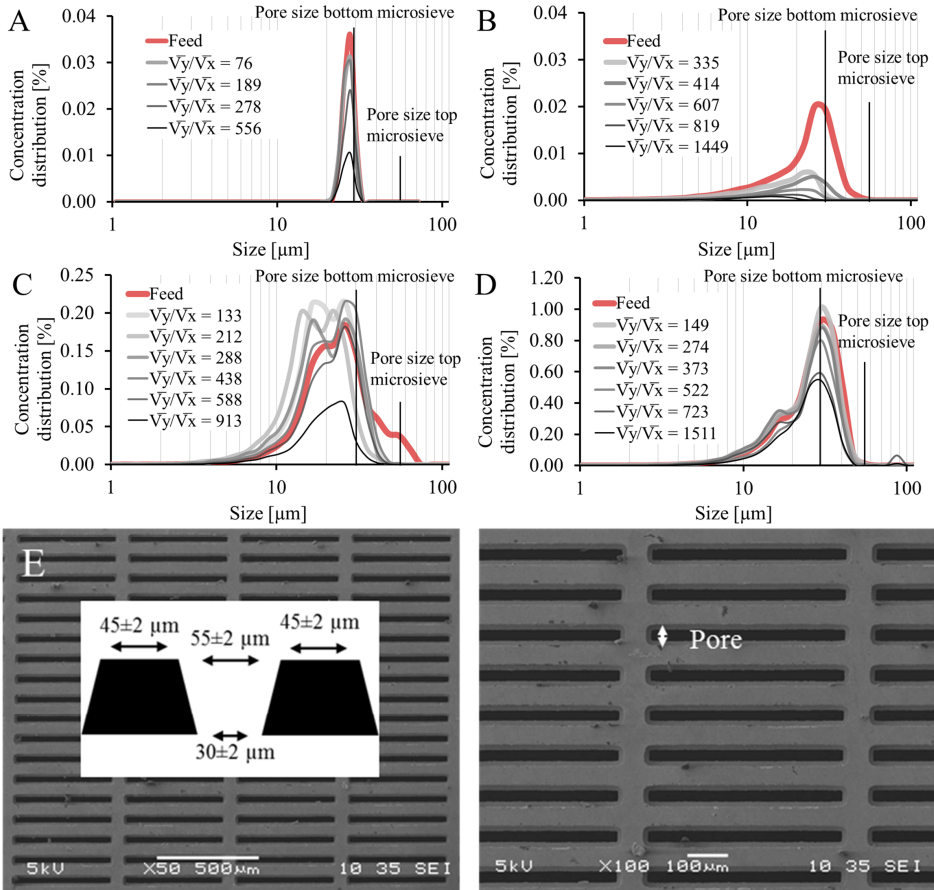


Figure 6.7: Particle concentration distribution of the permeate (Figure 6.6) with lines to indicate the size of the pores on both sides of the microsieve. The feed contained: (A) 0.1 v/v% PMMA particles, (B) 0.1 v/v% hexadecane, (C) 1 v/v% hexadecane and (D) 5 v/v% hexadecane. (E) SEM images of a representative microsieve that was used in the experimental module with different magnification ( $\times 50$  and  $\times 100$ ). IMAGEJ was used to measure the size of the pores (top:  $55 \pm 2 \mu\text{m}$  by  $500 \pm 5 \mu\text{m}$  and bottom:  $30 \pm 2 \mu\text{m}$  by  $475 \pm 5 \mu\text{m}$ ).

These results demonstrate that our hypothesis is correct; particle displacement does *not* require a distinct DLD design (e.g. angle, size of the gaps or obstacle size) but can be achieved by control of the hydrodynamic conditions, and can even be applied to existing separation techniques such as microfiltration. This proves the potential of the deterministic lateral displacement separation principle for dispersion separation on industrial scale.

## 6.5. Conclusion

Deterministic displacement of dispersions was successfully achieved in a cross-flow microsieve module that had pores *larger* than the diameter of the rigid particles or deformable oil droplets to be separated. It was shown that the separation depends on the ratio of crossflow velocity to the permeate velocity. This was confirmed for varying operating conditions and verified with high speed imaging. Concentration experiments with particles and droplets showed successful separation at the appropriate operation conditions and the existence of an optimum range with acceptable permeate flux and particle displacement. With higher concentrations, the performance of the separation declines. Our results show that the deterministic displacement principle can be applied in cross-flow microsieve devices. This facilitates the design of a system that can use a microfluidic separation principle to process neutrally buoyant and deformable dispersions on an industrial scale with lower energy requirements.







# Seven

## General discussion and outlook

I often listened to *Wake Up* from *AWOLNATION* during the writing of this chapter

## 7.1. Introduction

This thesis reports on the separation of particles and/or droplets from dispersions by deterministic lateral displacement (DLD), which is a microfluidic separation principle that could potentially be applied at an industrial scale. The technique is promising because it allows separation of particles and/or droplets that are *smaller* than the smallest gaps in a DLD device, thereby reducing risk of internal fouling and minimising pressure drop. Translation of this technique towards industrial production volumes would be a breakthrough, even though it is a challenge. Larger-scale DLD systems were constructed using microsieves that can process much larger volumes compared to a single microfluidic device. For this purpose, we investigated the influence of the system design and hydrodynamics on the separation performance. These investigations provided additional understanding of the separation principle, which in its turn led to the proposition of a more conventional and scalable process, which is a hybrid between DLD and microfiltration. This latter device meets the original objective of this study to develop a scalable device based on a combination of microsieve(s) and microfluidic DLD technology.

The main findings and conclusions of our investigations are discussed in this chapter. Subsequently, we evaluate the feasibility of the cross-flow microsieve module and qualitatively compare it with conventional microfiltration. Following, we provide an outlook to discuss further research required to develop CFM into large-scale technology that are robust towards different applications.

## 7.2. Main findings

Microfiltration may be considered state-of-the-art technology to separate particles with sizes  $0.1 - 10 \mu\text{m}$  from suspensions for industrial production volumes. More recently new microfluidic separation techniques have been developed that may have potential to be translated to industrial volumes. Even though the throughput of microfluidic techniques can be directly increased by placing systems in parallel, volumetric scale up is preferred for use on industrial scale, because it reduces the required amount of materials per unit output (economy of scale). Besides, the possibility to place systems in parallel after increasing the single-unit throughput remains. The latter appears especially feasible for inertial microfluidic separation devices, such as DLDs. Therefore, a qualitative comparison was made between state-of-the-art microfiltration systems with various hydrodynamic techniques to enhance separation and several inertial microfluidic systems for their potential on industrial scale (*Chapter 2*). The three most promising techniques were: fluid skimming microfiltration, sparse lateral displacement and an inertial spiral microchannel for which we illustrated their conceptual large-scale design. Even though these three techniques may be promising, each requires further research before they can be applied on industrial scale.

The throughput of a sparse lateral displacement array can be increased by making the channel cross-section larger, which is possible by using taller obstacles. However, tall obstacles are too vulnerable and break easily, rendering the process too fragile. A possible solution to increase the mechanical strength of the obstacles is to use (micro)sieves instead. Microsieves having long parallel slots as pores, are a mechanically stronger alternative because they basically represent an array of interconnected, infinitely long obstacles. In *chapter 3*, a study is presented on increasing the throughput of a sparse lateral displacement device by replacing obstacle columns by sieves. The system was operated using sieves that varied in porosity, but the particle concentration in the targeted outlet did not increase substantially. We found that to separate particles in the targeted outlet, it is necessary to keep the pressure difference along the length

of sieve constant. A constant pressure difference along the sieve was achieved by changing the outflow conditions. This improved the separation and confirmed the possibility to displace particles with a sieve-based lateral displacement device, although only under the correct operating conditions.

Displacing particles with a sieve-based lateral displacement device was successful but existing theoretical design rules do not apply. For this reason, in *chapter 4* we discussed the influence of the geometric parameters on particle displacement in a sieve-based lateral displacement systems and showed the differences compared to an original (asymmetric) DLD system. Using 2D computational fluid dynamics (CFD), the velocity profiles for systems of different size was simulated, and the effects of it on the critical particle diameter along the length of the channel was shown. These results provided the basis of our hypothesis that the hydrodynamics can be used to control the flow lanes and thus the separation.

The influence of the local hydrodynamics on separation was investigated in a sieve-based lateral displacement system. To investigate the hydrodynamics, the flow velocity field was quantified using  $\mu$ PIV (microscopic particle image velocimetry), which was compared with 2D numerical simulations in *chapter 5*. This demonstrated the direct influence of the flow velocity on the size of the flow lanes and therefore, the local flow velocity near the pores was further analysed with CFD models. A relationship was found between the ratio of the velocity components of fluid near a pore (velocity ratio) and the size of the corresponding flow lane. Thus, careful control of the velocity ratio gives control of the size of the flow lanes and the critical particle diameter. This means that the separation characteristics are not only a function of the design of the device but also of the process conditions. As result, one can adjust the separation with the hydrodynamic, which makes scale up to process large volumes easier. Based on this idea, a simple cross-flow microfiltration like system was operated over a range of different flow conditions (velocity ratios) and evaluated for deterministic displacement of particles and oil droplets (*chapter 6*). 2D CFD simulations provided information on the

required hydrodynamic conditions to obtain stable flow lanes, which was verified by the experimentally visualized flow fields. In addition to the flow field, both particles and oil droplets were tracked to confirm whether they were deterministically displaced. The separation performance was evaluated by measuring the transmission for different feed concentrations. For a low feed concentration, the retention was high and no effect apparent of the deformability of oil droplets was observed. For an increased concentration of oil in the feed the performance declined.

On the basis of the results described in this thesis we can conclude that microsieves are promising elements for the construction of upscaled DLD-based separation devices that can process large volumes. In the process of replacing obstacles in deterministic lateral displacement devices by microsieves we obtained understanding of the DLD separation mechanism, which led to the concept for deterministically displacing particles in a much simpler hybrid microsieve-based device design, which increases the feasibility to implement the DLD principle on industrial scale.

### 7.3. Evaluation of feasibility deterministic displacement of dispersions on industrial scale

Deterministic displacement has potential to separate dispersions on an industrial scale because it allows amongst others separation of particles or droplets that are smaller than the smallest gaps in the system. This results in a lower pressure drop and lower risk of particles (irreversibly) blocking the gaps. However, deterministic displacement of dispersions on industrial scale is not (yet) feasible because current DLD systems are unable to process large volumes. Direct application of microfluidic DLD systems would require mass parallelization, which is not an effective strategy to scale-up to very large volumes. Therefore, alternative systems designs and operating conditions were investigated in this thesis to come up with a separation system that is able to handle increased throughput and is easier to manufacture.

The cross-flow microsieve (CFM) module was proposed to deterministically displace particles on large scale. In such a device separation mainly depends on the careful control of the hydrodynamic conditions and the geometry is of less importance. Because the geometry is less important, this system is simpler to manufacture and allows a certain range of control on the cut-off diameter by changing the hydrodynamic conditions. Here, the feasibility to deterministically displace particles on industrial scale is evaluated and compared to the current state-of-the-art technique cross-flow microfiltration.

### **Cross-flow microsieve module (CFM)**

#### *Future design & operation*

Insight into the influence of the hydrodynamics on particle separation was the inspiration to construct a cross-flow microsieve module (CFM). In this system the microsieve is positioned parallel to the initial feed flow direction. Since the sieve is not placed at an angle, the design can be simplified into a T-shaped flat sheet cross-flow module (*Figure 7.2AB*). As result, the construction of this system is straightforward and the throughput can easily be elevated by increasing the surface area of the microsieves. The microsieve in our system was 105 mm<sup>2</sup>. Increasing the area of the microsieves, however, must be accompanied by the required hydrodynamic balance (velocity ratio). There are two main approaches to increase the surface area without affecting the hydrodynamic balance in flow direction over a single microsieve. The most direct method is to extend the sieve dimensions in the transverse direction (z) with respect to the direction of the main flow. Even though it is, to a limited extent, also possible to increase the sieve dimensions in the longitudinal direction (y), this will (eventually) decrease the velocity in the main channel and thus affect the hydrodynamic balance and the separation performance. The second method to increase the surface area without affecting the hydrodynamic balance is to have multiple side channels in series with controlled permeate flow (*Figure 7.2C*).

Because the flow velocity in the main channel decreases after fluid is syphoned off by the side channels, the permeate flow of the consecutive side channels must also decrease to maintain the same hydrodynamic balance. The consequence is that the flux decreases for each consecutive compartment in downstream direction.

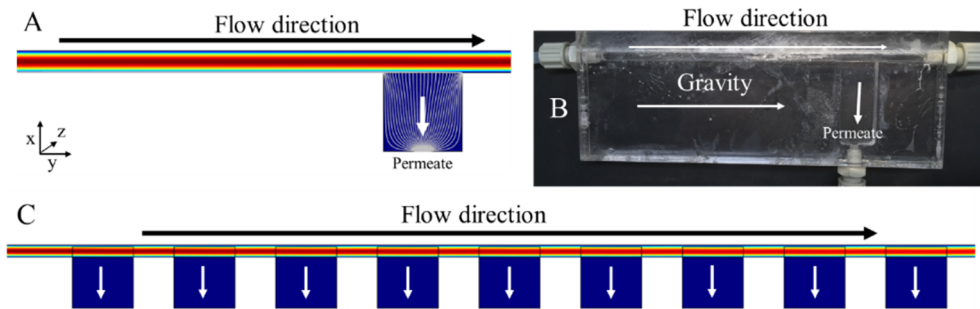


*Figure 7.2:* (A) A two dimensional CFD model of the cross-flow microsieve module. (B) The cross-flow microsieve module used for our experiments. The microsieve surface area was 105 mm<sup>2</sup>. (C) A conceptual design of a cross-flow microsieve module with a larger microsieve surface area and higher permeate flow. Red indicates a high flow velocity and blue a low flow velocity.

Even though the microsieve surface area can be increased, it is ambitious to achieve a similar surface area per module as currently is achieved in tubular or spiral wound modules, and maintain the required hydrodynamic balance. Furthermore, the specific hydrodynamic balance that is required to deterministically displace particles, limits the flux at which the system can be operated. A too high flux will cause more particles to pass through the microsieve, while a too low flux leads to inefficient use of the available microsieve surface area. Despite the fact that the flux is confined in a specific range by the separation principle, the possible flux is still estimated in the range of 2000 – 7000 L/m<sup>2</sup>/h, which is high compared to conventional microfiltration.

Deterministic displacement in a CFM system on large scale will operate at low transmembrane pressure, steady fluxes, and will exhibit less fouling. Because the (macroscopic) effects of fouling on particle displacement was not investigated in this thesis, we performed a preliminary

experiment to characterize the flux decline in a CFM system while processing an oil in water emulsion. The emulsion was prepared with demineralized water, 0.1w/v% BiPRO Whey Protein Isolate (Davisco Foods, USA) and 0.1v/v% (1000ppm) hexadecane (Sigma Aldrich 6703), and was homogenized at 9000 RPM for 15 minutes using an Ultra-turrax digital T25 (IKA, USA). The obtained emulsion had an average droplet diameter of 27  $\mu\text{m}$ . The pressure at the inlet and outlets were measured (Jumo Midas C18SW) and the permeate flow was determined with a balance. The emulsion was continuously recirculated through the system by pumping (Masterflex L/S, Cole Parmer, US) it from a collection vessel into a pressure vessel and back through the CFM module (Figure 7.3). The permeate flow was collected in a separate vessel.

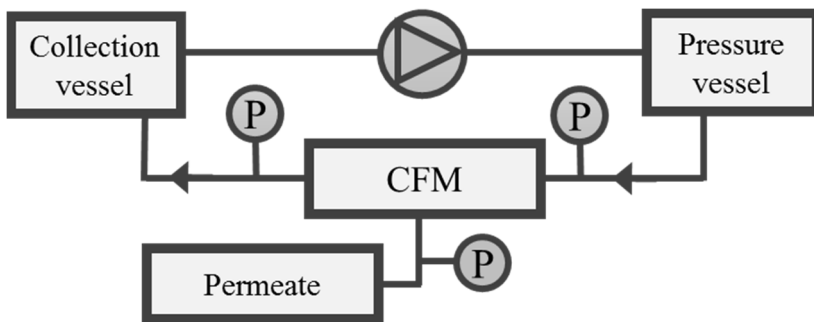


Figure 7.3: Scheme of the experimental setup. The pump is indicated by the symbol of the triangle inside the circle and the P shows the location of the pressure sensors.

#### Results & discussion

The flux and the pressure difference over the microsieve were measured while deterministically displacing oil droplets in water. During operation no hydrodynamic effects (e.g. back-flushing or back-pulsing) were used to maintain a high flux. The pressure difference was calculated using the pressure at the inlet and at the permeate outlet and was between 10 - 20 mbar. The highest permeate flow rate was 9.0 mL/minute after starting up the experiment after which it slowly declined to 5.4 mL/minute. Because of the small surface area of the microsieve, the measured flow rates correspond to a flux of 5140  $\text{L}/\text{m}^2/\text{h}$  and 3070  $\text{L}/\text{m}^2/\text{h}$  respectively.



Not taking outliers into account, the permeability falls between 100 000 and 500 000 L/m<sup>2</sup>/h/bar. The performance of oil/water separation in a the CFM module was evaluated by comparing it to cross-flow microfiltration experiments reported in literature [107]. Because different operational conditions were used, the systems are compared by normalizing the permeability (L/m<sup>2</sup>/h/bar divided by the initial L/m<sup>2</sup>/h/bar). The normalized permeability over time is shown in *Figure 7.4A*, in which indicates the rate of fouling in the CFM module and a conventional cross-flow microfiltration module. In addition, the normalized permeability is plotted against the total volume processed per filtration area (*Figure 7.4B*). It can be observed that the rate of fouling in both situations is less when oil droplets are deterministically displaced in a CFM module.

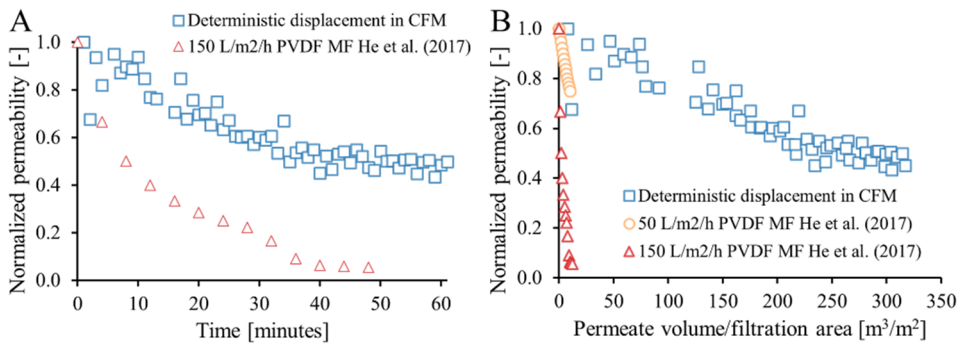


*Figure 7.4:* Performance of a cross-flow microsieve module deterministically displacing oil droplets (1000ppm) in an o/w emulsion compared with a polyvinylidene fluoride microfiltration (PVDF MF) membrane (1500ppm) [107]. (A) Shows the normalized permeability (L/m<sup>2</sup>/h/bar divided by the initial L/m<sup>2</sup>/h/bar) over time for two systems, where the PVDF MF module is operated above its threshold flux (57 L/m<sup>2</sup>/h). In (B) the normalized permeability is shown for total volume processed per filtration area for the CFM, for the PVDF MF module operated below the threshold flux (50 L/m<sup>2</sup>/h) and for the PVDF MF module operated above the threshold flux (150 L/m<sup>2</sup>/h).

In *Figure 7.4B* fouling in the PVDF MF module is reduced by operating it below a certain threshold flux (57 L/m<sup>2</sup>/h). It can be observed that fouling is less pronounced in the PVDF MF module operated with a constant flux of 50 L/m<sup>2</sup>/h (orange) compared to the system operated with a constant flux of 150 L/m<sup>2</sup>/h (red). However, the improvement is only small

compared to when oil droplets are deterministically displaced in a CFM module (blue). Note that the oil droplets and the pores in the microsieve were much larger compared to what is described by He et al., besides the influence of the different surfactants is not taken into account. Even though *Figure 7.4* cannot fairly be compared, the results give an impression of the benefits of deterministic displacement in a CFM module, namely, a high flux (for very low pressure difference across the microsieve) and a relatively low risk of (irreversible) fouling. Still, the decline of the permeability indicates that the CFM module also suffers from fouling.

### **Comparing the cross-flow microsieve module with microfiltration**

In this section we briefly discuss and compare deterministic displacement in the cross-flow microsieve module (CFM) with conventional microfiltration, which is used as benchmark. We should bear in mind that the cross-flow microsieve module is not yet mature and will need significant development before it is robust enough to operate at larger scales, while microfiltration is an established technique that has already been optimized over the years.

A first advantage of the CFM system is the low pressure difference across the microsieve, which simplifies the peripheral process considerably. Commonly, a crossflow microfiltration set-up needs two pumps: one for the recirculating loop, and one to pressurize the feed. Because of the low pressure difference across the microsieve no additional pump is needed to pressurize the feed.

A second advantage of deterministic displacement in the CFM system is its lower sensitivity to fouling, as demonstrated in this chapter. Of course this remains to be verified with different types of feed suspensions, and with different membrane materials and structures.

A third advantage of deterministic displacement is the possibility to easily separate deformable particles and (oil) droplets. Such dispersions are generally difficult to separate using microfiltration because they can rapidly foul the membrane or penetrate through the membrane.

A disadvantage of the CFM system is its more complex module design, which requires precise positioning of the sieves, and makes the design of inexpensive modules such as a spiral wound configuration, more difficult.

As discussed before, the construction and operation of this system will initially bring challenges because of its novelty. However, we expect that the lower transmembrane pressure, lower risk of (irreversible) pore blocking and the possibility to separate deformable particles or droplets will ultimately lower the operation costs, which makes separation based on deterministic displacement attractive.

## 7.4. Outlook for further research

Even though separation on the basis of deterministic displacement has advantages, still many questions remain. In this section, some remaining questions are discussed that should be addressed to completely understand the potential of deterministic displacement on a large scale. This thesis established better insight in the separation principles, and an indication of the feasibility of a cross-flow module that combines some of the advantages of deterministic lateral displacement (DLD) and microfiltration (MF). The next step would be to scale the systems from bench scale to pilot and commercial scales. This will involve much work on the exact module design.

The experiments were carried out with droplet and particles that were larger than is typically relevant for industrial separations, but required to enable direct microscopic visualization of the displacement performance. The principles found will also be valid for smaller particles and droplets as long as their size is larger than  $\sim 1 \mu\text{m}$ ; however, this remains to be verified.

Deterministic displacement of particles or droplets is less effective for more densely concentrated dispersions. The effect of concentration on particle displacement was previously investigated and connected to particle-particle interactions in the layer at the obstacle surface

[60]. In addition to particle-particle interactions, hydrodynamic interaction of multiple particles can affect the fluid flow [34, 110, 111]. If the concentrated layer of particles on the microsieve surface indeed disturb the flow (lanes) it may affect particle separation. While the DLD separation principle is mostly suitable for applications with relatively dilute dispersions, system design will certainly be of influence on the maximum volume fraction that can be successfully processed. Fouling is intrinsic to technologies that use membranes and/or physical interactions between particles and structures. Thus, fouling also occurs in deterministic displacement systems as was observed in *Figure 7.4*. However, the fact that the dimensions of a typical gap or pore can be larger than the particles that are separated, makes deterministic displacement techniques intrinsically less susceptible to fouling. However, other fouling mechanisms can still increase the membrane resistance overtime. For instance, when particles or droplets adsorb onto the microsieve surface or in the pores. Fouling during deterministic displacement in a cross-flow microsieve module should be further studied to confirm whether the risk of (irreversible) fouling is indeed reduced.

## 7.5. Conclusions

Dispersed systems can be separated with various techniques, each with its benefits and drawbacks. This thesis showed the possibility to use a microfluidic dispersion separation principle, called deterministic lateral displacement (DLD), in a system design(s) that can be scaled up more easily to process large volumes.

This thesis has contributed to more efficient and more resource efficient separations compared to existing techniques. For one, the gaps (pores) are larger than the diameter of the particle or droplets of dispersed phase, which lowers the required transmembrane pressure and lowers the risk of (irreversible) fouling. The second reason is that the used microsieves can be very thin and have a high porosity. Besides, microsieves are made of inert material, which is easier to clean. Especially hybrid techniques, such as the combination of the DLD and MF, may offer the best of both worlds.



# References

One of my favorite songs while reading these articles was *Strong* from *London Grammar*

1. Wakeman, R., *The influence of particle properties on filtration*. Separation and Purification Technology, 2007. **58**(2): p. 234-241.
2. Wakeman, R.J., *Selection of equipment for solid/liquid separation processes*. Filtration & Separation, 1995. **32**(4): p. 337-341.
3. Jaffrin, M.Y., *Hydrodynamic techniques to enhance membrane filtration*. Annual Review of Fluid Mechanics, 2012. **44**: p. 77-96.
4. Warkiani, M.E., et al., *Investigation of membrane fouling at the microscale using isopore filters*. Microfluidics and Nanofluidics, 2015. **19**(2): p. 307-315.
5. Kuiper, S., et al., *Ceramic microsieves: influence of perforation shape and distribution on flow resistance and membrane strength*. Journal of Membrane Science, 2002. **196**(2): p. 149-157.
6. Kuiper, S., et al., *Development and applications of very high flux microfiltration membranes*. Journal of Membrane Science, 1998. **150**(1): p. 1-8.
7. Whitesides, G.M., *The origins and the future of microfluidics*. Nature, 2006. **442**(7101): p. 368-373.
8. Sajeesh, P. and A.K. Sen, *Particle separation and sorting in microfluidic devices: a review*. Microfluidics and Nanofluidics, 2013. **17**(1): p. 1-52.
9. Kulrattanak, T., et al., *Classification and evaluation of microfluidic devices for continuous suspension fractionation*. Advances in Colloid and Interface Science, 2008. **142**(1-2): p. 53-66.
10. Lubbersen, Y.S., *Deterministic ratchets for large-scale separation of suspensions*. 2014, Wageningen University: Wageningen.
11. Belfort, G., R.H. Davis, and A.L. Zydney, *The Behavior of suspensions and macromolecular solutions in crossflow microfiltration*. Journal of Membrane Science, 1994. **96**: p. 1-58.
12. van Dinther, A.M.C., C.G.P.H. Schroën, and R.M. Boom, *High-flux membrane separation using fluid skimming dominated convective fluid flow*. Journal of Membrane Science, 2011. **371**(1-2): p. 20-27.
13. Altena, F.W. and G. Belfort, *Lateral migration of spherical particles in porous flow channels: application to membrane filtration*. Chemical engineering science, 1984. **39**(2): p. 343-355.



14. van Dinther, A.M.C., *Understanding flow-induced particle migration for improved microfiltration*. 2012, Wageningen University: Wageningen.
15. Winzeler, H.B. and G. Belfort, *Enhanced performance for pressure-driven membrane processes: the argument for fluid instabilities*. *Journal of Membrane Science*, 1993. **80**: p. 35-47.
16. Brans, G., et al., *Membrane fractionation of milk: state of the art and challenges*. *Journal of Membrane Science*, 2004. **243**(1-2): p. 263-272.
17. Schutyser, M. and G. Belfort, *Dean Vortex Membrane Microfiltration Non-Newtonian Viscosity Effects*. *Industrial & Engineering Chemistry Research*, 2002. **41**(3): p. 494-504.
18. Li, H.-y., C.D. Bertram, and D.E. Wiley, *Mechanisms by which pulsatile flow affects cross-flow microfiltration*. *American Institute for Chemical Engineers*, 1998. **44**: p. 1950-1961.
19. Knol, H.G., *Sieve material of metal, and method for its production*. 2010.
20. Gironès, M., et al., *Polymeric microsieves produced by phase separation micromolding*. *Journal of Membrane Science*, 2006. **283**(1-2): p. 411-424.
21. Femmer, T., A.J.C. Kuehne, and M. Wessling, *Print your own membrane: direct rapid prototyping of polydimethylsiloxane*. *Lab on a Chip*, 2014. **14**(15): p. 2610-2613.
22. van Dinther, A.M.C., C.G.P.H. Schroën, and R.M. Boom, *Particle migration leads to deposition-free fractionation*. *Journal of Membrane Science*, 2013. **440**(0): p. 58-66.
23. Davis, R.H. and D.T. Leighton, *Shear-induced transport of a particle layer along a porous wall*. *Chemical Engineering Science*, 1987. **42**(2): p. 275-281.
24. Kromkamp, J., *Particle separation and fractionation by microfiltration*. 2005, Wageningen University: Wageningen, the Netherlands.
25. Mondor, M. and C. Moresoli, *Experimental verification of the shear-induced hydrodynamic diffusion model of crossflow microfiltration, with consideration of the transmembrane pressure axial variation*. *Journal of Membrane Science*, 2000. **175**(1): p. 119-137.
26. Di Carlo, D., *Inertial microfluidics*. *Lab on a Chip*, 2009. **9**(21): p. 3038-3046.
27. Martel, J.M. and M. Toner, *Inertial Focusing in Microfluidics*. *Annual Review of Biomedical Engineering*, 2014. **16**(1): p. 371-396.

28. Amini, H., W. Lee, and D. Di Carlo, *Inertial microfluidic physics*. Lab on a Chip, 2014. **14**(15): p. 2739.
29. Zhou, J. and I. Papautsky, *Fundamentals of inertial focusing in microchannels*. Lab Chip, 2013. **13**: p. 1121-1132.
30. Segre, G. and A. Silberberg, *Radial Particle Displacements in Poiseuille Flow of Suspensions*. Nature, 1961. **189**(4760): p. 209-210.
31. Bhagat, A.A.S., S.S. Kuntaegowdanahalli, and I. Papautsky, *Inertial microfluidics for continuous particle filtration and extraction*. Microfluidics and Nanofluidics, 2008. **7**(2): p. 217-226.
32. Amini, H., et al., *Engineering fluid flow using sequenced microstructures*. Nature Communications, 2013. **4**: p. 1826.
33. Chung, A.J., et al., *Microstructure-induced helical vortices allow single-stream and long-term inertial focusing*. Lab on a Chip, 2013. **13**(15): p. 2942.
34. Amini, H., et al., *Intrinsic particle induced lateral transport in microchannels*. PNAS, 2012. **109**(29): p. 11593-11598.
35. Bhagat, A.A.S., S.S. Kuntaegowdanahalli, and I. Papautsky, *Continuous particle separation in spiral microchannels using dean flows and differential migration*. Lab on a Chip, 2008. **8**(11): p. 1906.
36. Di Carlo, D., et al., *Continuous inertial focusing, ordering, and separation of particles in microchannels*. Proceedings of the National Academy of Sciences, 2007. **104**(48): p. 18892-18897.
37. Guan, G., et al., *Spiral microchannel with rectangular and trapezoidal cross-sections for size based particle separation*. Sci. Rep., 2013. **3**.
38. Di Carlo, D., et al., *Particle Segregation and Dynamics in Confined Flows*. Physical Review Letters, 2009. **102**(9).
39. Bhagat, A.A.S., S.S. Kuntaegowdanahalli, and I. Papautsky, *Enhanced particle filtration in straight microchannels using shear-modulated inertial migration*. Physics of Fluids, 2008. **20**(10): p. 101702.
40. Seo, J., M.H. Lean, and A. Kole, *Membraneless microseparation by asymmetry in curvilinear laminar flows*. Journal of Chromatography A, 2007. **1162**: p. 126-131.

41. Yoon, D.H., et al., *Size-selective separation of micro beads by utilizing secondary flow in a curved rectangular microchannel*. Lab Chip, 2009. **9**(1): p. 87-90.
42. Gossett, D. and D. Di Carlo, *Particle focusing mechanisms in curving confined flows*. Analytical Chemistry, 2009. **81**: p. 8459-8465.
43. Hur, S.C., A.J. Mach, and D. Di Carlo, *High-throughput size-based rare cell enrichment using microscale vortices*. Biomicrofluidics, 2011. **5**(2): p. 022206.
44. Lee, M.G., S. Choi, and J.-K. Park, *Inertial separation in a contraction--expansion array microchannel*. Journal of Chromatography A, 2011. **1218**: p. 4138-4143.
45. Park, J.-S., S.-H. Song, and H.-I. Jung, *Continuous focusing of microparticles using inertial lift force and vorticity via multi-orifice microfluidic channels*. Lab on a Chip, 2008. **9**(7): p. 939-948.
46. Chung, A.J., D.R. Gossett, and D. Di Carlo, *Three Dimensional, Sheathless, and High-Throughput Microparticle Inertial Focusing Through Geometry-Induced Secondary Flows*. Small, 2013. **9**(5): p. 685-690.
47. Sollier, E., et al., *Size-selective collection of circulating tumor cells using Vortex technology*. Lab Chip, 2014. **14**(1): p. 63-77.
48. Zhang, J., et al., *Inertial focusing in a straight channel with asymmetrical expansion-contraction cavity arrays using two secondary flows*. Journal of Micromechanics and Microengineering, 2013. **23**(8).
49. Wang, X. and J.P. Zhou, I., *Vortex-aided inertial microfluidic device for continuous particle separation with high size-selectivity, efficiency and purity*. Biomicrofluidics, 2013. **7**.
50. Stoecklein, D., et al., *Micropillar sequence designs for fundamental inertial flow transformations*. Lab on a Chip, 2014. **14**(21): p. 4197-4204.
51. Mao, W. and A. Alexeev, *Hydrodynamic sorting of microparticles by size in ridged microchannels*. Physics of Fluids (1994-present), 2011. **23**(5): p. 051704.
52. Hsu, C.-H., et al., *Microvortex for focusing, guiding and sorting of particles*. Lab on a Chip, 2008. **8**(12): p. 2128.
53. Stoecklein, D., et al., *Micropillar sequence designs for fundamental inertial flow transformations*. Lab on a Chip, 2014. **14**(21): p. 4107-4296.

54. Huang, L.R., et al., *Continuous Particle Separation Through Deterministic Lateral Displacement*. Science, 2004. **304**(5673): p. 987-990.
55. Lubbersen, Y.S., M.A.I. Schutyser, and R.M. Boom, *Suspension separation with deterministic ratchets at moderate Reynolds numbers*. Chemical Engineering Science, 2012. **73**(0): p. 314-320.
56. Lubbersen, Y.S., et al., *Visualization of inertial flow in deterministic ratchets*. Separation and Purification Technology, 2013. **109**(0): p. 33-39.
57. Bowman, T.J., G. Drazer, and J. Frechette, *Inertia and scaling in deterministic lateral displacement*. Biomicrofluidics, 2013. **7**(6).
58. Bhagat, A.A.S., *Inertial Microfluidics for Particle Separation and Filtration*, in *Electrical and Computer Engineering*. 2009, University of Cincinnati: Cincinnati. p. 90.
59. Kuntaegowdanahalli, S.S., et al., *Inertial microfluidics for continuous particle separation in spiral microchannels*. Lab on a Chip - Miniaturisation for Chemistry and Biology, 2009. **9**(20): p. 2973-2980.
60. Lubbersen, Y.S., et al., *Particle suspension concentration with sparse obstacle arrays in a flow channel*. Chemical Engineering and Processing: Process Intensification, 2015. **95**: p. 90-97.
61. Xiang, N., et al., *Improved understanding of particle migration modes in spiral inertial microfluidic devices*. RSC Advances, 2015. **5**(94): p. 77264-77273.
62. Clime, L., et al., *Twin tubular pinch effect in curving confined flows*. Scientific Reports, 2015. **5**: p. 9765.
63. Warkiani, M.E., et al., *Membrane-less microfiltration using inertial microfluidics*. Scientific Reports, 2015. **5**.
64. Davis, J.A., et al., *Deterministic hydrodynamics: Taking blood apart*. Proceedings of the National Academy of Sciences, 2006. **103**(40): p. 14779-14784.
65. Louthback, K., et al., *Deterministic separation of cancer cells from blood at 10 mL/min*. AIP Advances, 2012. **2**(4): p. -.
66. Zeming, K.K., S. Ranjan, and Y. Zhang, *Rotational separation of non-spherical bioparticles using I-shaped pillar arrays in a microfluidic device*. Nature Communications, 2013. **4**.

67. Holm, S.H., et al., *Separation of parasites from human blood using deterministic lateral displacement*. Lab on a Chip, 2011. **11**(7): p. 1326-1332.
68. Xiang, N. and Z. Ni, *High-throughput blood cell focusing and plasma isolation using spiral inertial microfluidic devices*. Biomedical Microdevices, 2015. **17**(6): p. 1-11.
69. D'Avino, G., *Non-Newtonian deterministic lateral displacement separator: theory and simulations*. Rheologica Acta, 2013. **52**(3): p. 221-236.
70. Beech, J.P., et al., *Sorting cells by size, shape and deformability*. Lab on a Chip, 2012. **12**(6): p. 1048-1051.
71. Hur, S.C., et al., *Deformability-based cell classification and enrichment using inertial microfluidics*. Lab on a Chip, 2011. **11**(5): p. 912-920.
72. Masaeli, M., et al., *Continuous Inertial Focusing and Separation of Particles by Shape*. Physical Review X, 2012. **2**(3).
73. Ranjan, S., et al., *DLD pillar shape design for efficient separation of spherical and non-spherical bioparticles*. Lab on a Chip, 2014. **14**: p. 4250-4262.
74. Inglis, D.W., M. Lord, and R.E. Nordon, *Scaling deterministic lateral displacement arrays for high throughput and dilution-free enrichment of leukocytes*. Journal of Micromechanics and Microengineering, 2011. **21**(5): p. 054024.
75. Inglis, D.W., et al., *Critical particle size for fractionation by deterministic lateral displacement*. Lab on a Chip, 2006. **6**(5): p. 655-658.
76. Dijkshoorn, J.P., et al., *A comparison of microfiltration and inertia-based microfluidics for large scale suspension separation*. Separation and Purification Technology.
77. Roos, Y.H., et al., *Food Engineering at Multiple Scales: Case Studies, Challenges and the Future—A European Perspective*. Food Engineering Reviews, 2016. **8**(2): p. 91-115.
78. Zeming, K.K., et al., *Asymmetrical Deterministic Lateral Displacement Gaps for Dual Functions of Enhanced Separation and Throughput of Red Blood Cells*. Scientific Reports, 2016. **6**.
79. Lubbersen, Y.S., R.M. Boom, and M.A.I. Schutyser, *High throughput particle separation with a mirrored deterministic ratchet design*. Chemical Engineering and Processing: Process Intensification, 2014. **77**(0): p. 42-49.
80. COMSOL, M., in *v. 5.3*, COMSOL AB: Stockholm, Sweden.

81. Warkiani, M.E., et al., *Large-Volume Microfluidic Cell Sorting for Biomedical Applications*. Annual Review of Biomedical Engineering, 2015. **17**(1): p. 1-34.
82. Dijkshoorn, J.P., et al., *A comparison of microfiltration and inertia-based microfluidics for large scale suspension separation*. Separation and Purification Technology, 2017. **173**: p. 86-92.
83. Schroën, K., A. van Dinther, and R. Stockmann, *Particle migration in laminar shear fields: A new basis for large scale separation technology?* Separation and Purification Technology, 2017. **174**: p. 372-388.
84. Liu, Z., et al., *Rapid isolation of cancer cells using microfluidic deterministic lateral displacement structure*. Biomicrofluidics, 2013. **7**(1): p. 011801-10.
85. Dijkshoorn, J.P., et al., *Sieve-based lateral displacement technology for suspension separation*. Separation and Purification Technology, 2017. **175**: p. 384-390.
86. Hyun, J.-c., et al., *Improved pillar shape for deterministic lateral displacement separation method to maintain separation efficiency over a long period of time*. Separation and Purification Technology, 2017. **172**: p. 258-267.
87. Kulrattanarak, T., et al., *Mixed motion in deterministic ratchets due to anisotropic permeability*. Journal of Colloid and Interface Science, 2011. **354**(1): p. 7-14.
88. Vernekar, R., et al., *Anisotropic permeability in deterministic lateral displacement arrays*. arXiv:1610.08427, 2016.
89. Kim, S.-C., et al., *Broken flow symmetry explains the dynamics of small particles in deterministic lateral displacement arrays*. Proceedings of the National Academy of Sciences, 2017. **114**(26): p. E5034-E5041.
90. Kulrattanarak, T., et al., *Analysis of mixed motion in deterministic ratchets via experiment and particle simulation*. Microfluidics and Nanofluidics, 2011. **10**(4): p. 843-853.
91. de Jong, J., R.G.H. Lammertink, and M. Wessling, *Membranes and microfluidics: a review*. Lab on a Chip, 2006. **6**(9): p. 1125-1139.
92. Devasenathipathy, S., et al., *Particle imaging techniques for microfabricated fluidic systems*. Experiments in Fluids, 2003. **34**(4): p. 504-514.

93. Silva, G., N. Leal, and V. Semiao, *Micro-PIV and CFD characterization of flows in a microchannel: Velocity profiles, surface roughness and Poiseuille numbers*. International Journal of Heat and Fluid Flow, 2008. **29**(4): p. 1211-1220.
94. Sinton, D., *Microscale flow visualization*. Microfluidics and Nanofluidics, 2004. **1**(1): p. 2-21.
95. Dijkshoorn, J.P., et al., *Reducing the critical particle diameter in (highly) asymmetric sieve-based lateral displacement devices*. Scientific Reports, 2017. **7**(1): p. 14162.
96. de Valença, J.C., et al., *Influence of Rayleigh-Bénard convection on electrokinetic instability in overlimiting current conditions*. Physical Review Fluids, 2017. **2**(3): p. 033701.
97. Vernekar, R., et al., *Anisotropic permeability in deterministic lateral displacement arrays*. Lab on a Chip, 2017.
98. Barros, A.I., et al., *Harvesting techniques applied to microalgae: A review*. Renewable and Sustainable Energy Reviews, 2015. **41**: p. 1489-1500.
99. Green, J.V., M. Radisic, and S.K. Murthy, *Deterministic Lateral Displacement as a Means to Enrich Large Cells for Tissue Engineering*. Analytical Chemistry, 2009. **81**(21): p. 9178-9182.
100. Henry, E., et al., *Sorting cells by their dynamical properties*. Scientific Reports, 2016. **6**: p. 34375.
101. Dijkshoorn, J.P., et al., *Visualizing the hydrodynamics in sieve-based lateral displacement systems*. Scientific Reports, 2018. **8**(1): p. 12861.
102. Wu, W.-Y., S. Weinbaum, and A. Acrivos, *Shear flow over a wall with suction and its application to particle screening*. Journal of Fluid Mechanics, 1992. **243**: p. 489-518.
103. Yan, Z.-Y., A. Acrivos, and S. Weinbaum, *Fluid skimming and particle entrainment into a small circular side pore*. Journal of Fluid Mechanics, 1991. **229**: p. 1-27.
104. Yamada, M. and M. Seki, *Hydrodynamic filtration for on-chip particle concentration and classification utilizing microfluidics*. Lab on a Chip, 2005. **5**(11): p. 1233-1239.
105. Brito-de la Fuente, E., et al., *Microfiltration of whole milk with silicon microsieves: Effect of process variables*. Chemical Engineering Research and Design, 2010. **88**(5): p. 653-660.

106. Warkiani, M.E., et al., *A high-flux isopore micro-fabricated membrane for effective concentration and recovering of waterborne pathogens*. Biomedical Microdevices, 2012. **14**(4): p. 669-677.
107. He, Z., et al., *The effect of permeate flux on membrane fouling during microfiltration of oily water*. Journal of Membrane Science, 2017. **525**: p. 25-34.
108. Tanudjaja, H.J., et al., *Effect of cross-flow velocity, oil concentration and salinity on the critical flux of an oil-in-water emulsion in microfiltration*. Journal of Membrane Science, 2017. **530**: p. 11-19.
109. Ullah, A., et al., *Microfiltration of deforming oil droplets on a slotted pore membrane and sustainable flux rates*. Journal of Membrane Science, 2011. **382**(1): p. 271-277.
110. Wang, Y., R. Mauri, and A. Acrivos, *The transverse shear-induced liquid and particle tracer diffusivities of a dilute suspension of spheres undergoing a simple shear flow*. Journal of Fluid Mechanics, 1996. **327**: p. 255-272.
111. Rohatgi, A., *Shear-Induced Diffusion in Dilute Suspensions*, in *Chemical and Biomolecular Engineering*. 2012, University of Notre Dame.



# Acknowledgements

Caught you!! I suggest you start reading at the beginning.. (smile)

Well ok, for many the acknowledgements is a very important part of this book. Though, most of the effort was mine, I am sure that without your help this book would not have existed. Now, looking back, I am very grateful and want to thank you from the bottom of my heart for all your; support, laughs, discussions, patience, jokes, adventures, nudges, drinks, comfort, parties, massages, smiles and whatever more you did to help me over the past four years. Partly because of you, I managed to finish this book!

I would like to start by expressing my utmost gratitude for my supervisors. *Martijn*, ik ben erg blij dat jij mijn begeleider bent geweest over de afgelopen 4 jaar. Ik denk met veel plezier terug naar onze gesprekken die nog wel eens afdwaalde (basketball of klussen). Ook door onze, niet al te beste, humor was het meestal leuk maar ook in de wat lastigere periodes stond je voor me klaar. Mijn dank voor alles. *Maarten*, ik ben blij dat je aan mij dacht toen dit project beschikbaar kwam. Bedankt voor ons, meestal nuttig, wekelijks telefonisch overleg, waarvoor ik dan eigenlijk geen agenda had en dat we tot de conclusie kwamen dat we het deze keer wel konden overslaan. Bedankt voor de pizzadiner(s) al waren die toch best wel ver weg. Maar vooral bedankt voor je eindeloze geduld, ik heb enorm veel van je geleerd! Ik vond het heel fijn om met je samen te werken. *Remko* bedankt voor al je ideeën, betrokkenheid en enthousiasme. Onze gesprekken waren altijd zeer interessant en de daardoor ontstane inzichten resulteren zich in dit boekje!

*Jorge Ricardo Apolinario Machado da Bachert-Cunha* and *BDRik*! I remember my first day like yesterday, Rikkie and Ricardinho all the way at the back of the office. Ricardinho staring out of the window most of his time and Rik pretending to be busy when he was actually checking dumpert! Thank you so much for the past 4 years, it was a pleasure to have spent most of our time in the same office. It is my honour to have you as my Paranymps!

Special thanks go to *Moses*, *Mundis* and *Ton*. Thanks for all your effort and dedication with the work in the lab and to teach me how to be a supervisor!

Dear officemates, I want you to know that you made my day, every day! Thank you, *Vytautas* (you \$%#@#) for all the pranks and *Pom* for the help starting up. *Maurits* for all your advice and help designing my system! *Paulina* for your cat-massages and the awesome Mexico-trip but not for getting me water. *Maarten* for the astrophysics lectures and of course all your help. *Karine* for being insane(ity 2.0), for the delicious food, vodka and all the sweets (Аленка)! *Stan* for the laughs and the (Belgium) beers you made! *Nimmy* for the laughs, for being clumsy and for getting me water! *Steffen* for our table tennis sessions that I always lost. 'New' guy lil' *Chris*, technically you did not even start yet but all the best in the next four years!

I want to thank everybody at Wetsus for the amazing time. *Harm* super bedankt voor al je advies en je werk aan mijn setup en systeempjes en voor de praatjes in de gang, zonder jou was het nooit gelukt. *JJ & Marco* voor jullie hulp en onuitputtelijke enthousiasme. *Gerben*, bedankt voor de opfleurende praatjes en voor de uitstekende zorg (bv. als ik weer eens een broodje vergat te bestellen). *Wim*, *Ernst*, *Jan T.*, *Marianne*, *Rienk*, *Jelmer*, *Agnieszka*, *Ton*, *Wiebe*, *Janneke*, *Mieke*, *Riet*, *Catharina* bedankt voor jullie hulp in het lab, in het kantoor en de kantine. Natuurlijk wil ik ook *Jan de G.*, *Anke*, *Geke*, *Linda*, *Helena*, *Roely*, *Jeanette*, *Trienke*, *Tineke* en juffrouw *Jannie* bedanken voor praatjes, grapjes (het Jorrit-effect) en jullie hulp. Ook wil ik *Cees*, *Johannes & Bert* bedanken voor de fantastische werkplek die Wetsus is en voor de luchtige praatjes/geintjes bij de borrel, lunch of koffie pauzes. I want to thank, *Maarten B.* and the *AWT members* for their input and interesting discussion during the theme meetings.

*Joeri* bedankt voor de interessante gespreksonderwerpen en hulp bij het PIVen. *Mark & Mariana* and *Tijn*, thanks for the occasional drinks (that did not happen often enough). *Philipp W.* for all the pranks and being weird. *Terica*.. thanks for... pinching someone else! Still makes me smile. *Hector* for organizing the Mexico trip and laughing.. loud! *Victor* for being awesome! No you are awesome! *Jorrit* for being my Doppelgänger. *João* for being my staring buddy and *Lisette* for the fun with the kids & the HSC. There are many more, so *Gonçalo*, *Natascha*,

*Prashanth, Thomas, Rebeca, Pedro, Rachel, Roel, Janneke, Doekle, Jos, Louis, Slawek, Sam, Adam, Tom, Sebastian, Gijs, Gerwin, Oliver, Hester, Lucia and Jordi* thanks for the help and all the nice moments!

Though I spend most of my time in Leeuwarden, I have much to thank to the Food Process Engineering (FPE) Group in Wageningen. For your desk that I probably used, for the nice dinners, beers and coffee breaks that somehow always had cakes or sweets! *Marjan*, you always picked up the phone in the most impressive way! Thanks for all the help you have given me over the years. *Martin* thanks for the fun talks and for reminding me every month to fill in 'my projects' followed by an email to correct it. I want to thank *Laura* for always offering me your guest (red) room and the alcohol-free glühwein, it was delicious! *Filippos* for all the interesting discussions and gags you send me. *Meinou*, thank you for advising me to do my PhD and for your positivity! *Victor Q* it was always nice to have lunch with you and thanks for letting me use your Netflix! *Victor A* for our nice (music) discussions, soon we will be like Dexter Holland!! *Juliana* thanks for the fun ☺ and your company when traveling to Fryslân. *Emmie* and *Steffie* bedankt voor de fantastische Canada trip en het spotten van een beer! *Andrea, Pina* and *Patricia*, thanks for having me stay over, for the nice table talks and the amazing food..! *Fiona* for teaching me Chinese, I am fluent now! *Zulhaj* thanks for the nice food and answering all my annoying questions. *Anton* for the relaxing time and all the ice-creams in Nice! *Dimitri*, it was my pleasure sitting across of you ;). Of course I also want to thank *Lu, Angelica, Kelly, Marlies, Jos, Ali, Jun, Maurice, Eline, Ties, Karin, Jochem, Floor, Jan* and *Nynke*.

Special thanks go to the Bolivian Family (yteicos terces) and all the related people. *Christian & Pamela, Wilco & Grace, Ori, Bella and Lauri* thanks a million for always making me feel welcome and all the amazing times! *Patrick, Bart, Gijs, Edwin en Jurre* bedankt voor de barre weekendjes en feestjes! Het is nog altijd helemaal goud! *Esther en Lidwien* het valt niet altijd mee om af te spreken maar de zeldzame 'dates' zijn altijd fantastisch!

Zonder dat jullie het misschien zelf doorhebben heb ik heel veel aan jullie te danken en niet alleen in deze vier jaar. En ondanks dat ik heel ver weg woon en ik jullie de afgelopen

jaren een stuk minder heb gezien is het altijd fijn om weer in Maasland te zijn. *Jeffrey & Amy (Jason)*, *Kevin & Kelly (Vinz en Lynn)*, *Edwin K. & Chantal*, *Coen & Sanne (Guus)*, *Stanley & Lianne*, *Edwin G. & Robiene (Quin)*, *Ben & Kelly*, *Erik, Sven en Jan* bedankt voor alle steun!

Ook wil ik mijn super lieve familie bedanken! Alle *Buurtjes en Dijkshoorns* bedankt voor jullie interesse, steun en alle leuke vragen! Met name *Pim & Maaïke (Sil)* en *Willem & Moniek (Duuk)* wil ik bedanken voor hun interesse en steun!

*Pa & Ma, Jan Willem & Joella* en kleine *Liz*, ik hou van jullie! Bedankt voor alles wat jullie voor mij gedaan hebben! Bedankt voor jullie hulp, tips, zorgen en steun! Nu dit avontuur is afgelopen kunnen jullie even rustig ademhalen. Maar niet te lang want het volgende avontuur staat alweer klaar! *JW*, (lieve) grote broer, er is enorm veel om jou voor te bedanken teveel om het hier even op te noemen. In het kort, ik ben super blij met een broer als jij! Ik heb dus nog een paar van die extra stevige knuffels voor je in petto (alleen als *Liz* niet kijkt).

Voor veel zijn de laatste paar maanden van een PhD het zwaarst, een snel naderende deadline waarin veel teveel tegelijk af moet. Door jou vlogen deze laatste maanden zonder enige moeite voorbij! *Birgit* ik ben heel blij dat we allebei de laatste loodjes van ons PhD met elkaar mogen delen en hoop dat ons nog veel mooie momenten te wachten staan!

# About the author

Jaap (Jacob Paulus) Dijkshoorn was born on May 22, 1987 in Delft, The Netherlands. His primary education started at Maputo International School in Mozambique and finished in 2000 at 't Spreeuwenest in Maasland. In 2005, he obtained his HAVO diploma at the Christelijk Lyceum Delft and in the same year he started his study in Food Technology at the University of Applied Sciences (InHolland) in Delft.



During his BSc, Jaap investigated the inactivation of lipase in lecithin using protease at Unilever and finished his BSc thesis at Cosun R&D where he developed glazing agents. After obtaining his BSc degree, he started his MSc at the Wageningen University and specialised on process and product design. For his MSc thesis, Jaap investigated suspension separation using Deterministic Lateral Displacement (DLD) arrays at Wetsus, European Centre of Excellence for Sustainable Water Technology. He concluded his MSc in 2012 with an internship about processing of Vicia Faba at the University of Helsinki.

After obtaining his MSc degree, Jaap started a project at Unilever where he investigated the effect of surface active components on the adherence of spreads. He continued his career as food technologist in the department of product and process development at Cargill Cocoa & Chocolate in Wormer. In 2014, Jaap started his PhD in the Food Process Engineering (FPE) Department of Wageningen University but was stationed at Wetsus in Leeuwarden. There he continued his research on the separation principle of DLD to separate particle suspensions on large-scale. The results of his work are presented in this thesis.

# List of Publications

- J.P. Dijkshoorn**, M.A.I.S. Schutyser, R.M. Wagterveld, C.G.P.H. Schroën, R.M. Boom (2017), A comparison of microfiltration and inertia-based microfluidics for large scale suspension separation. *Separation and Purification Technology* 175, 86-92
- J.P. Dijkshoorn**, R.M. Wagterveld, R.M. Boom, M.A.I.S. Schutyser (2017), Sieve-based lateral displacement technology for suspension separation. *Separation and Purification Technology* 175, 384-390
- J.P. Dijkshoorn**, M.A.I.S. Schutyser, R.M. Boom, R.M. Wagterveld (2017), Reducing the critical particle diameter in (highly) asymmetric sieve-based lateral displacement devices. *Scientific Reports* 7(1), 14162
- J.P. Dijkshoorn**, J.C. de Valença, R.M. Wagterveld, R.M. Boom, M.A.I.S. Schutyser (2018), Visualizing the hydrodynamics in sieve-based lateral displacement systems. *Scientific Reports* 8, 12861
- J.P. Dijkshoorn**, R.M. Wagterveld, R.M. Boom, M.A.I.S. Schutyser (2018), Deterministic displacement of particles and oil droplets in a cross-flow microsieve module. Accepted in *Journal of membrane science*.

# Overview of completed training activities

## Discipline specific activities

- The Netherlands Process Technology Symposium (NPS), The Netherlands 2014
- European Congress of Chemical Engineering (ECCE), France 2015
- FILTECH conference, Germany 2016
- Int. Membrane Science and Technology Conference (IMSTEC), Australia 2016
- Group of Users of Technology for Separation (NLGUTS), The Netherlands 2016
- Wetsus Congress, The Netherlands 2014-2018
  
- Statics and dynamics of soft and granular materials, The Netherlands (JMBC) 2016
- Modelling and Simulations in Food & Bio Processing, Italy (MSFS) 2016
- Process Economics and Cost Engineering, The Netherlands (ISPT) 2016
- Measurement Techniques, The Netherlands (JMBC) 2017

## General courses

- Personal development plan, The Netherlands (Wetsus) 2014
- Student supervision course, The Netherlands (Wetsus) 2014
- Vlag PhD week, The Netherlands (VLAG) 2015
- Authoring a PhD, The Netherlands (UCF) 2015
- Image Processing for Scientists, The Netherlands (Wetsus) 2016
- Scientific Writing, The Netherlands (WGS) 2017
- Business Development, The Netherlands (Climate-KIC) 2017
- Talent Course, The Netherlands (Wetsus) 2017
- Career Perspectives, The Netherlands (WGS) 2018

## Optionals

- Preparation of research proposal 2014
- Advanced Water Treatment meetings 2014-2018
- Food Process Engineering Symposia 2014-2018
- Wetsus Internal Congress 2014-2018
- PhD study tour, Germany and Switzerland 2016
- PhD study tour, Canada 2018

This work was performed in the cooperation framework of Wetsus, centre of excellence for sustainable water technology ([www.wetusus.nl](http://www.wetusus.nl)). Wetsus is co-funded by the Dutch Ministry of Economic Affairs and Ministry of Infrastructure and Environment, the European Union Regional Development Fund, the Province of Fryslân, and the Northern Netherlands Provinces. The author would like to thank the participants of the research theme Advanced Waste Water Treatment for the fruitful discussions and their financial support.

Cover design by Douwe Hoendervanger.

This thesis is printed by ProefschriftMaken.nl in 100 copies